How does lithospheric configuration relate to deformation in the Alpine region?

Cameron Spooner

Kumulative Dissertation
zur Erlangung des akademischen Grades
"doctor rerum naturalium"
(Dr. rer. nat.)
in der Wissenschaftsdisziplin Geologie

eingereicht an der
Mathematisch-Naturwissenschaftlichen Fakultät
Institut für Geowissenschaften
der Universität Potsdam
und
Sektion 4.5 Sedimentbeckenanalyse
Deutsches GeoForschungsZentrum Potsdam

Ort und Tag der Disputation: Campus Golm, Universität Potsdam, 26/07/2021

Hauptbetreuer:
- Priv. Doz. Dr. Sascha Brune.....University of Potsdam

Betreuer*innen:
- Prof. Dr. Magdalena Scheck-Wenderoth.....RWTH Aachen University
- Prof. Dr. Michael Weber.....University of Potsdam

Gutachter*innen:
- Prof. Dr. Magdalena Scheck-Wenderoth.....RWTH Aachen University
- Prof. Dr. Hans-Jürgen Götze.....Christian-Albrechts-Universität zu Kiel
- Prof. Dr. Eline Le Breton.....Freie Universität Berlin

Published online on the
Publication Server of the University of Potsdam:
https://doi.org/10.25932/publishup-51644
https://nbn-resolving.org/urn:nbn:de:kobv:517-opus4-516442

Abstract

Forming as a result of the collision between the Adriatic and European plates, the Alpine orogen exhibits significant lithospheric heterogeneity due to the long history of interplay between these plates, other continental and oceanic blocks in the region, and inherited features from preceeding orogenies. This implies that the thermal and rheological configuration of the lithosphere also varies significantly throughout the region. Lithology and temperature/pressure conditions exert a first order control on rock strength, principally via thermally activated creep deformation and on the distribution at depth of the brittle-ductile transition zone, which can be regarded as the lower bound to the seismogenic zone. Therefore, they influence the spatial distribution of seismicity within a lithospheric plate. In light of this, accurately constrained geophysical models of the heterogeneous Alpine lithospheric configuration, are crucial in describing regional deformation patterns. However, despite the amount of research focussing on the area, different hypotheses still exist regarding the present-day lithospheric state and how it might relate to the present-day seismicity distribution.

This dissertaion seeks to constrain the Alpine lithospheric configuration through a fully 3D integrated modelling workflow, that utilises multiple geophysical techniques and integrates from all available data sources. The aim is therefore to shed light on how lithospheric heterogeneity may play a role in influencing the heterogeneous patterns of seismicity distribution observed within the region. This was accomplished through the generation of: (i) 3D seismically constrained, structural and density models of the lithosphere, that were adjusted to match the observed gravity field; (ii) 3D models of the lithospheric steady state thermal field, that were adjusted to match observed wellbore temperatures; and (iii) 3D rheological models of long term lithospheric strength, with the results of each step used as input for the following steps.

Results indicate that the highest strength within the crust (~ 1 GPa) and upper mantle (> 2 GPa), are shown to occur at temperatures characteristic for specific phase transitions (more felsic crust: 200 – 400 °C; more mafic crust and upper lithospheric mantle: ~600 °C) with almost all seismicity occurring in these regions. However, inherited lithospheric heterogeneity was found to significantly influence this, with seismicity in the thinner and more mafic Adriatic crust (~22.5 km, 2800 kg m^{-3}, 1.30E^{-06} W m^{-3}) occuring to higher temperatures (~600 °C) than in the thicker and more felsic European crust (~27.5 km, 2750 kg m^{-3}, 1.3–2.6E^{-06} W m^{-3}, ~450 °C). Correlation between seismicity in the orogen forelands and lithospheric strength, also

show different trends, reflecting their different tectonic settings. As such, events in the plate boundary setting of the southern foreland correlate with the integrated lithospheric strength, occurring mainly in the weaker lithosphere surrounding the strong Adriatic indenter. Events in the intraplate setting of the northern foreland, instead correlate with crustal strength, mainly occurring in the weaker and warmer crust beneath the Upper Rhine Graben.

Therefore, not only do the findings presented in this work represent a state of the art understanding of the lithospheric configuration beneath the Alps and their forelands, but also a significant improvement on the features known to significantly influence the occurrence of seismicity within the region. This highlights the importance of considering lithospheric state in regards to explaining observed patterns of deformation.

Zusammenfassung

Als Resultat der Kollision zwischen der Adriatischen und Europäischen Platte ist das Alpenorogen durch eine ausgeprägte Heterogenität der Lithosphäreneigenschaften gekennzeichnet, die auf die Geschichte der beiden Platten, ihre Interaktion, Wechselwirkungen mit anderen kontinentalen und ozeanischen Blöcken der Region und strukturell vererbte Merkmale aus früheren Orogenesen zurückzuführen sind. Entsprechend ist zu erwarten, dass die thermische und rheologische Konfiguration der Lithosphäre ebenfalls grundlegend innerhalb der Region variiert. Lithologie und Temperatur-/Druckbedingungen steuern maßgeblich die Festigkeit der Lithosphäre indem thermisch aktiviertes Kriechen die Tiefenlage der spröd-duktilen Übergangszone – die sogenannte brittle-ductile transition (BDT) bestimmt. Diese Tiefenlage kann als untere Grenze der seismogenen Zone betrachtet werden kann, weshalb sie die räumliche Verteilung der Seismizität in der Lithosphärenplatte entscheidend beeinflusst. Trotz der langjährigen und umfangreichen Forschung zur Dynamik und Struktur der Alpen gibt es immer noch verschiedene Hypothesen zum heutigen physikalischen Zustand des Systems und dazu, wie dieser mit der Verteilung und dem Auftreten von Seismizität zusammenhängt.

Diese Dissertation hat das Ziel, die Lithosphärenkonfiguration der Alpen zu beschreiben und Zusammenhänge zwischen der Verteilung lithosphärischer Eigenschaften und Deformation, insbesondere der Verteilung der Seismizität abzuleiten. Dies wird durch einen integrierten Modellierungsansatz erreicht, mit dem verfügbare geophysikalische Beobachtungen in 3D Modellen zusammengeführt werden, die die heterogene lithosphärische Konfiguration abbilden. Dazu wird (1) ein mit geologischen, seismischen und gravimetrischen Daten konsistentes 3D-Dichtemodell erzeugt und genutzt, um Lithologien abzuleiten, (2) deren Konsequenzen für das dreidimensionale stationäre thermische Feld zu berechnen und, basierend darauf, schließlich (3) die räumliche Variation der Lithosphärenrheologie zu bestimmen. Diese räumliche Variation der rheologischen Eigenschaften wurde schließlich in Beziehung zur Verteilung der auftretenden Seismizität gesetzt.

Die Ergebnisse zeigen, dass die größte Festigkeit innerhalb der Kruste (~1 GPa) und im oberen Mantel (> 2 GPa) oberhalb der Bereiche auftritt, wo Temperaturbedingte Phasenübergänge zu erwarten sind. Für die felsische Kruste umfasst dies den Temperaturbereich bis etwa 400° C, für die mafische Kruste und den lithospärischen Mantel bis etwa 600°, wobei Seismizität jeweils oberhalb dieser Temperaturen auftritt. Zusätzlich

wurden Hinweise gefunden, dass diese Festigkeitsverteilung auf vererbte Lithosphäreneigenschaften zurückzuführen ist: so tritt seismische Aktivität in der dünneren und mafischen Adria Kruste (~22,5 km, 2.800 kg m^{-3}, 1.30E $^{-06}$ W m^{-3}) bei höheren Temperatur (~600° C) auf als in der dickeren und eher felsischen europäischen Kruste (~27.5 km, 2750 kg m^{-3}, 1.3–2.6E^{-06} W m^{-3}, ~450 °C).

Die Beziehung zwischen seismischer Aktivität und Lithosphärenfestigkeit im Bereich der Vorländer zeigt ebenfalls unterschiedliche Trends, die verschiedenene tektonische Randbedingungen wiederspiegeln. Während im Plattenrandsetting des südlichen Vorlands Seismizität in der rheologisch weicheren Lithosphäre in der Umrandung des adriatischen Indentors auftritt, korreliert die auftretende Seismizität im Intraplattensetting des nördlichen Vorlands räumlich mit wärmeren und rheologisch schwächeren Domänen im Bereich des Oberrheingrabens.

Somit liefern die Ergebnisse in dieser Arbeit nicht nur ein verbessertes Verständnis der Lithosphärenkonfiguration der Alpen und ihrer Vorländer , sondern auch einen bedeutenden Fortschritt dazu, welche Faktoren Seismizität innerhalb der Region beeinflussen können. Sie zeigen, dass es wichtig ist, die Lithosphärenkonfiguration zu kennen und sie zur auftretenden Deformation in Beziehung zu setzen.

Declaration of Author Contributions

In this cumulative dissertation, Chapters 2, 3, 4 and 5 consist of published or submitted studies where Cameron Spooner is either first author or co-author. Accordingly, the numbering of the figures tables and equations were adjusted to the style of this thesis. The related bibliography for these publications is also presented at the end of the dissertation.

Chapter 2 derives from "Spooner, C., Scheck-Wenderoth, M., Götze, H., Ebbing, J. and Hetényi, G. Density distribution across the Alpine lithosphere constrained by 3-D gravity modelling and relation to seismicity and deformation. Solid Earth, 10(6), pp.2073-2088, https://doi.org/10.5194/se-10-2073-2019, 2019", where Cameron Spooner carried out the gravity modelling workflow, interpreted the results and prepared the manuscript as a first author. Magdalena Scheck-Wenderoth advised on the entire workflow and the interpretation of results. Hans-Jürgen Götze and Jörg Ebbing contributed pre-existing gravity models from the region and advised on the gravity modelling workflow and utilisation of the software used to carry it out. György Hetényi contributed seismic data for the work and advised on the interpretation of the crust and Moho in the Eastern Alps. All authors contributed to redrafting of the manuscript.

Chapter 3 derives from "Spooner, C., Scheck-Wenderoth, M., Cacace, M., Götze, H. and Luijendijk, E. The 3D thermal field across the Alpine orogen and its forelands and the relation to seismicity. Global and Planetary Change, 193, p.103288, https://doi.org/10.1016/j.gloplacha.2020.103288, 2020", where Cameron Spooner carried out the thermal modelling workflow, interpreted the results and prepared the manuscript as a first author. Mauro Cacace developed the software used to carry out the thermal modelling workflow and provided support on its use throughout. Magdalena Scheck-Wenderoth and Hans-Jürgen Götze advised on the entire workflow and the interpretation of results. Elco Luijendijk contributed a dataset of Alpine temperature measurements and advised on the interpretation of results. All authors contributed to redrafting of the manuscript.

Chapter 4 has been submitted to Geoscientific Model Development (2021) as a manuscript entitled "How biased are our models? – A Case Study of the Alpine Region", where Cameron Spooner generated both the General-Focus and Crustal-Focus Alps model, interpreteted results and prepared the manuscript as a co-author. Denise Degen carried out the sensitivity analyses, interpreted results and prepared the manuscript as a first author. Mauro

Cacace and Magdalena Scheck-Wenderoth advised on the entire workflow and the interpretation of results. All authors contributed to redrafting of the manuscript.

Chapter 5 has been accepted for review in Solid Earth (2020, https://doi.org/10.5194/se-2020-202) as a manuscript entitled “How Alpine seismicity relates to lithospheric strength“, where Cameron Spooner carried out the rheological modelling workflow, interpreted the results and prepared the manuscript as a first author. Mauro Cacace and Denis Anikiev developed tools for calculations in the modelling workflow and the plotting of results. Magdalena Scheck-Wenderoth advised on the entire workflow and the interpretation of results. All authors contributed to redrafting of the manuscript.

Table of Contents

List of Figures

List of Tables

Conversion of Units

Centimetre–gram–second units have been used for gravitational acceleration throughout this dissertation. As a result of the small magnitudes dealt with, mGal is used, which can be converted into SI units using the equation: 1 mGal = $1E^{-5}$ m s^{-2}

Chapter 1. Introduction

The Alps and their forelands, stretching for 1200 km in an arc from Nice to Vienna are one of the most heavily industrialised and populated parts of Europe. Earthquakes have repeatedly struck the region, most noticeably in the Upper Rhine (Germany, France, Switzerland) and Friuli (Italy, Slovenia, Austria) areas, inflicting casualties and damaging properties. Investigating the underlying causes of this activity is therefore clearly of paramount importance. However, despite also representing one of the most geologically fascinating locations in Europe, the present-day distribution of seismicity is still poorly understood and presently debated with regards to heterogeneity in the subsurface of the Alpine orogen and its northern and southern forelands (Deichmann, 1992; Bonjer, 1997; Cattaneo et al., 1999; Singer et al., 2014; Eva et al., 2015).

Recent numerical work attributes the seismicity depth distribution across the region solely to plate tectonic features such as the relatively low plate convergence rate, with negligible influence from tectonic inheritance (Dal Zilio et al., 2018). As lithospheric heterogeneity and inheritance is ubiquitous throughout the region, a critical discussion of the correlation between modelled lithospheric strength variations and a comprehensive dataset of regional seismicity could test to identify, whether lithospheric heterogeneity plays a significant role in shaping the observed localisation of seismicity throughout the Alps and their forelands. The fundamental question that will therefore be addressed within this work is, 'How does lithospheric structure relate to deformation?'.

In the following introductory section, the state of the art knowledge prior to the initiation of this project will be highlighted, regarding how other works have attempted to tackle this question previously, along with a comprehensive geological history of the region. The contribution of more recent works will be examined later in the Discussion section.

1.1. Lithospheric Structure

One of the first hurdles in explaining seismicity distribution within the Alpine orogen and its forelands, is to accurately constrain the present-day physical state of the entire crust-mantle system. Due to the long and complex development of both the European Alps and their forelands, across numerous plates and orogens, lithospheric inheritance represents an important

feature throughout the region. Significant crustal heterogeneity of the European plate, constituting the northern foreland of the Alps, derives from the Carboniferous age Variscan orogeny (Franke, 2000). This resulted in large scale crustal differentiation, with terranes of contrasting physical properties juxtaposed, such as the Moldanubian and Saxothuringian terrains (Babuška and Plomerová, 1992; Freymark at al., 2017), and the assemblages of uplifted crystalline basement presently exposed in the Vosges, Black Forest and Bohemian massifs.

Within the Alpine crust of the orogen proper, lithospheric heterogeneity results from the Alpine orogeny, which initiated in the Cretaceous and continues to the present-day as a consequence of the collision of the Adriatic plate with the European plate (Handy et al., 2010). Mantle reorganisation occurring as a result of the orogeny influence the shallow geology of the region, with anomalously high crustal densities present in the Western Alps, at the Ivrea Zone and along its sub-surface continuation South to the Ligurian Sea. There, as a result of a South-East dipping mantle wedge, mantle and lower crustal rocks are present at upper crustal depths (Zingg et al., 1990) and even at the surface (Pistone et al., 2017 and therein).

Traditionally, the Alpine crust has been interpreted as distinct domains according to their plate provenance and observed physical properties such as petrology and metamorphic/tectono-thermal characteristics. This resulted in the Austro-Alpine and Southern nappes in the Eastern Alps being classified as Adriatic derived, whilst in the Western Alps, the Helvetic nappes are interpreted as European derived and the Penninic nappes as distal margin units and slivers of oceanic crust (Schmid et al., 1989). Although the Iberian plate influenced the development of the orogen to a much lesser extent, the Briançonnais crustal block that lies within the Penninic nappes of the Western Alps derives from it (Frisch, 1979). Different interpretations exist on the plate provenance of some features however, with more recent works using plate reconstruction models reinterpreting some features such as the Tauern Window from Penninic origin to European plate origin (Schmid et al., 2004). The present-day boundary of the European and Adriatic derived crust within the Alps broadly occurs at the surface along the East-West running Periadriatic Lineament, offset 100km in a North-East orientation in the Central Alps by the Giudicarie fold-and-thrust belt (Castellarin et al. 2006, Pomella et al. 2010).

Previous published interpretations of crustal features within the orogen have been primarily based upon 2D seismic sections (e.g Brückl et al., 2007), tending to result in overly simplistic models. However, due to the long and complicated development of both the European Alps and their forelands, with crust and mantle derived from multiple plates, across multiple orogens, that has resulted in significant lateral differences in crustal structure, even at

distances of ~15 km in the Alps (Hetényi et al. 2018a), the need remains for more integrative models that do not neglect inherent lithospheric heterogeneity in 3D.

Studies that have integrated multiple geo-scientific datasets to create 3D models of the region, have either included the Alps as part of a much larger study area (e.g. Tesauro et al., 2008), without dividing the model into distinct regions of differing physical properties, and those do represent lithospheric heterogeneity are focussed on smaller sub-sections of the region (Ebbing, 2002; Ebbing et al., 2006). Furthermore, the current state of the art regional Moho map (Spada et al. 2013) features gaps, therefore significant work is required to generate a complete 3D structural model of the Alpine lithospheric structure that respects all geoscientific observations within the region, before debates about how Alpine lithospheric structure relates to the present-day seismicity distribution can proceed.

Recent seismic images by Zhao et al. (2015) interpret continuing plate convergence in the region as driving the southward subduction of the European plate beneath the Adriatic plate in the Western Alps. However, in the Eastern Alps (east of the Giudicarie Fault) some seismic studies show a southward-dipping European Moho (Lüschen et al. 2006, Bleibinhaus & Gebrande 2006) that underlies the Adriatic Moho (Kummerow et al. 2004, Brückl et al. 2007), whilst others show the slab in the Eastern Alps as steeply to moderately inclined to the north (e.g Lippitsch et al. 2003; Mitterbauer et al. 2011). Switches in subduction polarity have also been proposed in the Alps: one in the Paleogene occurring at the transition of the Western Alps to the Apennines (Vignarolli et al. 2008, Molli et al. 2010) and the other in the Miocene at the transition of the Western and Eastern Alps (Lippitsch et al. 2003, Kissling et al. 2006). Controversy also persists over whether the slab anomaly beneath the Eastern Alps is part of the Adriatic or European plate (Mitterbauer et al. 2011, Handy et al. 2014) and a recent Moho map of this area (Spada et al. 2013) is not able to fully resolve the Moho depth in the region, instead indicating a Moho gap beneath part of the Eastern Alps. Given these discrepancies, it is evident that whilst slabs are known to be present throughout the region, a consistent model of their geometry or polarity is not available for the study area at present, a view recently backed up by a review of available literature from Kästle et al. (2019).

The foreland basins related to the orogen, forming contiguously with orogenesis (initiating in the Cretaceous) as a result of plate flexure, are the Po Basin and Veneto-Friuli Plain of the southern foreland and the Molasse Basin of the northern foreland. Also in the northern foreland, the Upper Rhine Graben formed as part of the European Cenozoic Rift System in the Eocene (Dèzes at el., 2004). Changes in surface uplift rate both laterally across the orogen and

through time can be identified through differential deposition rates in the foreland basins (e.g. Sinclair 1997).

1.2 Regional Dynamics and Deformation

In order to understand how lithospheric structure relates to seismicity patters, the regional dynamics must first be considered, so that their influence on seismicity can be identified. Different styles of deformation are apparent along the European-Adriatic plate boundary, from ongoing indentation in the Eastern Alps (Scharf et al. 2013; Restivo et al., 2016) to post-collisional extension and isostatic uplift in the Central and Western Alps (Sue & Tricart 2003). Geodetic measurements indicate that the rigid (i.e. mechanically stiff) Adriatic plate is currently rotating counterclockwise and indenting the Eastern Alps at ~2 mm/yr (Vrabec and Fodor, 2006; Vrabec et al. 2006; D'Agostino et al. 2008; Serpelloni et al., 2016), whereas in the Western Alps, the convergence rate is lower at ≤ 1mm/yr (Nocquet & Calais 2004, Tesauro et al. 2005).

Higher surface uplift rates than erosion rates in the Eastern Alps (Norton et al. 2011) contrast to the Central and Western Alps where the values are largely the same (Kahle et al. 1997; Wittmann et al. 2007). This pattern is often explained through the occurrence of two slab rupturing events: an Oligo-Miocene event in the Eastern and Central Alps (von Blanckenburg & Davies 1995) and a younger, possibly Plio-Pleistocene event in the Western Alps (Kissling et al. 2006, Fox et al. 2015). Both events appear to coincide with increased deposition rates in the foreland Molasse Basin (Sinclair 1997; Schlunegger & Willet 1999, Kuhlemann et al. 2002, Spiegel et al. 2000, 2002). However, the relative impact of glacial isostatic adjustment versus tectonic and mantle dynamic processes as causes of the observed present-day kinematic state of the Alpine region is still debated (e.g. Norton and Hampel, 2010; Chéry et al., 2016; Mey et al., 2017; Sternai et al., 2019). Nevertheless, some indications from the present-day uplift rates suggest that the seismicity in the eastern Alpine domain could be instead related to still ongoing viscous relaxation from the waning of the last ice cap.

Whilst some seismicity within the Alps corresponds to plate dynamics, such as at the convergence of the European and Adriatic plates in North-East Italy (Chiarabba et al., 2005; Restivo et al., 2016), regional seismicity is largely characterised by diffuse, shallow seismicity that does not necessarily follow geologically mapped faults or plate boundaries (e.g. Deich-

mann, 1992). Whereas the domain of highest convergence at the Alps-Dinarides junction indeed correlates with high rates of seismicity, such as the 1976 Mw 6.5 Friuli earthquake, destructive earthquakes have also affected areas where long-term convergence rates are low, for example, in the crustal root of the Central Alps in southern Switzerland (Fäh et al., 2011).

Numerous large historic seismic events (Fäh et al., 2011; Stucchi et al., 2012; Grünthal et al., 2013), such as the Magnitude 6.6 Basel earthquake in 1356 AD (Ustaszewski & Schmid, 2007) and the 1348 Villach earthquake (Reinecker & Lenhardt 1999), lie substantially intraplate in areas of the forelands with low amounts of horizontal surface strain (Sánchez et al., 2018). These observations suggest that factors other than only convergence rate, such as the stress state and crustal rheology of the region, affect earthquake activity. As with in the Alps, foreland seismicity generally occurs within the upper crust of the region, with a largely aseismic lower crust, however observations do show sporadic seismicity occurring in deeper layers in both the northern and southern forelands (Bonjer 1997; Chiarabba et al., 2005).

1.3 Physical Properties

Observations on the spread of seismicity across the region already suggest that more than just the dynamics of plate tectonics play a role in localisation, therefore the need also remains for an increased understanding of other factors that contribute to the localisation of seismicity within the lithosphere, such as the thermal field. As with structural models, previously published lithospheric thermal models that cover the entirety of the Alps and their forelands (Tesauro et al., 2009; Limberger et al., 2018) have largely not resolved the vertical and lateral heterogeneities observed mostly in the crustal domains sufficiently well to allow a quantitative assessment of their effects on the resulting temperature distribution. As the thermal field exerts a first order control on rock strength (e.g. Hyndman et al., 1995; Emmerson and McKenzie, 2007), principally via thermally activated creep deformation, it also plays a crucial role in controlling the spatial distribution of seismicity within a lithospheric plate, by influencing the distribution at depth of the brittle-ductile transition zone. Therefore, the effect that different crustal blocks with different thermal properties can have on seismicity localisation should not be neglected, further indicating the need for a well constrained regional model. Thermal models that do represent differentiated lithospheric layers and a heterogeneous crust have been published for the Upper Rhine Graben (Freymark et al., 2017) and the Molasse Basin

(Przybycin et al., 2015), however these only cover specific subdomains of the area under investigation.

Furthermore, despite its relevance in the current ongoing scientific debate, the cross-correlation between monitored seismicity and its localisation in space with respect to the long-term stress state of the whole lithosphere is also still lacking. As such, the generation of rheological models would also prove highly beneficial in addressing the regional localisation of seismicity. Previous lithospheric scale rheological models of the Alpine region, mainly rely on 2D sections across the Alpine chain such as the EGT (Okaya et al., 1996) and Transalp (Willingshofer and Cloetingh, 2003) profiles. Relatively few models exist that try to compute lithospheric strength variations across the entire orogen (e.g. Marotta and Splendore, 2014; Tesauro et al., 2009).

The need therefore remains for a fully 3D integrated modelling approach, utilising multiple geophysical techniques, that validates results with external observations, in order to fully understand how seismicity relates to lithospheric heterogeneity in the region, both structurally and in regards to thermal and rheological properties. The question therefore posed is, whether an integration of modelling techniques such as gravity, thermal and rheological models are able to shed light onto the localisation of deformation and seismicity in the region, such as why the upper crust and foreland of the Alps are seismic, whereas the lower crust and mantle lithosphere, including slabs in the eastern part of the Southern Alps where Adria-Europe convergence is still active, are largely aseismic?

1.4 Workflow

Here, a 3D structural and density model of the lithosphere of the Alps and their respective forelands, derived from integrating numerous geoscientific datasets, is adjusted to match the observed gravity field and available deep seismic surveys. Therefore, the generation of a 3D lithospheric scale, gravity constrained, structural model of the Alps and their forelands at an appropriate resolution is used to more accurately describe heterogeneity in the region by seeing how crustal blocks of different provenance are different structurally, in thickness and density. The possibility also remains to test whether the location, geometry or polarity of plates and subduction interfaces in the region are able to be constrained using current state of the art gravity modelling techniques.

In order to further assess how the present-day deformation within the Alpine region is related to the 3D thermal field, we have developed the first 3D steady state lithosphere-scale thermal field of the Alps and their forelands that takes into account the different thermal properties required to replicate the heterogeneous nature of the crust. This was carried out using the same model geometry constrained by gravity modelling, with thermal properties assigned based on seismic observations. The model is validated using a compiled dataset of wellbore temperatures from across the region. By carrying out a global sensitivity study on the generated thermal model, we additionally quantify the bias introduced in our models by focusing analyses purely on measurements. This is made possible through the construction of suitable surrogate models via the reduced basis method, allowing for the global sensitivity analysis to be carried out across the full parameter space, whilst preserving the physics at play.

The creation of measurement-constrained regional 3D models of lithospheric density distribution and thermal field then facilitate the generation of an observation-based rheological model of the Alps and their forelands. Long term lithospheric strength and viscosity is calculated for the entire orogen and its forelands. With multiple comparable geophysical models of the region, that each conform to additional observations, results can then be compared to a comprehensive catalogue of seismicity in order to illuminate driving factors for localisation. This also presents the benefit of answering other questions on the present-day state of the orogen, such as whether decoupling occurs within the orogenic crust or along the crust-mantle boundary beneath the orogen?.

Chapter 2. Density distribution across the Alpine lithosphere constrained by 3D gravity modelling and relation to seismicity and deformation

2.1. Introduction

The Alps are one of the best studied mountain ranges in the world, yet significant unknowns remain regarding their crustal structure and links that may exist between the localisation of deformation and seismicity in the region and crustal heterogeneity. Significant amounts of seismicity and deformation correspond to plate dynamics, such as at the convergence of the European and Adriatic plates in North-East Italy (Restivo et al., 2016) where the Adriatic plate is observed to act as a rigid indenter, moving northwards and rotating counter-clockwise against the weaker European plate (Nocquet and Calais, 2004; Vrabec and Fodor, 2006; Serpelloni et al., 2016). However, numerous large historic seismic events (Fäh et al., 2011; Stucchi et al., 2012; Grünthal et al., 2013), such as the Magnitude 6.6 Basel earthquake in 1356 AD, lie substantially intra-plate in areas with low amounts of horizontal surface strain (Sánchez et al., 2018) suggesting that possible inherited features within the crust are also significant factors to their localisation.

Crustal heterogeneities in the European plate, constituting the northern foreland of the Alps, principally derive from different terranes that collided during the Carboniferous age Variscan orogeny (Franke, 2000). Collision during orogenesis resulted in the juxtaposition of crustal domains with differing properties next to one another, such as Moldanubia and Saxothuringia, (Babuška and Plomerová, 1992; Freymark at al., 2016) and also resulted in the creation of the Vosges, Black Forest and Bohemian massifs. The locations of all relevant tectonic features within the region can be found in Figure 2.1a.

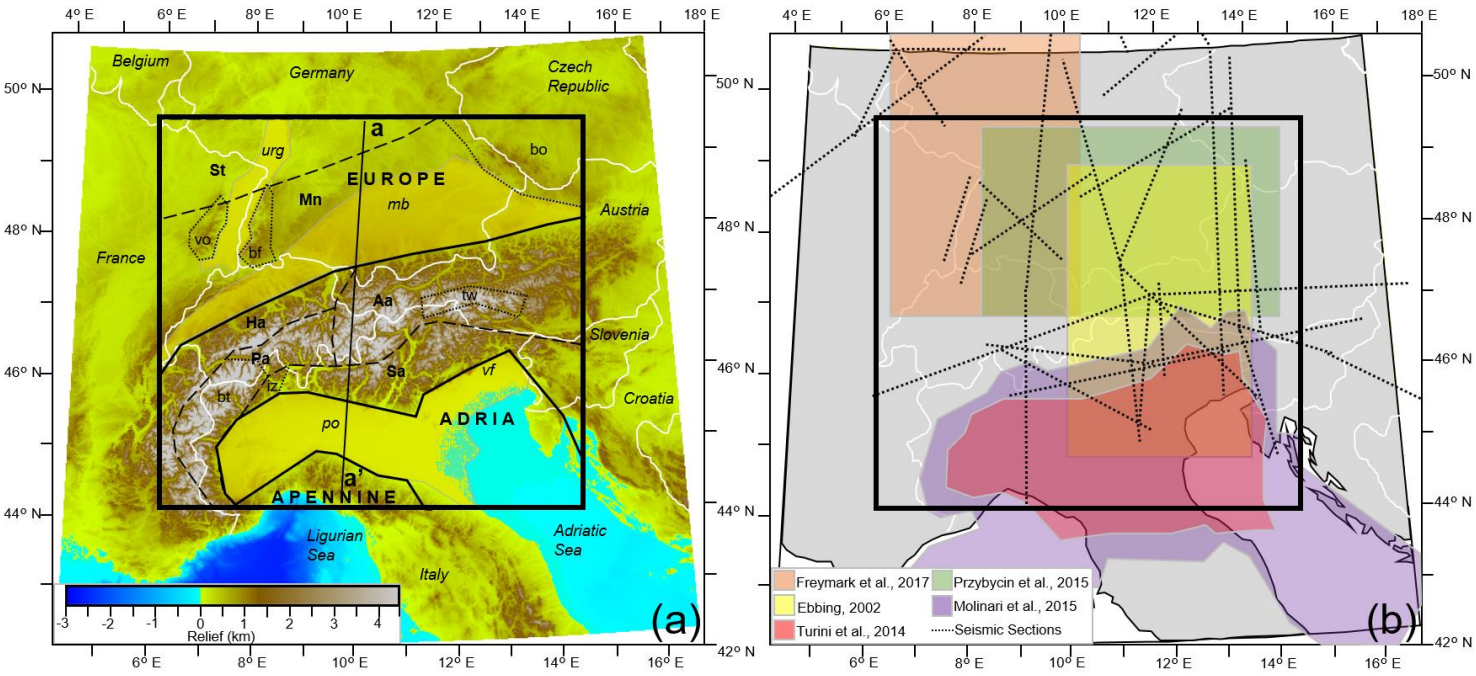

Figure 2.1. a) *Topography and bathymetry from Etopo 1 (Amante and Eakins, 2009) shown across the Alpine region with the key tectonic features overlain. Study area is indicated with a black box. a-a' represents the cross section in Figure 2.3. Solid black lines demark the boundaries of the non-deformed European and Adriatic Plates, the location of the Apennine plate is also marked. Dashed black lines indicate different geological domains (St – Saxothuringian; Mn – Moldanubian; Aa – Austro-Alpine Zone; Ha – Helvetic Alps; Pa – Penninic Alps; Sa – Southern Alps). Dotted black lines indicate the extent of other tectonic features within these domains (bo – Bohemian Massif; vo – Vosges Massif; bf – Black Forest Massif; tw – Tauern Window; bt – Briançonnais Terrane; iz – Ivrea Zone). Yellow areas bound by a solid grey line indicate the extent of sedimentary basins (urg – Upper Rhine Graben; mb – Molasse Basin; po – Po Basin).* ***b)*** *Input data source extents: Upper Rhine Graben gravity constrained model (Freymark et al., 2017); Molasse Basin gravity constrained model (Przybycin et al., 2015); TRANSALP gravity constrained model (Ebbing, 2002); Po Basin seismically constrained models (Turini et al., 2014; Molinari et al., 2015); and Seismic Sections (IESG, 1978; IESG & ETH Zuerich, 1981; Strößenreuther, 1982; Mechie et al., 1983; Zucca, 1984; Gajewski & Prodehl, 1985; Deichmann et al., 1986; Gajewski et al., 1987; Gajewski & Prodehl, 1987; Yan and Mechie, 1989; Zeis et al., 1990; Aichroth et al., 1992; Guterch et al., 1994; Ye et al., 1995; Scarascia and Cassinis, 1997; Enderle et al., 1998; Bleibinhaus & Gebrande, 2006; Brückl et al., 2007; Hetényi et al., 2018).*

As a consequence of the collision of the Adriatic plate with the European plate from the Cretaceous until the present (Handy et al., 2010), heterogeneity within the Alpine orogen is also very pronounced, however different interpretations exist on the plate provenance of some features. Traditionally, the Alps have been split into distinct zones according to their plate of origin and metamorphic history, such as the Adriatic derived Austro-Alpine and Southern Alps, the European derived Helvetic Alps and the Penninic zone representing distal

margin units and slivers of oceanic crust (Schmid et al., 1989). The Briançonnais crustal block that lies within the Penninic zone derives from the Iberian plate (Frisch, 1979). More recent works examining the plate provenance of Alpine zones have reinterpreted some features such as the Tauern Window from Penninic origin to European plate origin (Schmid et al., 2004).

Density distribution throughout the lithosphere of the region is also affected by mantle features and sedimentary depocentres. The three main depocentres within the region are the Po Basin of the southern foreland, the Molasse Basin of the northern foreland and the Upper Rhine Graben, also within the northern foreland, that formed as part of the European Cenozoic Rift System in the Eocene (Dèzes at el., 2004). Anomalously high densities within the crust are present in the Western Alps, in the Ivrea Zone and along its sub-surface continuation to the South to the Ligurian Sea, as a result of a South East dipping mantle wedge, where mantle and lower crustal rocks are present at upper crustal depths (Zingg et al., 1990) and even at the surface (Pistone et al., 2017 and therein).

Previous published interpretations of crustal features within the orogen have been primarily based upon 2D seismic sections (e.g Brückl et al., 2007), tending to result in simple models. However, lateral differences in crustal structure have been demonstrated, even at short wavelength, for example through the deployment of parallel seismological profiles, spaced 15 km apart across the Eastern Alps (Hetényi et al. 2018a), indicating the need for more complex models. Studies that have integrated multiple geo-scientific datasets to create 3D models of the region, have either focussed on smaller sub-sections of the Alps (Ebbing, 2002; Ebbing et al., 2006) or included the Alps as part of a much larger study area (E.g. Tesauro et al., 2008). Therefore, the generation of a 3D, crustal scale, gravity constrained, structural model of the Alps and their forelands at an appropriate resolution could be used to more accurately describe crustal heterogeneity in the region. The generation of such an Alpine-wide specific model is made possible by the existence of seismological results from numerous published deep seismic surveys (e.g. Zuerich, 1981; Gajewski & Prodehl, 1985; Yan and Mechie, 1989; Ye et al., 1995; Brückl et al., 2007) that have been completed throughout the region, and available high quality global gravity field models (e.g. Förste et al., 2014). Within this current work, such data is integrated in a common frame to give insights into the distribution of densities within the crust as constrained by 3D gravity modelling across the vast majority of the Alpine region and its forelands for the first time, so that questions about the relationship between the distribution of densities within the crust and seismicity and deformation patterns can be addressed.

2.2. Input Data

Existing geological and geophysical observations from previous published works about the Alps and their respective forelands were used as constraints for the generation of the 3D structural model. Topography and bathymetry were utilised unaltered from ETOPO1 (Amante and Eakins, 2009), as shown in Figure 2.1a. The data integrated to constrain sub-surface lithospheric features are shown in Figure 2.1b and include: regional scale, gravitationally and seismically constrained models of the TRANSALP study area (Ebbing, 2002), the Molasse Basin (Przybycin et al., 2014) and the Upper Rhine Graben (Freymark et al., 2017); regional scale, seismically constrained models of the Po Basin, such as MAMBo (Turrini at al., 2014; Molinari et al., 2015); and seismic reflection/conversion depths and their associated P wave velocity from projects such as ALP'75, EGT'86, TRANSALP, ALP 2002 and EASI (IESG, 1978; IESG & ETH Zuerich, 1981; Strößenreuther, 1982; Mechie et al., 1985; Zucca, 1984; Gajewski & Prodehl, 1985; Deichmann et al., 1986; Gajewski et al., 1987; Gajewski & Prodehl, 1987; Yan and Mechie, 1989; Zeis et al., 1990; Aichroth et al., 1992; Guterch et al., 1994; Ye et al., 1995; Scarascia and Cassinis, 1997; Enderle et al., 1998; Bleibinhaus & Gebrande, 2006; Brückl et al., 2007; Hetényi et al., 2018a). The Lithosphere-Asthenosphere Boundary (LAB) was utilised unaltered from Geissler (2010), which was obtained by S receiver functions of teleseismic events.

Constraining data coverage for most sub-surface lithospheric features was sufficient; however, thicknesses of unconsolidated sediments were not available across the full modelled region. In regions of less dense data coverage, continental scale, seismically constrained, integrative best fit models, EuCRUST-07 and EPcrust (Tesauro et al., 2008; Molinari and Morelli, 2011) were also used. Both models provided complete coverage of major structural interfaces and P wave velocities over the whole modelled area at a coarse resolution. Detailed values of unconsolidated sediment thicknesses were only available for the Upper Rhine Graben, the Molasse Basin and the Po Basin, as the seismic sections utilised lacked the resolution for shallower features and the continental scale models did not differentiate between sedimentary strata.

The free-air anomaly used was calculated from the global gravity model EIGEN-6C4 (Förste et al., 2014), at a fixed height of 6 km above the datum (Figure 2.2, further referred to as observed gravity). As the gravity data source is a hybrid, terrestrial and satellite dataset, the potential exists for it to be lacking some of the short wavelength response that a fully terrestrial dataset would possess. The fixed height of 6 km was utilised to account for this, so that the

vertical component of the gravity response from the generated regional structural model (further referred to as calculated gravity) and observed gravity can be directly compared during the gravity modelling process.

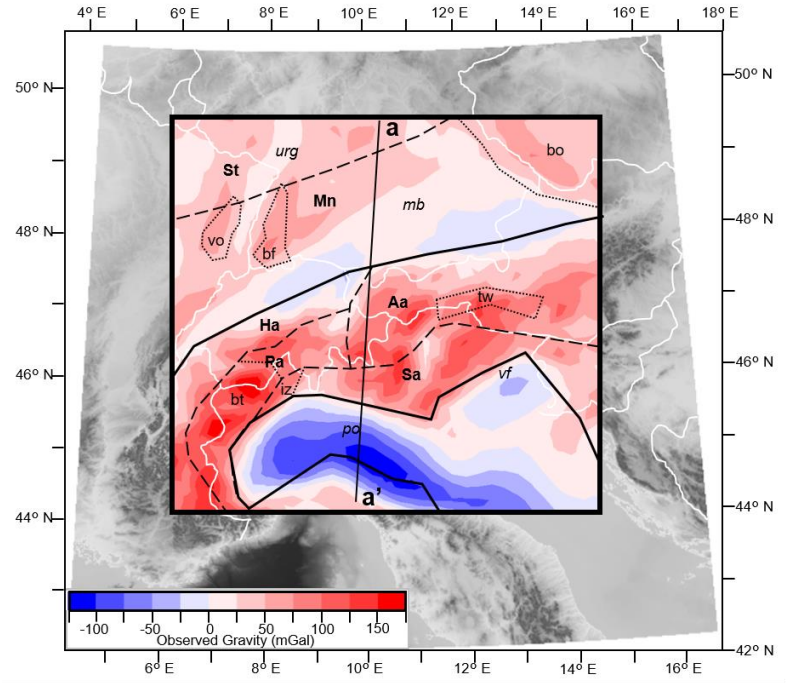

Figure 2.2. *Observed gravity of the region. Values calculated from a spherical approximation at 6km above datum of EIGEN-6C4 global gravity model (Förste et al., 2014). a-a' represents the cross section in Figure 2.3. Locations of key tectonic features are overlain (definitions shown in Figure. 2.1 caption). N.B. Whilst we refer to the EIGEN-6C4 data as gravity observations, it is in actuality a highly sophisticated potential field model.*

2.3. Method

Data from numerous existing geoscientific datasets (see Input Data section) were integrated to create a gravity constrained, 3D, structural and density model of the lithosphere of the Alps and their respective forelands. The study area of this work, indicated in both Figures 2.1a and b, focuses on a region of 660 km x 620 km where the highest density of constraining data coverage was compiled. The vast majority of the Alps and their forelands are included, with the Central and Eastern Alps and the northern foreland being the best covered regions.

The software package Petrel (Schlumberger, 1998) was used for the creation and visualisation of the modelled surfaces in 3D, representing the key structural and density contrasts within the region. These modelled surfaces were: 1. top water; 2. top unconsolidated sediments; 3. top consolidated sediments; 4. top upper crust; 5. top lower crust; 6. top

lithospheric mantle; 7. top asthenospheric mantle. All surfaces were generated with a grid resolution of 20 km x 20 km using Petrel's convergent interpolation algorithm.

The above mentioned model layers were generated by correlation and integration between data sources, with the exception of the following: 1. The water layer was generated from cropping ETOPO1 to 0 m a.s.l. No freshwater bodies were added as they are too small to be of impact at the model resolution utilised; 2. The top unconsolidated sediment surface used in the modelling corresponds to topography and bathymetry, which is plotted in Figure 2.1a; 3. As a result of unconsolidated sediment thicknesses from the data sources only being present in the Upper Rhine Graben, the Molasse Basin and the Po Basin, outside of these regions a thickness of 0 was used. This was deemed acceptable because unconsolidated sediment thicknesses are not large enough as to be of impact at the model resolution, outside these regions; 4. The LAB was used unedited from the data source, in spite of its low resolution as it does not represent a significant density contrast. Alpine nappe stacks were included within the consolidated sediments layer of the model.

During correlation and integration, a hierarchy of data source types was used and in the case of contradiction between the different data sources, those of the highest hierarchy were accepted. The hierarchy was derived from the quality, resolution and consistency of data sources and was as follows: 1. regional scale, gravitationally and seismically constrained models; 2. regional scale, seismically constrained models; 3. individual seismic reflection surfaces and interpreted sections; 4. continental scale, seismically constrained, integrative best fit models.

No subduction interfaces were modelled, as multiple studies within the region have shown that the effect of different subduction polarities as well as the presence or lack of subducting plates is small. Previous 2D gravity modelling across the TRANSALP profile has demonstrated that the differences in gravity response between a model of both different subduction polarities and a model setup with no subducted crust were negligible (Deutsch, 2014). Lowe (2019) showed that the contribution of subducting slabs in the region to the gravity field is relatively small, in the range of 30 mGal).

The 3D gravity modelling software IGMAS+ (Schmidt et al., 2010) was used, which operates by creating triangulated meshes between points on input surfaces and vertical parallel planes, around a body of homogenous density, to calculate their volumetric contribution to the gravity response. Gravity in the model was calculated at 6 km above the datum to be concurrent with the observed gravity. In this way, the short wavelength response of the calculated gravity was not overestimated as mentioned before. The top of the model was also set to a height of 6

km with a density of 0 used to represent the column of air between it and topography. To account for the edge effect of the gravity field, the model was extended by ~50% (330 km) in all horizontal directions of the studied area using the surfaces from EuCrust-07 (Tesauro et al., 2008).

The free-air gravity response was used because this work is focussed on the crustal composition of the Alpine region and considering that up to 4.8 km of crust lies above sea level within the modelled area, removing this from the gravity signal was deemed unacceptable. Additionally, the complex geological setting of the Alps implies that the removal of Alpine topography as a Bouguer slab of homogenous density would potentially introduce errors.

The process of gravity modelling involved the modification of an initial 3D structural model, comprising surface heights and densities, such that through multiple iterations the resulting model produced a gravity field similar to the observed one. Best practice of such an iterative process allows only one input parameter, density or surface heights, to be altered. Here, the surfaces generated as part of the integration work were not modified during the gravity modelling process as they were better constrained than the densities, leaving only density as a free parameter. However, this approach can't reduce the ambiguity in the interpretation of potential field modelling.

For the calculation of the densities used in the initial structural model, P wave velocities from seismic data sources were converted using the experimentally derived empirical relationship detailed in Brocher (2005). In the absence of seismic data, P wave velocities from the continental scale models listed in the Input Data section were used to supplement, giving coverage over the entire study area. Densities of 1025 kg m^{-3} and 3320 kg m^{-3} were assigned to the water layer and the asthenospheric mantle, respectively.

The densities derived from the P wave velocity conversions were then used in conjunction with densities from the input regional scale, gravitationally and seismically constrained models, to split the layers of the generated model laterally into domains of different density, to reflect the heterogeneous nature of the crust within the region. During the generation of the model, preference was given to the resolution of major density contrasts. Consequently, units of known differing lithology, age and/or provenance were grouped together, when they appeared to have a similar density to best fit the gravity in the region. An overview of the mean densities of each modelled body, derived from seismic P wave velocities, is presented in Table 2.1.

Unit	Mean Density indicated by P Wave Velocities (Kg/m3)	Density Used in Final Model (Kg/m3)
1. Unconsolidated Sediments	2530	2450
2. Unconsolidated Sediments – East Molasse	2540	2470
3. Unconsolidated Sediments - Po	2610	2470
4. Consolidated Sediments	2680	2670
5. Consolidated Sediments – East Molasse	2670	2680
6. Consolidated Sediments - Po	2700	2700
7. Upper Crust – Saxothuringia	2690	2670
8. Upper Crust – Moldanubia	2710	2700
9. Upper Crust – Bohemia	2720	2740
10. Upper Crust – Vosges and Black Forest	2690	2660
11. Upper Crust – East Molasse	2720	2720
12. Upper Crust – East Alps	2740	2740
13. Upper Crust – West Alps	2740	2670
14. Upper Crust – Po	2740	2730
15. Upper Crust – North East Adria	2780	2660
16. Upper Crust – Ivrea	-	2790
17. Upper Crust – East Adria	2780	2700
18. Upper Crust – Apennine	2770	2720
19. Lower Crust – Saxothuringia	2900	2920
20. Lower Crust – Europe	2890	2800
21. Lower Crust – Alps	2880	2950
22. Lower Crust – Ivrea	-	3100
23. Lower Crust – Northern Adria	2990	2750
24. Lower Crust – East Adria	2950	3040
25. Lithospheric Mantle – Less Dense	3340	3305
26. Lithospheric Mantle – More Dense	3260	3335
Water	-	1025
Asthenospheric Mantle	-	3320

Table 2.1. *The density of each domain in the model calculated by converting from its mean P wave velocity using the empirical relationship detailed in Brocher (2005) and the density of all domains used in the final model of the region that best reproduce the indications of both the seismic data sources and the gravity field. Locations of each density domain can be found in Figure 2.4.*

To determine how well the structural model fits the gravity field in the region, the calculated gravity was subtracted from observed gravity during interactive modifications of the location of different domains within each layer and their densities, and the result (further referred to as residual anomaly) interrogated. No filtering for specific wavelengths was done during gravity modelling, with the full signal being used. No presumptions were made about which tectonic features would require domains of different density, with their location ultimately derived from the gravity modelling process.

In the case of anomalies in the residual gravity field, the depth of the source was estimated to be half the width of the anomaly wavelength and the density of the body lying at that depth was increased for a positive residual anomaly or decreased for a negative residual anomaly. Successive iterations of the model were then generated by modifying the distribution of densities within the model layers. This was repeated until a 3D structural density model of the region was obtained, that best reproduces the indications of both the seismic data sources and the gravity field.

2.4. Results

Figure 2.3 shows a North-South cross section through the generated model illustrating the thickness of all main structural layers, the density domains defined within them and the calculated and observed gravity of the section. The location of the cross section can be seen in Figure 2.1a and is also marked on all figures illustrating the setup of the model.

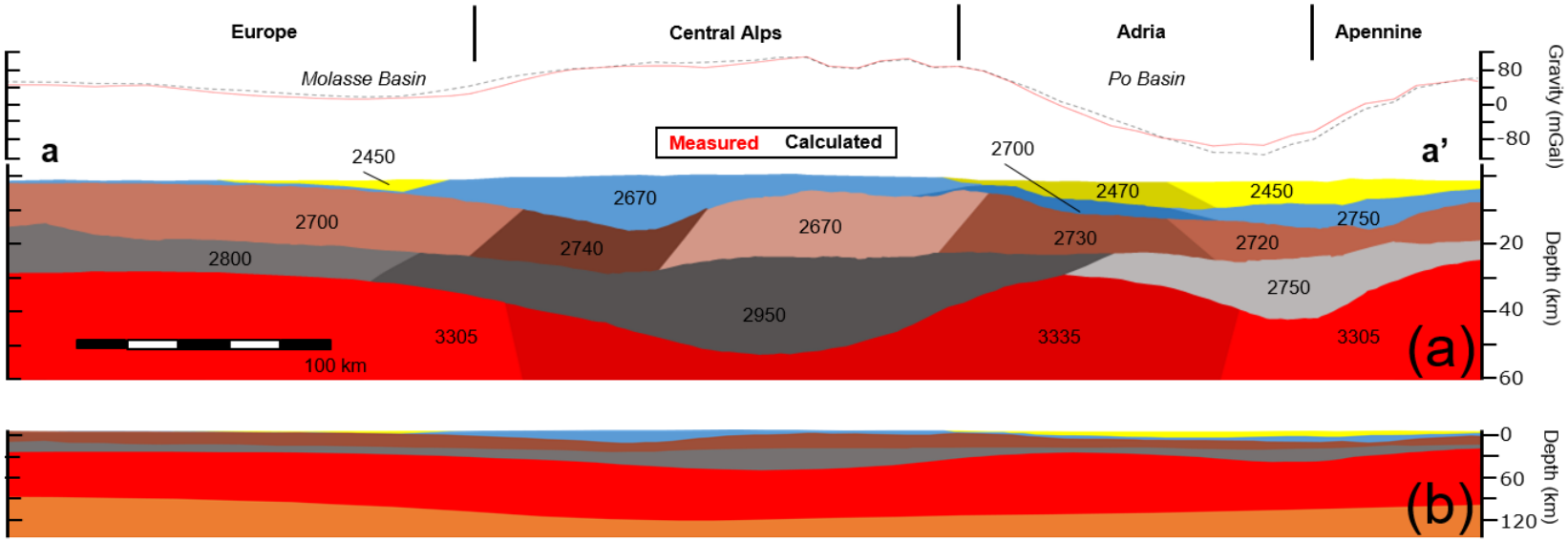

Figure 2.3. *Cross sections through generated model showing thickness of model layers. Location is marked in Figures 2.1.a, 2.2. and 2.4-6 as a-a'. 1a. Lithospheric mantle layer is shown in red, lower crust is shown in grey, upper crust is shown in brown, consolidated sediments are shown in blue and unconsolidated sediments are shown in yellow. In Figure 2.3.* ***a)*** *Density domains within each layer are shown as a change of shade and the density of each domain is labelled. On top, the observed and calculated gravity anomalies along the cross section are shown. Fig.* ***b)*** *is*

Our model indicates that more heterogeneity is required in the crust, than in other model layers, to replicate the gravity field and that significant differences exist between the crust of the European and Adriatic plates. Sedimentary thicknesses, both unconsolidated and consolidated, are thinner in the Molasse Basin than in the Po Basin and crustal densities and thicknesses also differ between the plates. Beneath the orogen itself, the result of incorporating all Alpine nappes within the consolidated sediment layer can be observed, with higher thicknesses beneath the central Alps. The whole crust is thickest below the central Alps and is compensated by higher thickness and density of the lower crust. The observed gravity along with the calculated gravity of the model can also be observed, showing a good fit.

Figure 2.4. shows the thicknesses of the layers of the generated model, which were created as a result of the correlation and integration work, with the areal extent of all density domains overlain on top. An overview of the final density of all the bodies composing the model required to fit the gravity field can be found in Table 2.1.

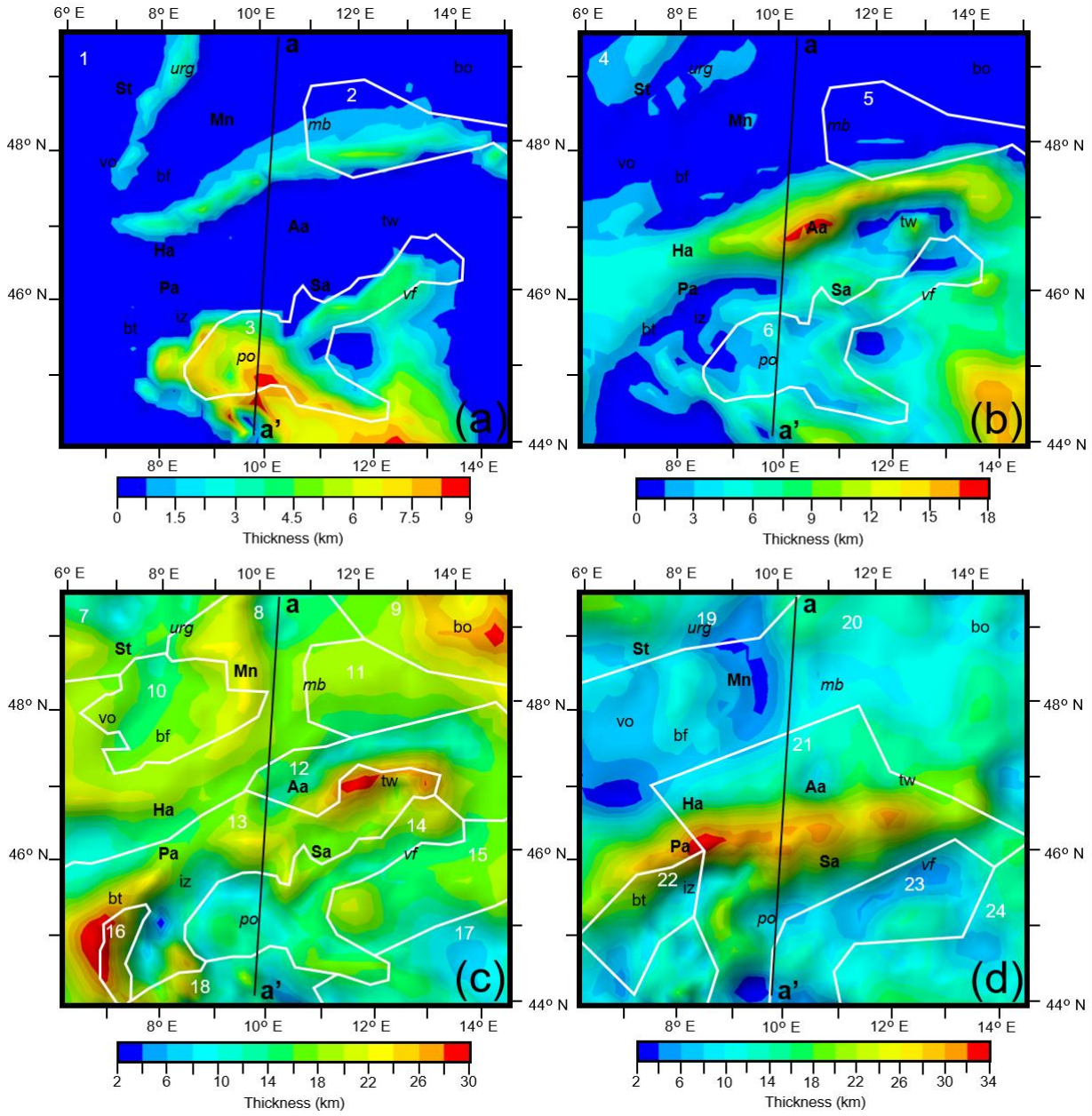

Figure 2.4. *Thickness of* ***a)*** *unconsolidated sediments,* ***b)*** *consolidated sediments,* ***c)*** *the upper crust and* ***d)*** *the lower crust across the modelled area. Density domains required during modelling within the layer are overlain in white, domain numbers are shown in white and correspond to Table 2.1. Locations of key tectonic features are overlain (abbreviations shown in Figure 2.1. caption).*

Both sedimentary layers shown in Figure 2.4. reflect trends across the region previously identified along the cross section presented in Figure 2.3., with thicker and denser sediments in the Po Basin than in the Molasse Basin, and large thicknesses of consolidated sediments in the central Alps (18 km) representing the Alpine nappe stacks. Maximum thicknesses of 9 km and 12 km were used in the Po Basin for unconsolidated and consolidated sediments respectively, whilst 6 km and 9 km were used in the Molasse Basin. Thicknesses of 3.75 km

unconsolidated sediments were used in the deepest part of the Upper Rhine Graben with consolidated sediment thicknesses of up to 3 km. In both of the sedimentary layers, separate density domains were necessary in the Eastern Molasse Basin (2470 kg m^{-3} and 2680 kg m^{-3}) and the Po Basin (2470 kg m^{-3} and 2700 kg m^{-3}) that were denser than the sediments in the rest of the region (2450 kg m^{-3} and 2670 kg m^{-3}).

The European upper crust (domains 7-11 in Figure 2.4.c and Table 2.1.) is thicker, but has a similar density on average (20 km and 2700 kg m^{-3}), compared to the Adriatic upper crust (12 km and 2700 kg m^{-3}, domains 14, 15 and 17 in Figure 2.4c and Table 2.1). The densities given for the European and Adriatic crusts are averages of the density domains that comprise them. The thickest regions of upper crust can be found around the Bohemian massif in the northern foreland and the Briançonnais Terrane and Tauern Window in the Alps reaching a thickness of up to 30 km, whilst thinned upper crust with thicknesses of only 4 km is found below the Adriatic Sea and the Ivrea Zone. Multiple density domains in the upper crust correspond to known tectonic features in the modelled region such as the Variscan domains of Saxothuringia (2670 kg m^{-3}) and Moldanubia (2700 kg m^{-3}), the massifs of Bohemia (2740 kg m^{-3}) and Vosges/Black Forest (2660 kg m^{-3}) that lie close enough together in the model to be grouped, the Briançonnais Terrane (2790 kg m^{-3}) and the Apennine belt (2720 kg m^{-3}). However, in the Alps and the Adriatic Sea the modelled density domain boundaries do not correspond to specific tectonic features. The Alps are divided roughly North East (2740 kg m^{-3}) to South West (2670 kg m^{-3}), being denser in the NE, while the Adriatic Sea is split roughly North (2660 kg m^{-3}) to South (2700 kg m^{-3}), being denser in the south.

The configuration of the European lower crust (domains 19 and 20 in Figure 2.4c and Table 2.1) is of similar thickness, but less dense on average (10 km and 2860 kg m^{-3}) than the Adriatic (10 km and 2910 kg m^{-3}; domains 21, 23 and 24 in Figure 2.4c and Table 2.1). The lower crustal Alpine root is thicker and denser (2950 kg m^{-3} and 34 km) than in the rest of the region. Density domains within the lower crust show less correspondence with known tectonic features than those in the upper crust. Of the domains in the lower crust only two correspond roughly to tectonic features, one to the Saxothuringian Variscan domain (2920 kg m^{-3}) and the other to the Briançonnais Terrane (3100 kg m^{-3}). A large region of similar density within the lower crust exists, mostly in the European Plate, covering an area including the Moldanubian Variscan domain, the Bohemian Massif and the Western and Eastern Alps (2800 kg m^{-3}). The central Alps and the Western Po Basin are also grouped as a region of similar density (2950 kg m^{-3}). As with the upper crust, the lower crust beneath the Adriatic Sea is split roughly North

(2750 kg m^{-3}) to South (3040 kg m^{-3}) with a denser domain in the south. Some lower crustal density domains in the European and Adriatic plates have been modelled as low as 2800 kg m^{-3} (domain 20 in Figure 2.4c and Table 2.1) and 2750 kg m^{-3} (domain 23 in Figure 2.4c and Table 2.1) respectively, and although necessary to fit the gravity anomaly, these values are similar to upper crustal density values. The other density domains in the lower crust of the region have values that would be expected for this depth level.

Figure 2.5 shows the depths of the Moho and LAB used in this work. The Moho is shallowest below the Ligurian Sea (20 km) but also shallow beneath the Ivrea Zone (22.5 km) and below the Upper Rhine Graben (25 km). It reaches its deepest point in the crustal root of the Alps at 55 km. The trends in Moho depth noted here correspond well to trends in the Moho map of Spada et al., (2013). However the minimum (Ivrea Zone: 12 km) and maximum (Alpine crustal root: 60 km) depths of the Spada et al., Moho are more extreme and likely represent more local values than those used in this work. Additionally, our integrated Moho does not contain large vertical steps (28 km in the Northern Apennines) between defined plate domains, such as in the Spada et al. (2013) Moho as these would create large density contrasts within the 3D model that would present severe difficulties when trying to fit the observed gravity in the region.

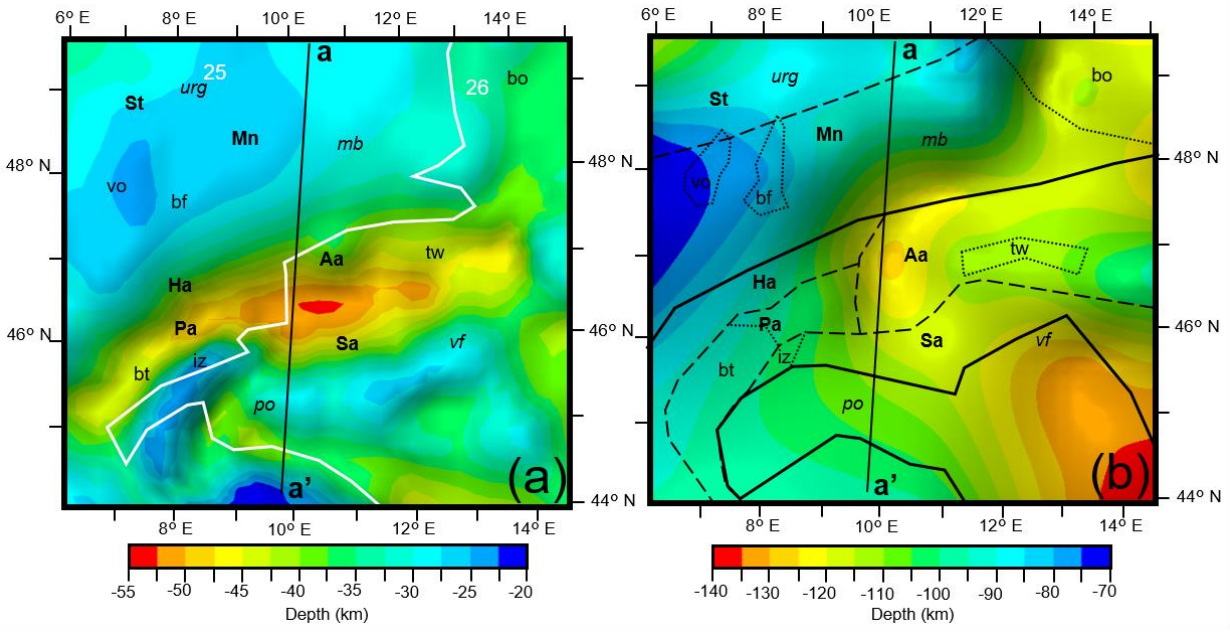

Figure 2.5. a) *Depth to the Moho across the modelled area. Density domains required during modelling within the lithospheric mantle are overlain in white, domain numbers are shown in white and correspond to Table 2.1.* ***b)*** *Depth to the LAB from Geissler et al (2010) across the modelled area. Locations of key tectonic features are overlain for both figures (definitions shown in Figure 2.1. caption).*

From the gravity modelling process it was found necessary to have variation in the density of the lithospheric mantle, and that the regions of different density correspond to different thicknesses of the lithosphere (Geissler et al., 2010). Broadly, the lithosphere is thinnest and least dense to the North-West of the region (70 km and 3305 kg m^{-3}) whilst being thickest and densest to the South-East (140 km and 3335 kg m^{-3}) below the Adriatic Sea. The shallowing of the LAB below the Alps could correspond to the boundary between the Austro-Alpine and Helvetic/Penninic Alps.

The observed gravity in the modelled region is visible in Figure 2.2, while the calculated gravity response is shown in Figure 2.6. The residual anomaly can be observed in Figure 2.6. demonstrating the good fit achieved by the generated structural model. Almost all of the modelled area reproduces the observed gravity to ± 25 mGal with the exception of a couple of isolated regions where the misfit between observed and calculated gravity slightly exceeds that value. As the polarity of both anomalies indicates less density is required to fit the gravity field, they correspond to Moho highs and their wavelength would suggest the top surface of the Moho as the source of the anomaly, the anomalies likely stem from isolated Moho depths that are slightly too shallow. As crustal densities were not the source of these anomalies and surface heights remained fixed during the modelling process, no changes were made to account for these anomalies so that a more representative density configuration of the regional crust could be calculated.

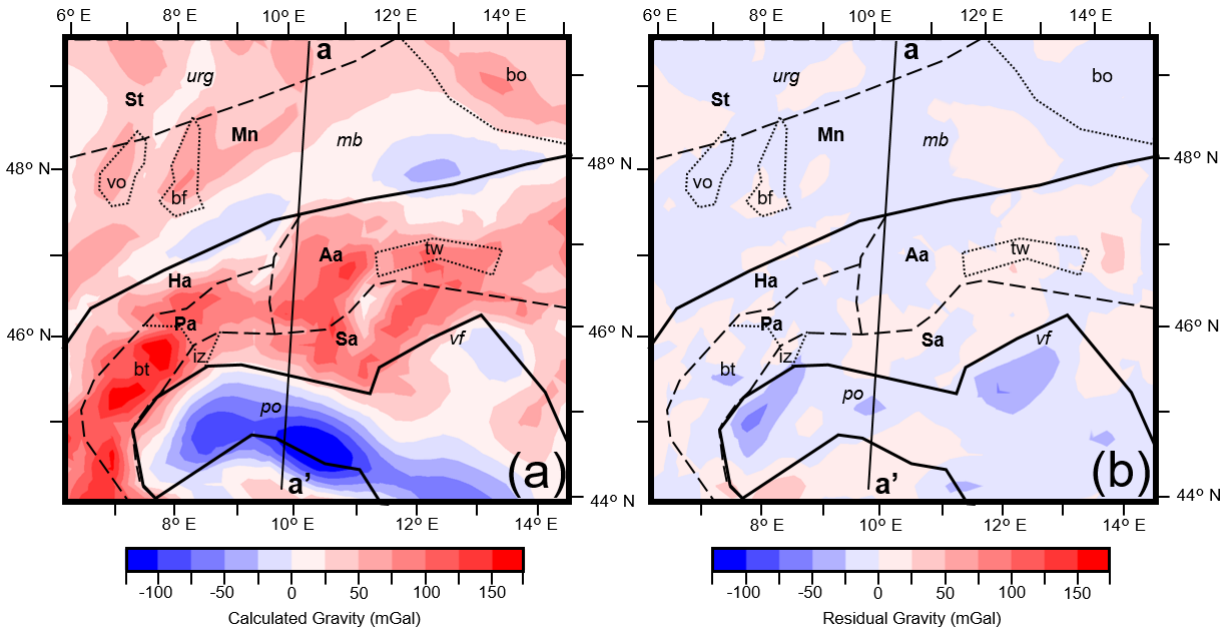

Figure 2.6. a) *Calculated gravity at 6 km above the datum resulting from the final structural and density model.* ***b)*** *Residual gravity (observed gravity - calculated gravity) of the best fit model. Locations of key tectonic features are overlain for both figures (definitions shown in Figure 2.1. caption).*

The thickness and average density of the modelled crust throughout the region are shown in Figure 2.7. The lateral variation in average density is obtained as a weighted average calculated from the thicknesses and densities of the upper crust and the lower crust at every point in the model. Overall the crust is thicker and less dense on average in the European plate (27.5 km and 2750 kg m^{-3}) compared to the Adriatic (22.5 km and 2850 kg m^{-3}). The thickest crust corresponds to the crustal root of the Central Alps (55 km). Areas of thinned crust are found below the sedimentary depocentres of the Po Basin and the Upper Rhine Graben, which can additionally be seen extending South and West of its surface location, however the crust does not appear significantly thinned beneath the Molasse Basin. Whilst the Adriatic crust is denser on average than the European crust, it has more extreme density variations within it, such as a modelled low density crust in the North of the Adriatic indenter that coincides with the Veneto-Friuli plain (2700 kg m^{-3}), immediately adjacent to much denser crust lying to the South below the Adriatic Sea (2900 kg m^{-3}).

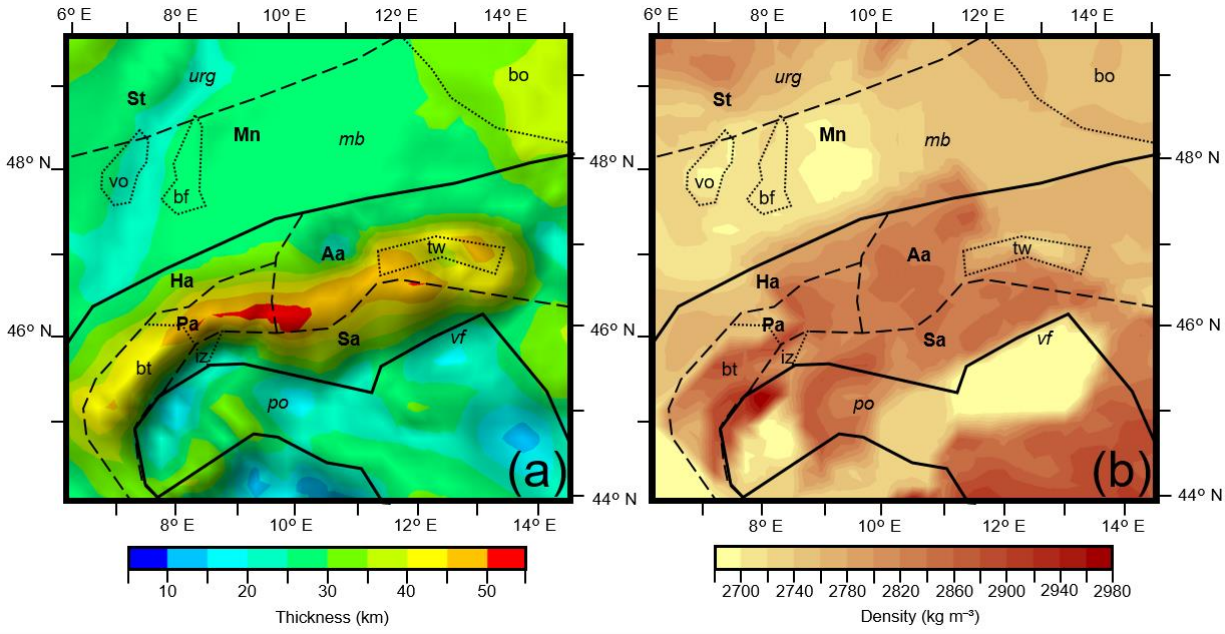

Figure 2.7. a) *Thickness and* ***b)*** *average density of the entire crust across the modelled area. Solid lines demark the boundaries of Alpine zones, the dotted black lines indicate the extent of the non-accreted Adriatic plate. Locations of key tectonic features are overlain (definitions shown in Figure 2.1. caption).*

Density contrasts within the crust correlate spatially with the locations of some Alpine zone boundaries as defined in the literature (Schmid et al., 1989; Schmid et al., 2004). The Briançonnais Terrane can be seen as a higher density block contrasting with the rest of the zones that surround it. The Southern Alps can also be identified as a dense block, with its borders to the Briançonnais Terrane and the Austro-Alpine zone clearly defined in the East of the modelled region. The Tauern Window can also be clearly identified as a relatively lower density zone within the Austro-Alpine zone.

Figure 2.8 also shows the thickness and average density of the modelled crust, but additionally shows their correspondence with large earthquakes and ongoing surface deformation. The thickness of the crust is overlain with present day vertical displacement rates (Sternai et al., 2019) in Figure 2.8a and the average density of the crust is overlain with present day horizontal surface strain distribution (Sánchez et al., 2018), earthquakes of a moment magnitude of 6 or larger (Fäh et al., 2011; Stucchi et al., 2012; Grünthal et al., 2013) and the location of modelled upper crust domain boundaries in Figure 2.8b, so that relationships between crustal features and recent deformation and seismicity can be interrogated.

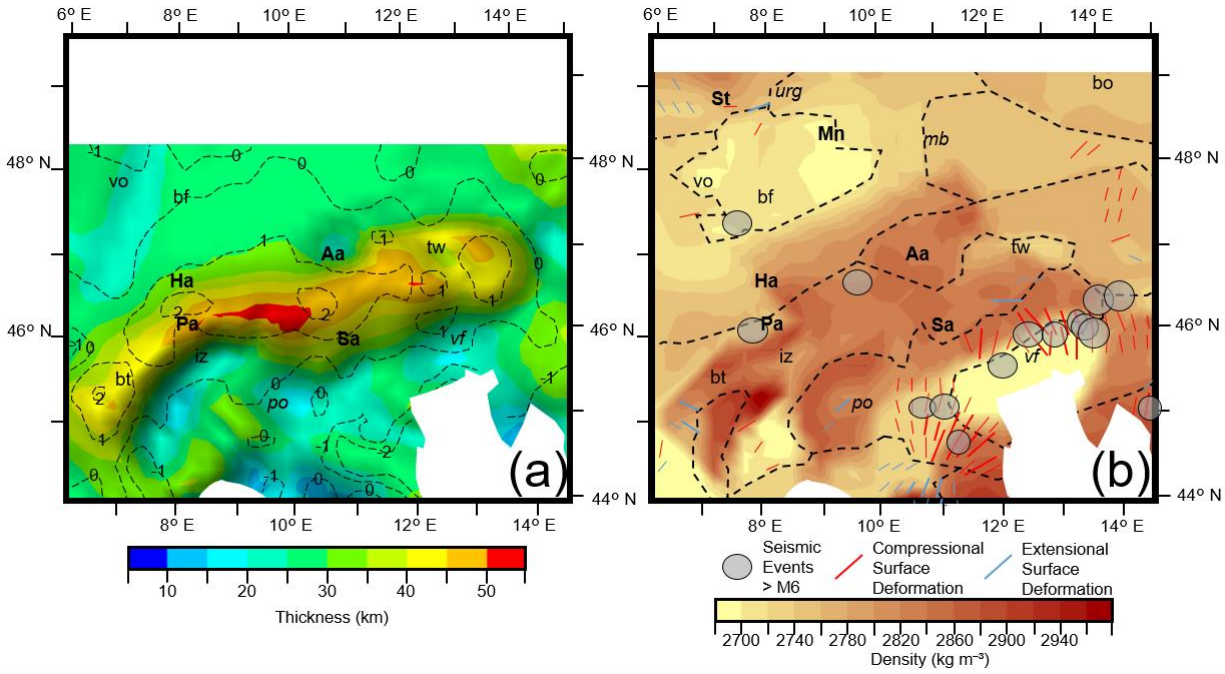

Figure 2.8. a) *Thickness of the crust across the modelled area overlain with vertical displacement rates (Sternai et al., 2019). Dotted black lines indicate isolines of the vertical displacement rates in mm/yr.* ***b)*** *Average density of the crust across the modelled area overlain with geodetically derived horizontal surface strain distribution (Sánchez et al., 2018) and seismic events of a moment magnitude larger than 6 (Fäh et al., 2011; Stucchi et al., 2012; Grünthal et al., 2013). Bar orientation indicates orientation of maximum surface strain. Dotted black lines indicate the upper crust density domains of the final structural and density model. Regions where the overlain data was not available have been whited out in both figures. Locations of key tectonic features are overlain for both figures (abbreviations shown in Figure 2.1. caption).*

Within the Alps a strong correlation exists between the thickness of the crust and vertical displacement rates at the surface. Regions of modelled thickened crust correspond to high positive rates of vertical displacement. Regions of thinned crust, such as the Po Basin and the Upper Rhine Graben, were found to correspond to negative vertical displacements. Differing rates of vertical displacement can also be observed in the Western Molasse and Eastern Molasse Basin, with the west uplifting and the east subsiding. The transition between these two behaviours in the Molasse Basin corresponds to the boundary of the modelled density domain boundaries in the sedimentary and upper crustal layers, separating the denser eastern region of the basin and the less dense western portion of the basin.

Among regions with a pronounced change in the density of the crust, such as the plate boundary between Adria and the Southern Alps, there is coincidence with large earthquakes (Figure

2.8b). Whilst not every large earthquake corresponds to a contrast in the average density of the crust, they all correspond to the location of density domain boundaries within the upper crust as defined in the generated model. Horizontal surface strain distribution also corresponds to the location of density domain boundaries within the upper crust as defined in the model, with the direction of maximum horizontal strain predominantly perpendicular to the domain boundaries.

2.5. Discussion

2.5.1. Alpine Zone Provenance

Differing methods of classifying the Alpine zones have been adopted over time, however the results presented here would support works that utilise tectonic reconstructions and constrain zones based on the plate the crust originated from (e.g. Schmid et al., 2004). Crust derived from different terranes could potentially be assumed to have differing properties such as density, and from the model produced in this work that is found to be the case. From the results, correlation can be observed between zones of different density in the model and Alpine zones as defined by tectonic reconstructions and paleogeography, such as the dense Briançonnais Terrane and Southern Alps and the less dense Tauern Window.

As no density domain geometries were pre-defined during the modelling stage, the correlation of these domains within the generated model to known features adds validity to the generated model. However, caution should be exercised with the exact location of domain boundaries due to many geological cross sections (e.g., Schmid et al., 2004) showing that tectonic domains cropping out at the surface are offset or not continuous at depth. As this was not possible to implement during the gravity modelling workflow, an offset is often present between features in the average crustal densities (Figure 2.7c) and the location of the associated feature at the surface. Two examples of this are in the North of the Briançonnais Terrane and the Tauern Window, suggesting these features have subsurface geometries that differ from their surface expression. Nevertheless, the bulk average densities allow for the location of density distinct tectonic features in the crust.

Additionally, Alpine zones of Adriatic provenance were found, in general, to be denser than those of European provenance, a trend also noted in the present day densities of the Adriatic and European crusts, potentially indicating that prior to orogenesis this was also the case. Alpine zones derived from Adriatic continental crust such as the Austro-Alpine and

Southern Alps appear denser, in general, than the European continental crust derived Helvetic zone and Tauern Window. The Briançonnais Terrane derives from neither Europe nor Adria and appears as such in our model, as the region of highest density in the area. These observations are consistent with the interpretation that the provenance of crust within the Alps can potentially be indicated by its properties, such as density, implying that as the Alpine zones were emplaced at different times during orogenesis, the respective plates prior to orogenesis could have had similar crustal properties to the present day ones.

Regions in the generated model exist with similar provenance and differing densities, indicating that factors other than provenance would also influence their densities. This is exemplified by the Helvetic and Penninic Alps, both deriving from the European plate, which possess a boundary between them that corresponds to an average crustal density contrast. Additionally, some expected boundaries between crusts of different provenances are obscured by other elements of the model. The transition from the European, Helvetic and Peninnic, to Adriatic Austro-Alpine units corresponds to the thickest area of the crustal root, where lower crust percentages are much higher than upper crustal ones, creating a region of high density crust in the model that masks the transition from European to Adriatic crust, when looking at average crustal densities.

2.5.2. Deformation and Seismicity

Correlation between present day horizontal surface deformation and large seismic events with density contrasts within the crust in the generated model would suggest localisation of deformation along these features. Previous works have also shown correspondence between the localisaton of seismicity at density contrasts within the crust, such as at crustal block boundaries (Dentith and Featherstone, 2003), providing further validity to our model. As we are working with a coarse resolution crustal model to identify major features we found it appropriate to compare to a sparse seismic catalogue comprising only the largest (M>6) events allowing for a first-order identification of this correlation. Due to the complex structural nature of an active orogen it is difficult to relate seismicity purely to density contrasts in the crust at higher spatial resolution, as the interplay of faults and collisional processes play a major role in localising seismicity (Serpelloni et al., 2016), while a non-negligible part of earthquakes occurs away from known faults (Hetényi et al. 2018b). However, due to the inherently different properties of crustal blocks of different provenance, it presents the likelihood that major faults

and other structures likely to accommodate seismicity would form at the boundaries between these blocks.

All large seismic events in the region coincide with the modelled location of upper crustal density domain boundaries, however not all correlate to contrasts in the average density of the crust. This fact would suggest that within the Alps, upper crustal density contrasts are a more likely location for the localisation of seismicity than lower crustal ones. Observations of the occurrence of seismicity at depth within the Alps have shown that it is predominantly present within the upper crust (Deichmann, 1992; Serpelloni et al., 2016; Wiemer, et al., 2017), supporting interpretations made from the derived model. However, regions exist within the model that have both average crustal density contrasts and upper crustal density domain boundaries that do not coincide with seismic events, indicating that there are additional controlling factors to the localisation of seismicity.

Observations of the correlation between positive vertical displacement at the surface (Sternai et al., 2019) and thickened crust within the modelled region, and negative vertical displacement and thinned crust also strengthen the validity of the model, with this behaviour expected due to isostasy. The crust is significantly thinned beneath the Po Basin of the southern foreland while it is not in the Molasse Basin of the northern foreland, explaining the discrepancy in sedimentary thicknesses noted before. This could also indicate different driving mechanisms for the formation of either basin, with the Molasse Basin potentially lacking significant subsidence due to being formed predominantly through flexure and the Po Basin being formed through both flexural and active extensional processes. Alternatively the thinned crust below the Po basin could purely represent an inherited crustal feature. Deriving the driving processes for the sedimentary basins formation within the region remain outside of the scope of the present work, however the accurate constraint of the thinned crust in these regions through the use of gravity provides the scope for this to be identified in future projects.

The results presented in this work indicate crustal properties that would support observations from previous works (Sternai et al., 2019) on the dynamics of the region. Whilst correlation can be observed between vertical displacement at the surface and thickened or thinned crust, some regions such as the Molasse Basin show a crust of similar thickness throughout but present a change in the polarity of surface vertical motion. The crustal densities of the model generated here would support this change, with the transition occurring at the boundary of density domains in the crust and the denser eastern portion exhibiting subsidence and the less dense western portion exhibiting uplift.

Previous works on the dynamics of the Adriatic plate show that it acts as a more rigid indenter than the European plate as it moves northwards rotating counter-clockwise into it (Nocquet and Calais, 2004; Vrabec and Fodor, 2006; Serpelloni et al., 2016). Our model shows that the Adriatic crust is denser than the European crust and seismic velocities are also higher in the Adriatic crust than in the European crust (e.g. IESG, 1978; IESG & ETH Zuerich, 1981; Strößenreuther, 1982; Scarascia and Cassinis, 1997; Bleibinhaus & Gebrande, 2006; Brückl et al., 2007). Higher densities and velocities indicate an on average more mafic lithology for these domains, potentially suggesting that they may be stronger than the European crust. The properties of the plates, as modelled here, would suggest that in the present day convergence of the Eastern Alps the denser Adriatic crust would subduct under the European crust, which fits with the subduction polarity identified in teleseismic tomographies (Lippitsch et al., 2003) and high-resolution receiver function analysis interpreted with other datasets (Hetényi et al., 2018a). However, as stated by Kästle et al. (2019) there is no consistent model of Alpine subduction, it is a complex system that has evolved over time with more influencing factors than plate densities. Gravity constrained bulk average densities of the crust and lithospheric mantle in the region, however, provide strong constraints for future works to identify the nature of Alpine subduction.

2.5.3. Model Uncertainty

Whilst the densities used in the final best fit model often correspond very closely to those derived from the P wave velocities (Table 2.1), there are exceptions. In general these are not of concern, such as the opposite tendencies of the more and less dense lithospheric mantles, as the modelled bodies are large volumes of homogenous density that in the real world contain much more heterogeneity. The seismic velocities only provide a fraction of coverage through any of the bodies therefore it is expected that the density indicated by P wave velocity to density conversions will not accurately represent its bulk effect on the gravity field and as such they have been used for initial indications on density and the final densities indicated through gravity constraint.

In the European and North Adriatic domains of the lower crust, however, values are more typical of upper crust, which requires more scrutiny. The sensitivity of the model to density alterations in these crustal has been demonstrated in Figure 2.9. There, a model run with lower crustal densities in North Adria and Europe derived directly from P wave velocities

to density conversions, is shown. The density of the European lower crust has been raised from 2800 to 2890 kg m^{-3}, and the lower crust of North Adria has been raised from 2750 to 2990 kg m^{-3}. Figure 2.9a shows the residual gravity (calculated – observed) of this altered lower crust model and its difference to the residual of the best fit model is shown in Figure 2.9b.

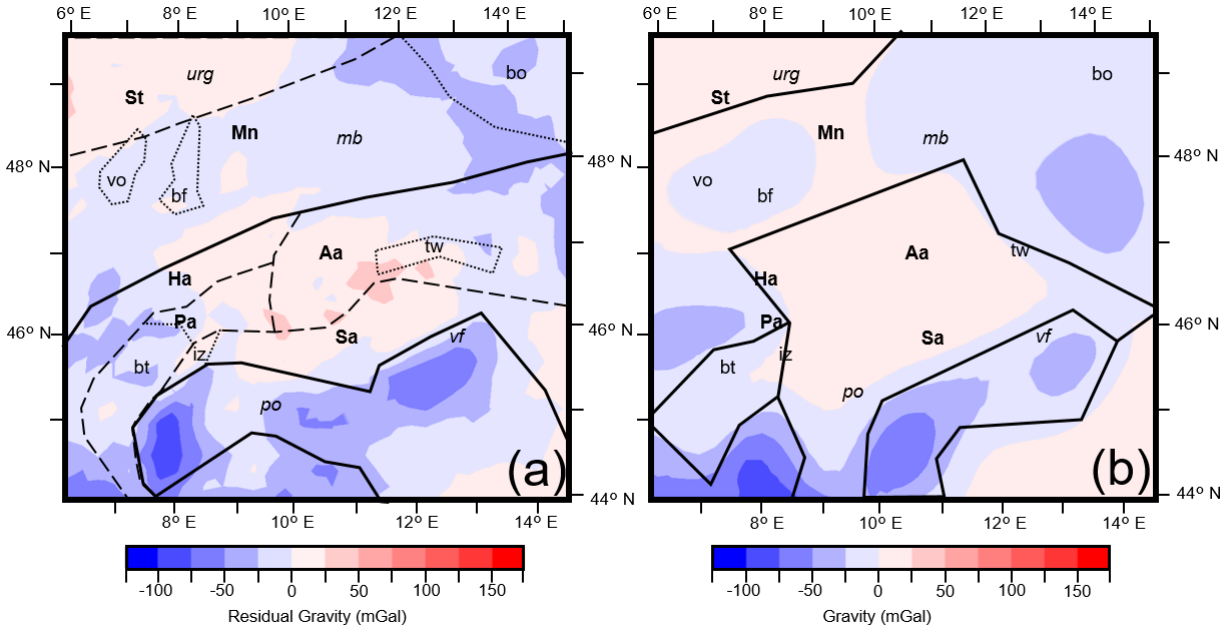

Figure 2.9. a) *Residual gravity (observed gravity - calculated gravity) of a test model with lower crust densities for the Europe and Northern Adria domains set to values indicated directly from P wave velocities using conversion suggested by Brocher (2005).* ***b)*** *Difference in gravity residual between the best fit model (Figure. 2.6b) and the model shown in the Figure 2.9a. Lower crustal density domains of the best fit model are overlain in black.*

The figure indicates that density changes in the lower crust ~ 100-200 kg m^{-3} can affect the gravity field by up to 100 mGal and that using lower crust densities indicated by the P wave velocity to density conversions in Europe and North Adria causes significant misfit. As mentioned prior, the only free parameter during the gravity modelling phase was density. With these low crustal densities required to fit the gravity field and the P wave velocity to density conversions from the upper crust regions fitting so closely, the likely explanations are that either the lower crust in those regions is in fact of a low density or the lower crust is thinner than in the initial structural model, in turn allowing for a slightly denser lower crust. In either case the average density of the crust as presented in Figure 2.8 would largely remain unchanged and these regions would still represent regions of low density crust.

Although correlations are noted between lateral variation in density distribution in the crust and observations such as plate dynamics and the localisation of large earthquakes and recent deformation, the causes of these observations must be further investigated. Planned future modelling will look closer at the features of the crust by creating thermal and rheological models to investigate the driving forces behind the observed correlations, and potentially helping to better explain trends noted in this work. Work is also progressing on constraining deeper structures in the region, such as the mantle, allowing for better constraints on crustal features in the future.

Although the generated model fits the observed gravity well across almost all of the modelled region, it represents a simplified version of the geology below the surface that is not able to account for all the complexity of the real world and as such, inaccuracies within the model exist. Additionally, whilst the location of density domains in the model remains a non-unique solution, efforts were made to minimise errors by using seismic data and indications from previous modelling (see Input Data section 2.2) to constrain the densities within each layer and density domain boundaries. Although these uncertainties cannot fully be accounted for, by only dealing with features and trends appropriate to the scale of the model they are severely mitigated. At the scale of the Alps and their forelands as described in this work, irrespective of localised changes to surface heights or densities, the overall trends identified would not be altered.

2.6. Conclusions

By creating the first gravity constrained, 3D structural and density model of the lithosphere focused on the Alps and their respective forelands, insights were gained into the distribution of densities at depth within the crust. The findings suggest that the present day Adriatic crust is both thinner (22.5 km) and denser (2800 kg m^{-3}) than the European crust (27.5 km, 2750 kg m^{-3}). Crust derived from different terranes was also found to have significantly different densities with Alpine zones of Adriatic provenance. The Austro-Alpine and Southern Alps were found to be denser and those of European provenance such as the Helvetic Zone and Tauern Window to be less dense, indicating the respective plates prior to orogenesis may be assumed to have had similar crustal properties to the present day.

Our modelled anomaly showed a good fit to the observed gravity with maximum misfits of around ± 25 mGal across the whole region. It was further validated by density domains

defined in the model corresponding to known tectonic features, large earthquakes corresponding to crustal density contrasts and surface vertical displacements corresponding to crustal thicknesses. The causes of these observations and correlations cannot be explained solely from the results of this work. Therefore, planned future modelling will generate thermal and rheological models to give further insight into the crustal architecture of the region as well the causes of the localisation of deformation and seismicity.

Chapter 3. The 3D thermal field across the Alpine orogen and its forelands and the relation to seismicity

3.1. Introduction

One in three people globally live at risk of being affected by seismicity (Pesaresi et al., 2017), therefore the need remains for an increased understanding of the factors that contribute to the localisation of seismicity within the lithosphere. As temperature exerts a first order control on rock strength and seismicity (e.g. Hyndman et al., 1995; Emmerson and McKenzie, 2007), a systematic knowledge of the regional 3D temperature distribution is an essential step towards refining predictions of future seismic hazard.

The study area covered here, the Alps and their forelands, represents one of the most active locations for intraplate seismicity in Europe. Ongoing deformation is primarily driven by the convergence of the European and Adriatic plates in northeast Italy (Restivo et al., 2016), where the Adriatic plate is considered to act as a rigid (i.e. mechanically stiff) indenter, moving northwards with a radial counter-clockwise rotation against the weaker European plate (Nocquet and Calais, 2004; Vrabec and Fodor, 2006; Serpelloni et al., 2016).

Recent gravity modelling work of the region (Spooner et al., 2019) have shown that large seismic events cluster across density contrasts within the crust, that represent an inherited crustal configuration of differing petrological and tectono-thermal origin (Schmid et al., 2004). Previously published lithospheric thermal models that cover the entirety of the Alps and their forelands (Tesauro et al., 2009; Limberger et al., 2018) have largely not resolved the vertical and lateral heterogeneities observed mostly in the crustal domains sufficiently well to allow a quantitative assessment of their effects on the resulting temperature distribution. Thermal models that do represent differentiated lithospheric layers and a heterogeneous crust have been published for the Upper Rhine Graben (Freymark et al., 2017) and the Molasse Basin (Przybycin et al., 2014), however these only cover specific subdomains of the area under investigation. In order to further assess how the present-day deformation within the Alpine region is related to the 3D thermal field, we have developed the first 3D steady state lithosphere-scale thermal field of the Alps and their forelands that takes into account the different thermal parameters required to replicate the heterogeneous nature of the crust.

3.1.1. Geological Setting

Crustal heterogeneities represent an important feature in the European crust of the north Alpine foreland. Juxtaposition of terrains with differing properties next to one another, such as Moldanubia and Saxothuringia (Babuška and Plomerová, 1992; Freymark at al., 2017), derive from the Carboniferous age Variscan orogeny (Franke, 2000), that assembled crystalline basement presently exposed in the Vosges, Black Forest and Bohemian massifs. Heterogeneity within the Alpine orogen is also very pronounced as a result of the collision of the Adriatic plate with the European plate from the Cretaceous until the present (Handy et al., 2010).

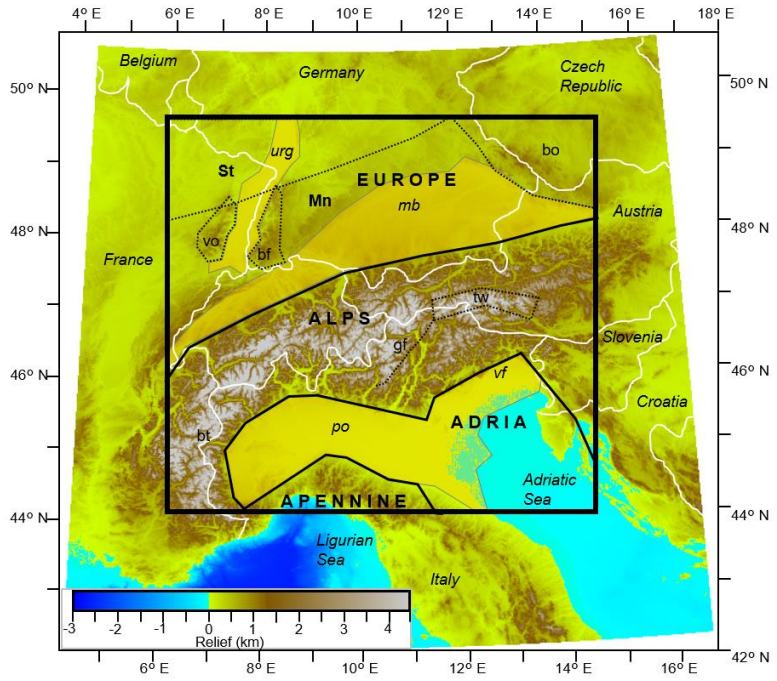

Figure 3.1. *Topography and bathymetry from Etopo 1 (Amante and Eakins, 2009) shown across the Alpine region with the key tectonic features overlain. Study area is indicated with a black box. Solid black lines demark the boundaries of the weakly deformed European and Adriatic plates, the location of the Apennine plate is also marked. Yellow areas bound by a solid grey line indicate the extent of sedimentary basins (urg – Upper Rhine Graben; mb – Molasse Basin; po – Po Basin; vf – Veneto Friuli plane). Dotted black lines indicate the extent of other tectonic features within the model (st – Saxothuringian Variscan domain; mn – Moldanubian Variscan domain; bo – Bohemian Massif; vo – Vosges Massif; bf – Black Forest Massif; tw – Tauern Window; gf – Giudicarie Fault; bt – Brianconnais Terrane). The Adriatic Sea is marked as (AS) in further figures.*

The different parts of the orogen-foreland system (Figure 3.1) are presently interpreted according to their provenance and metamorphic history, with the eastern and western Alps being derived from the Adriatic and European plates respectively (Schmid et al., 2004). The Briançonnais crustal block that lies within the western Alps derives from the Iberian plate (Frisch, 1979). The three main depocentres within the region are the Po Basin of the southern foreland, the Molasse Basin of the northern foreland and the Upper Rhine Graben, also within the northern foreland, that formed as part of the European Cenozoic Rift System in the Eocene (Dèzes at el., 2004).

3.2. Workflow

An existing 3D structure and density model of the Alpine lithosphere made by Spooner et al. (2019), was used to calculate the thermal field of the region. The model covers an area of 660 km x 620 km (shown in Figure 3.1) with a horizontal grid resolution of 20 km x 20 km and is the highest resolution 3D structural model of the Alps and foreland region that conforms to seismic and gravity based observations. The vertical resolution is variable, depending on the thickness of the 6 model layers, representing the key structural and density contrasts within the lithosphere: (1) water; (2) unconsolidated sediments (mostly Quaternary); (3) consolidated sediments (mostly Mesozoic); (4) upper crystalline crust; (5) lower crystalline crust; and (6) lithospheric mantle. Each layer (excluding water) is split into distinct domains representing the different tectonic blocks that comprise them. The thickness of each layer and location of the different domains within them are also shown in Figures 3.2 and 3.3a. No subduction interfaces are included in the model.

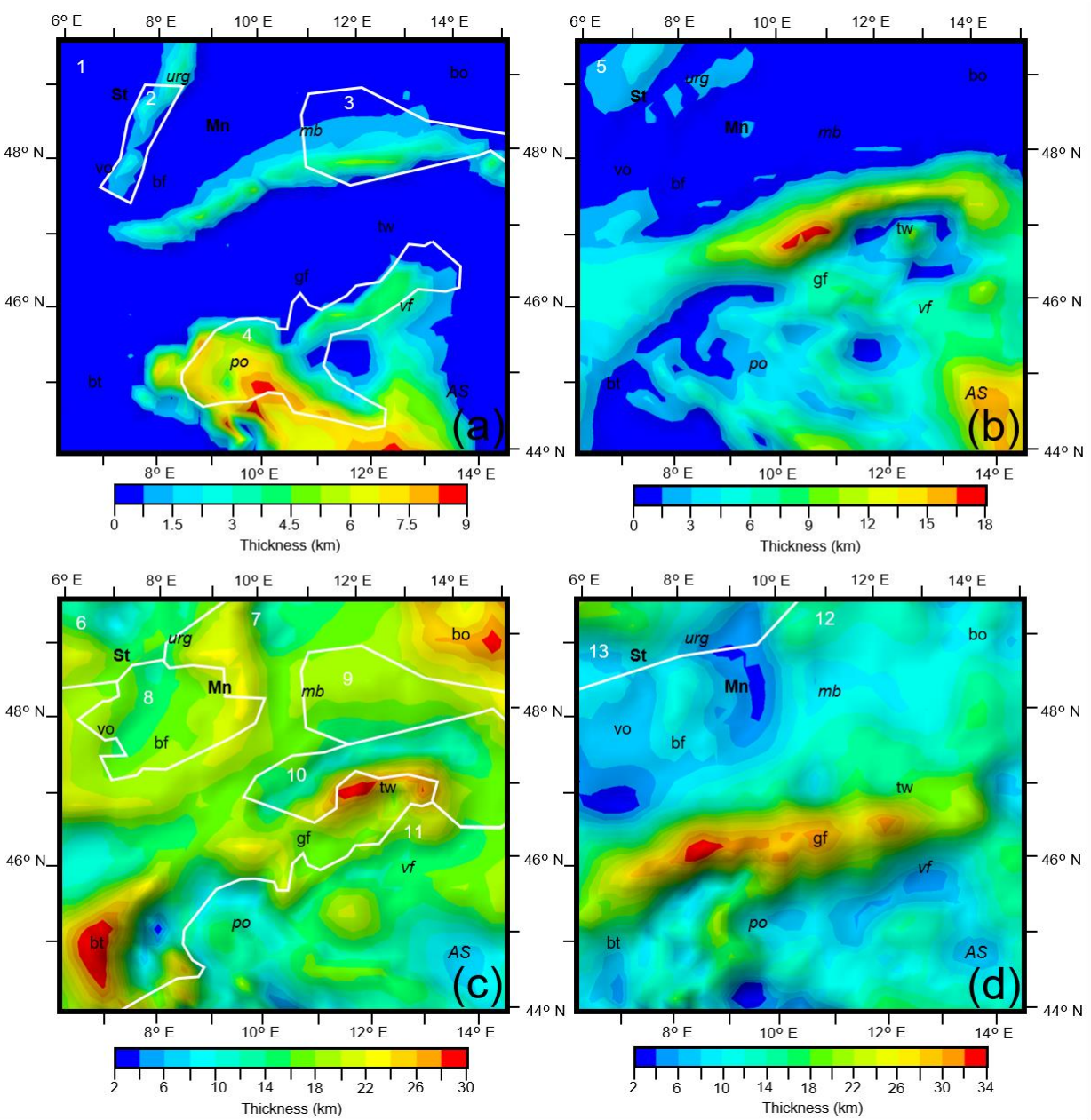

Figure 3.2. *Thickness of* ***a)*** *unconsolidated sediments (mostly Quaternary),* ***b)*** *consolidated sediments (mostly Mesozoic),* ***c)*** *the upper crystalline crust and* ***d)*** *the lower crystalline crust across the modelled area. Domains of different thermal parameters within each the layer are overlain in white, domain numbers correspond to Table 3.1. Locations of key tectonic features are overlain (abbreviations shown in Figure 3.1 caption).*

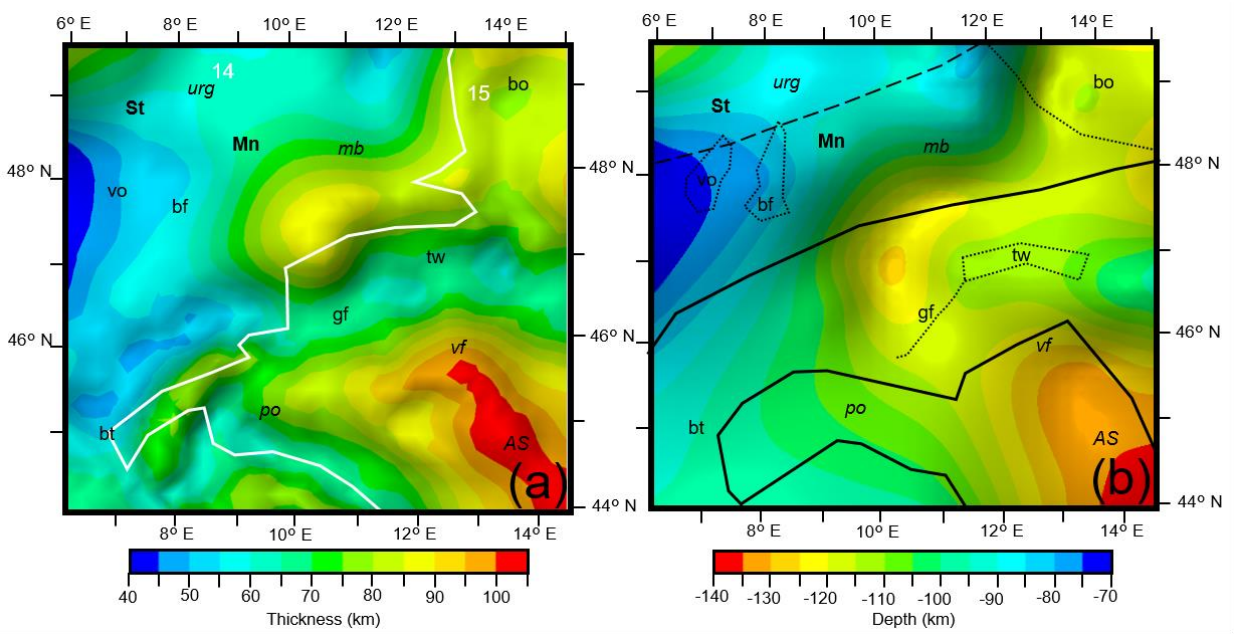

Figure 3.3. a) *Thickness of the lithospheric mantle layer from the structural model. Domains of different thermal parameters within the layer are overlain in white, domain numbers correspond to Table 3.1.* ***b)*** *Depth to the LAB from Geissler et al (2010) across the modelled area. Locations of key tectonic features are overlain (abbreviations shown in Figure 3.1 caption).*

Some refinements were made to the original structural model to make it of use for the thermal modelling effort. The water layer was discarded, with the surface representing topography and bathymetry used as the upper limit of the model (shown in Figure 3.1) and the Lithosphere-Asthenosphere Boundary (LAB) used as the base of the model (shown in Figure 3.3b). Additionally, thick unconsolidated sedimentary layers within the model, were vertically differentiated in terms of thermal parameters into two units to account for porosity changes within these layers due to compaction. As the majority of sedimentary porosity decrease takes place in the upper few kilometres (Allen and Allen, 2013) this transition was implemented at 2 km depth in the Po Basin and 1 km in other areas with less thick deposits of unconsolidated sediments. Further refinement of the model vertical resolution was tested but found to have little effect on the generated thermal field. Accordingly, the vertical resolution was not refined to minimise the computational demand.

A 3D finite element model (32,736 nodes) incorporating these refinements was then used to calculate the 3D conductive steady state thermal field of the study area using GOLEM

(Cacace and Jacquey, 2017), a numerical simulator of coupled Thermal-Hydraulic-Mechanical processes. For this study steady state conditions were assumed and the conductive thermal field was calculated. Therefore, the conductive heat equation solved for steady state conditions is

$$0 = \mathrm{div}(\lambda \nabla T) + S \tag{3.1}$$

where the ∇T is the temperature gradient (K/m), λ is the thermal conductivity (W/mK) and S is the radiogenic heat production (W/m3). The boundary conditions to close the system of equations comprise fixed temperatures along the top and bottom of the model (Dirichlet boundary condition), while all lateral boundaries are considered to be no-flow. The upper thermal boundary condition used (Figure 3.4a) corresponds to yearly average surface temperatures, comprising both land and sea floor measurements, from the WOA13 dataset (Locarini et al., 2013) the Histalp dataset (Böhm et al., 2009) and the GHCN_CAMS dataset (Fan and Van den Dool, 2008). Temperatures range from -10 °C in the Alps to 16 °C in the Adriatic Sea. The temperature distribution used across the lower thermal boundary condition (see Figure 3.4b), is derived from the conversion of shear wave velocities (Priestly and McKenzie, 2006; Meeßen, 2018) from Schaeffer and Lebedev's (2013) SL2013sv dataset, at a depth corresponding to the base of the model. Temperatures range from 1,250 °C below the Vosges massif to 1,400 °C beneath the Bohemian massif. Although the range of temperatures does not vary significantly, there is an overall spatial correlation between the thermal configuration and the topology of the LAB from the structural model (Spooner et al., 2019), an indication that assuming the LAB derived from seismology (Geissler et al., 2010) as a thermal boundary is justified.

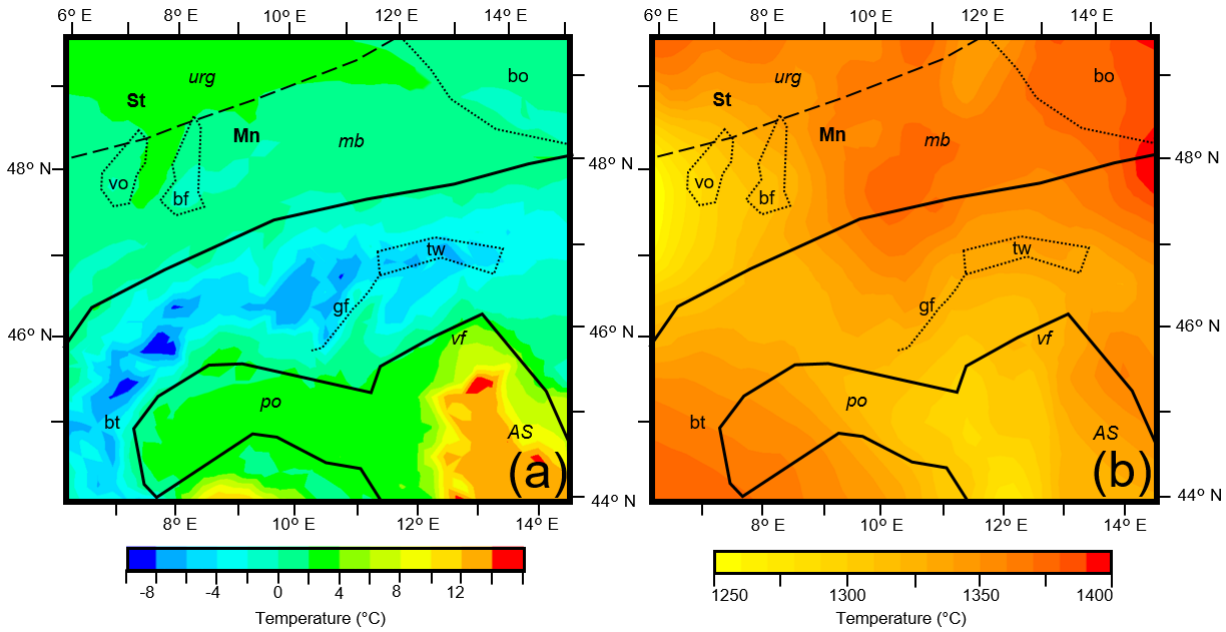

Figure 3.4. *Temperatures used as the* ***a)*** *upper and* ***b)*** *lower boundary condition for achieving steady state conditions of the thermal model. Temperatures for the upper boundary condition were derived from the WOA13 dataset (Locarini et al., 2013) the Histalp dataset (Böhm et al., 2009) and the GHCN_CAMS dataset (Fan and Van den Dool, 2008). Temperatures for the lower boundary conditions were calculated using the LAB of Geissler et al (2010) and Shaeffer and Lebedev's (2013) SL2013sv dataset. Locations of key tectonic features are overlain (abbreviations shown in Figure 3.1 caption).*

Model validation is carried out by comparing the obtained results against a dataset of measured sub-surface temperatures from across the region. Data for the southern foreland was derived from the Italian National Geothermal Database (Trumpy and Manzella, 2017), for the northern foreland from previously compiled databases of the Upper Rhine Graben (Freymark et al., 2017 and references therein) and the Molasse Basin (Przybycin et al., 2015 and references therein) and within the Alps a dataset compiled by Luijendijk et al. (2020) was used. The combined dataset represents 8,120 measurements from the surface down to 7.3 km below sea level, with a mean depth of 1.8 km. Temperature readings of a number of different types were used including, corrected bottom hole, continuous gradient and hot fluid readings, to give as broad a coverage across the region as possible.

In the first modelling stage, each model layer was assigned constant bulk thermal properties, from a range of values using in similar modelling work in the Upper Rhine Graben (Freymark et al., 2017) and Molasse Basin (Przybycin et al., 2015). The ranges of thermal

properties tested can be seen in Table 3.1. The values used were tested in an iterative fashion, starting at the midpoint of the tested range. The thermal parameters were altered in the lithospheric mantle domains first, at the base of the model, before altering the parameters in each domain successively moving up the layers of the structural model. In layers of the model where radiogenic heat production is expected to be low (unconsolidated sediments, consolidated sediments, lower crust and lithospheric mantle) the thermal conductivity was altered first to fit the measured temperatures before the radiogenic heat value was tweaked to get the best overall fit, with the opposite carried out for the upper crust where the radiogenic heat production is significant.

Unit	Final Bulk Thermal Conductivity (W/mK)	Bulk Thermal Conductivity Range Tested (W/mK)	Final Radiogenic Heat Production (W/m3)	Radiogenic Heat Production Range Tested (W/m3)
1. top 1km Unconsolidated Sediments - below 1km Unconsolidated Sediments	2 2.3	1.8 – 3	1.00E-06 1.00E-06	1.00E-06
2. top 1km Unconsolidated Sediments URG - below 1km Unconsolidated Sediments URG	1.1 1.4	1.1 – 1.8	1.00E-06 1.00E-06	1.00E-06
3. Unconsolidated Sediments Molasse	1.8	1.8 - 3	1.00E-06	1.00E-06
4. top 2km Unconsolidated Sediments Po - below 2km Unconsolidated Sediments Po	2 2.3	1.8 – 3	1.00E-06 1.00E-06	1.00E-06
5. Consolidated Sediments	2.3	2 – 3.5	1.00E-06	1.00E-06 - 1.30E-06
6. Upper Crust Saxothuringia	3	2.5 – 4	2.60E-06	1.00E-06 - 2.60E-06
7. Upper Crust Moldanubia and West Alps	2.6	2.3 – 3.1	1.80E-06	1.00E-06 - 2.60E-06
8. Upper Crust Vosges	2.8	2.3 – 3.1	2.00E-06	1.00E-06 - 2.60E-06
9. Upper Crust Molasse	2.4	2.3 – 3.1	1.30E-06	1.00E-06 - 2.60E-06
10. Upper Crust East Alps	2.4	2.2 – 3.1	1.60E-06	1.00E-06 - 2.60E-06
11. Upper Crust Adria and Apennine	2.4	2.3 – 3.1	1.30E-06	1.00E-06 - 2.60E-06
12. Lower Crust	2	2 – 2.7	3.00E-07	1.50E-07 - 7.00E-07
13. Lower Crust Saxothuringia	2.3	2 – 2.7	6.00E-07	1.50E-07 - 7.00E-07
14. Lithospheric Mantle North West	3	3 – 3.95	3.00E-08	2.00E-08 - 3.00E-08
15. Lithospheric Mantle South East	3	3 – 3.95	2.00E-08	2.00E-08 - 3.00E-08

Table 3.1. *Final thermal parameters used and the tested range for all domains of the structural model.*

The best fit thermal field was then compared to the seismic event catalogue of the International Seismological Centre (International Seismological centre, 2020) for the study area. The catalogue was filtered for events larger than magnitude 2 between January 2000 and January 2018, as the catalogue completeness drops significantly outside of these parameters. This provided a dataset of 4,571 seismic events so that relationships between the depth, temperature, and location of seismicity could be explored.

3.2.1. Methodological Limitations

The model generated here represents the first attempt to calculate the 3D steady state thermal field of the Alps and their forelands using different thermal parameters for different tectonic domains, validated with a dataset of wellbore temperatures from across the region, however limitations remain in the current workflow. The resolution of the thermal model generated is a result of the available data sources, which although state of the art, are limited in their resolution, coverage, and differentiation of Alpine lithospheric units, allowing for a first order comparison of relative thermal trends between large scale crustal features.

The method used to derive thermal parameters produces values representing the bulk average properties of the domain rather than an exact lithology or metamorphic facies. The availability of highly detailed geological information across the entire study area does not support the creation of such a high resolution model, especially at depth. As such, rather than use specific rock values, we test a range of parameter values likely in such a setting. Therefore, indications of lithology derived from the modelled thermal parameters are relative to one another, based upon how thermal parameters act in more mafic or felsic rocks (e.g. Hasterok and Webb, 2017). Despite the sparse nature of higher resolution data, wherever present they have been used to validate the thermal parameters derived from the workflow. Existing P-wave velocity models through the region (e.g. Bleibinhaus and Gebrande, 2006), suggest similar radiogenic heat production values to those we have modelled, when converting using the methodology of Hasterok and Webb (2017).

The thermal field presented here is a first attempt at a truly multidisciplinary study, integrating data from a wide array of sources. Interpretations used as a basis for the calculated thermal field, including prior work such as the structural model (Spooner et al., 2019) and the thermal parameters assigned to crustal domains, both represent non-unique solutions. To

remedy this, at each stage multiple external data sources, such as gravity anomalies, seismicity or wellbore temperatures, have been used for validation.

Limitations of the data used for validation also impacts the modelling effort. The distribution of wellbore measurements represent a significantly heterogeneous data coverage, with regions of interest for geothermal or hydrocarbon exploitation overrepresented and the orogen itself containing sparser coverage. The coverage negates the potential for an accurate deterministic solution to constrain thermal parameters in most regions, and this is further complicated by the required use of different types of measured wellbore temperatures in order to maximise coverage. Therefore, at this time, a qualitatively derived solution for a 3D thermal field of the region represents the best possible solution. In locations where these limitations have been encountered, further mention has been made in the text. Work to quantify the sensitivities of regional thermal parameters to the spread of measurement data is underway.

Another limitation of the workflow is that the model is made with the assumption that the thermal field is in a present day steady state, meaning that it has achieved thermodynamic equilibrium and will not change over time unless the system state is altered. To progress from steady state to other thermal modelling methods, such as transient thermal fields, where changes through time are calculated, further observations need to be gathered on the contributions of other influencing factors to the thermal field. These include: the effects of hydrothermal convection (e.g. Smith and Chapman, 1983; Ehlers and Chapman, 1999; Sippel et al., 2014); rapid sedimentation rates (Ehlers 2005); regional glacial history (Mey et al., 2017); present day surface vertical motion (Sternai et al., 2019); and long term exhumation rates (Fox et al., 2016). In locations where these other effects are interpreted to have affected our results, further mention has been made in the text.

3.3. Results

3.3.1. Modelled Temperature Distribution

Figure 3.5 illustrates depth slices through the thermal field of the best fit thermal model at 2, 5, 10 and 20 km below sea level. Observations of first order temperature trends at a depth of 2 km, indicate that the pattern of heat distribution correlates spatially to the topography, with the coldest areas in the Ligurian Sea (40 °C) and the hottest areas corresponding to the Alps (140 °C). However, irrespective of similar topographies the western Alps appear generally warmer (140 °C) than the eastern Alps (130 °C). The warmest temperatures outside of the

orogen are observed to occur beneath the Upper Rhine Graben (120 °C), corresponding to negative relief with respect to its surroundings whilst being significantly warmer than they are (80 °C). There is also an observable temperature contrast between both the northern and southern alpine forelands with the European domain in the north around 20 °C warmer (80 °C) than the Adriatic domain of the southern foreland (60 °C).

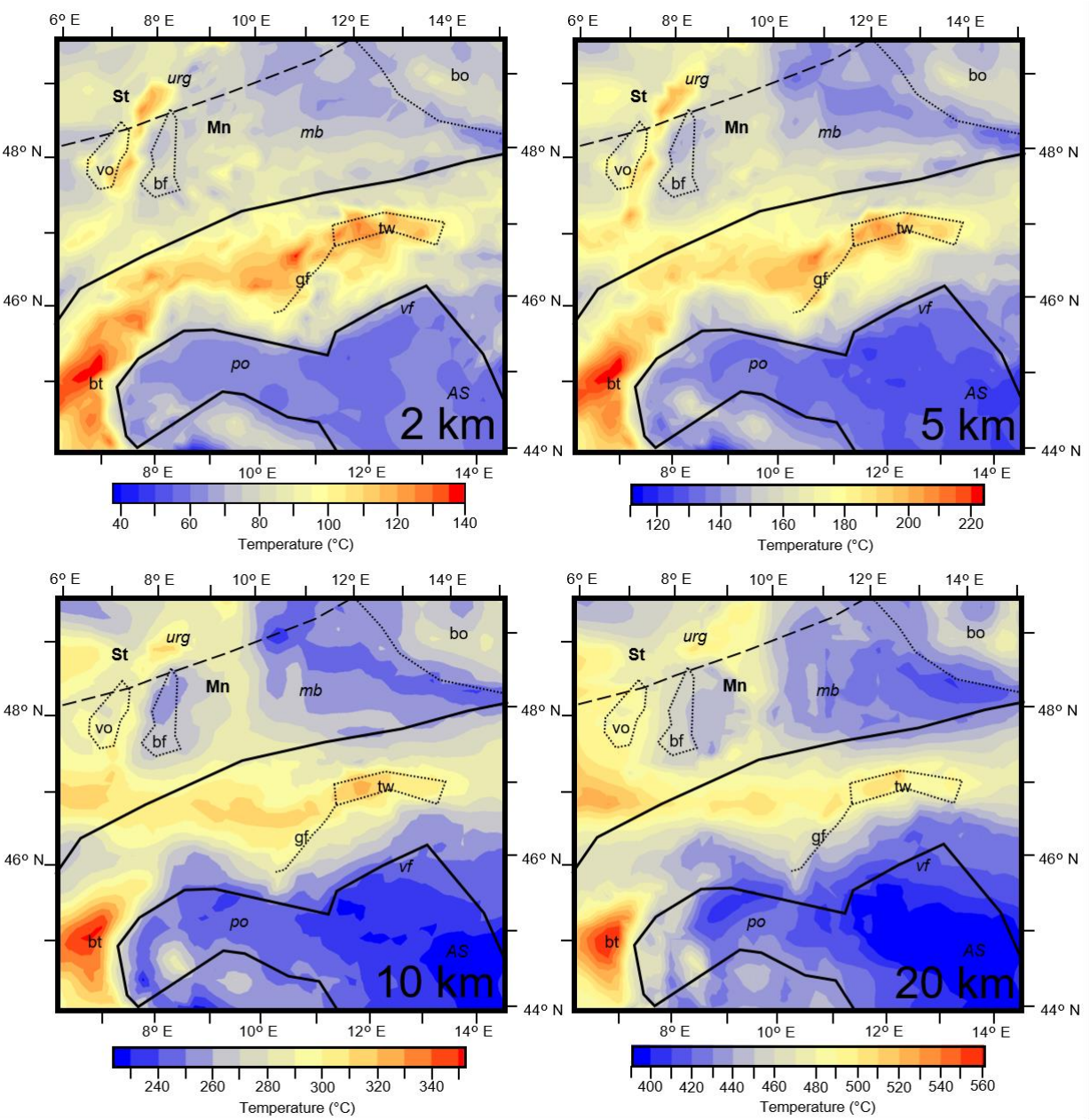

Figure 3.5. *Temperature maps through the final model at depths below sea level of 2 km, 5 km, 10 km and 20 km. Locations of key tectonic features are overlain (abbreviations shown in Figure 3.1 caption).*

Similar trends are also noted in the 5 km depth slice. The highest temperatures are found in the western Alps (220 °C), with the eastern Alps and Upper Rhine Graben around 20 °C cooler (200 °C). At this depth, the northern foreland begins to appear warmer in the west (170 °C) and cooler in the east (150 °C). Locally higher temperatures in the northern foreland are detected to correspond to thicker deposits of sediments in the basins. Deposits of around 4 km and 5 km thickness in the Upper Rhine Graben and Molasse Basin respectively raise temperatures by 20 °C compared to the surrounding foreland. Differentiation between tectonic blocks in the northern foreland is also visible, with the Vosges Mountains in the west of the study area displaying temperatures similar (170 °C) to those of the surrounding foreland, whilst the adjacent Black Forest appears cooler (155 °C). The Bohemian Massif in the east of the study area appears warmer (160 °C) than its surroundings. Such changeable lateral temperature variations are not widely noticed in the results from the southern foreland. Temperatures instead increase gradually moving westwards, from the coolest modelled values below the Adriatic Sea (130 °C), towards the thicker sedimentary deposits of the Po Basin (140 °C).

At a depth of 10 km, the warmest domain in the model (350 °C) corresponds to the location of the Brianconnais terrane, represented by a significantly thickened upper crust (30 km) in the structural model. Thinner upper crust immediately northwards (15 km thick) can be seen in the results as an area of lower temperatures (280 °C). Whilst not representing a zone of significant crustal thinning, the Giudicarie Line marks a thermal boundary within the Alps with crust 30 °C warmer (320 °C) in the West than in the East (290 °C). However, the Tauern Window represents an exception, lying east of the Guidicarie line it is indicated by a region of elevated temperatures (330 °C) that also corresponds to a thickened upper crust. The Bohemian Massif represents a thicker upper crust (28 km) than its surroundings and also possesses warmer temperatures (310 °C), whilst contrastingly the Black Forest also shows thickened upper crust but represents colder temperatures (260 °C). The coolest temperatures in the model still occur below the Adriatic Sea (225 °C), warming inland towards the Po Basin (250 °C), with both regions encompassing an area of significantly thinned upper crust (6 km). The northern foreland again displays a trend of warming westwards, with the western Molasse Basin appearing ~40 °C warmer (300 °C) than its eastern part (260 °C). The Upper Rhine Graben is no longer one of the hottest regions at this depth level (290 °C).

At 20 km below sea level, higher temperatures correlate less to high topographies with the majority of the Alpine orogen of a similar temperature to its northern foreland, and no observable links exist between thicknesses of sediment and temperature. However, the

correlation between temperature and thickness of the upper crust is noticeable, with the Brianconnais terrane the hottest region of the model (560 °C). Besides the Brianconnais terrane, the next warmest region lies in the western Molasse Basin, south of the Vosges Mountains. Temperatures there reach 540 °C and correspond to the shallowest region of the LAB (70 km), whereas below the coldest point of the model, in the Adriatic Sea (390 °C), the LAB is deepest (140 km). At this depth level the European crust still appears warmer than the Adriatic crust, with the LAB also shallower in general below Europe than Adria.

3.3.2. Model Parameterisation and Validation

The thermal properties used to achieve the best fit thermal field can be seen in Table 3.1. Unconsolidated sediment thermal conductivities vary significantly throughout the region. In the Upper Rhine Graben values at the lower limit of the tested range (1.1 and 1.4 W/mK) were found necessary to replicate the fit of the measured temperatures as close as possible. However in other basin settings more standard values ranging from 1.8 W/mK in the Molasse Basin to 2.3 W/mK in the Po Basin were used. Standard values for consolidated sediments were found to be sufficient throughout the region (2.3 W/mK and 1E-06 W/m3). Within the upper crust, large variations of thermal properties were found between different crustal blocks. The Saxothuringian block was found to require the highest thermal conductivity (3 W/mK) and radiogenic heat production (2.6E-06 W/m3), whilst much lower values (2.4 W/mK and 1.3E-06 W/m3) were found necessary for the upper crust beneath the Po Basin. The lower crust shows almost homogeneous thermal properties (2 W/mK and 3.0E-07 W/m3) with the exception of the Saxothuringian block that again was found to require higher values (2.3 W/mK and 6.0E-07 W/m3). Different radiogenic heat productions were also found necessary for the two lithospheric mantle domains with the less dense domain in the northwest requiring higher values (3.0E-08 W/m3) than in the denser southeast domain (2.0E-08 W/m3).

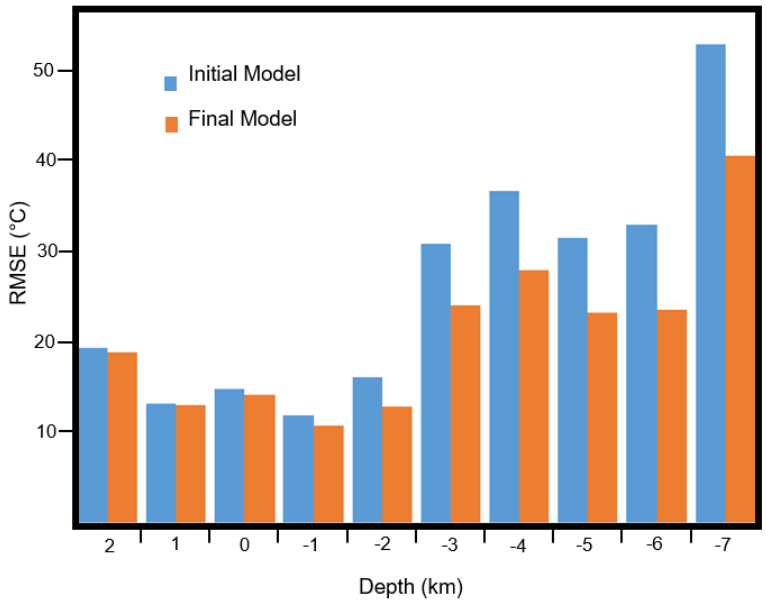

Figure 3.6. *Root mean square error (RMSE) of the difference between measured temperatures (°C) and the modelled temperatures (°C) from the initial and final best fit models.*

The improvement of the best fit model over the initial model (using the average value of the range tested in Table 3.1) is visualised in Figure 3.6, where the difference between the modelled temperatures and measured temperatures (root mean square error) is shown at different depths. The accuracy of shallower modelled temperatures (from 2 km asl to 2 km bsl) are only slightly improved (by ~1 °C) after iterative alterations to the thermal parameters. This is because modelled temperatures at this depth were already closely representing (±15 °C) their measurements from the initial model. However for the deepest measurements in the region (7 km), the accuracy of the best fit model (±40 °C) is more than 20% better than the initial model (±53 °C). Across the 8,120 measurements used in the region, the root mean square error of the best fit model is 15.42 °C, significantly better than the initial model (18.55 °C).

The correlation between measured and calculated temperatures of the best fit model are plotted against depth for both the whole model and specific regions of interest (Upper Rhine Graben, Molasse Basin, Po Basin, Alps) in Figures 3.7b and 3.8. Different regions of interest required different average geotherms to best match measured values. The highest thermal gradients are found in the sedimentary basins on the European plate with the Upper Rhine Graben requiring the highest value at 0.04 K/m, followed by the Molasse Basin with a value

of 0.035 K/m. Whilst measured values are sparser in the Molasse Basin, their trend is accurately replicated by our modelling results, leaving few outliers. Although the majority of Upper Rhine Graben measurements are well replicated, measured points in some regions deviate systematically from the regional geotherm (0.04 K/m), plotting along a localised higher geotherm (0.065 K/m). As a result, some modelled temperatures at depths of 2 km below the Upper Rhine Graben are ~60 °C cooler than their measurements suggest. Features such as local fluid movement and faults, known to affect the thermal filed in the Upper Rhine Graben (Freymark et al., 2019), are however not modelled using the present methodology.

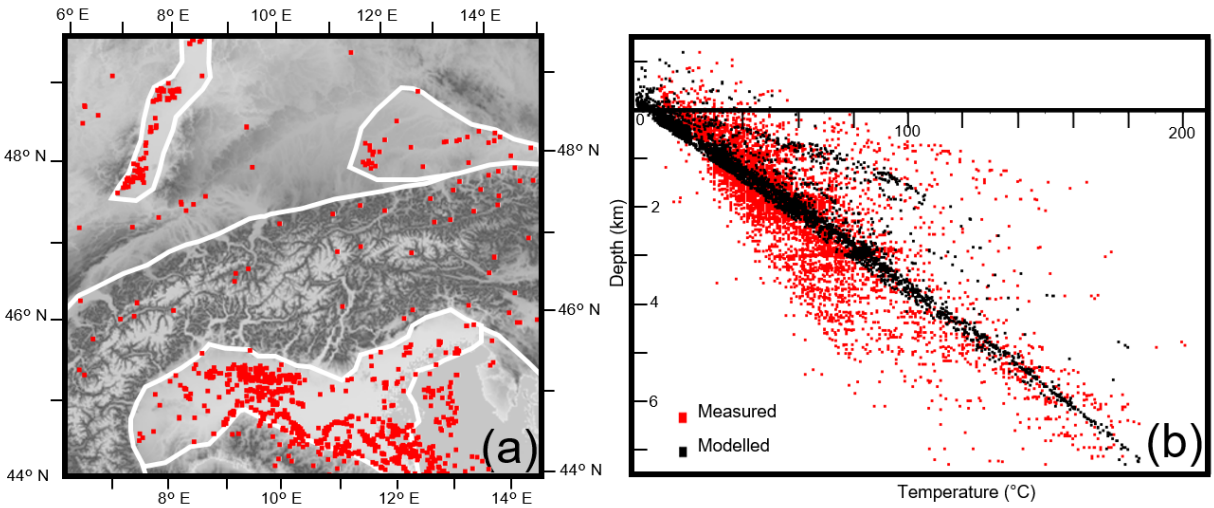

Figure 3.7. a) *Location of all wellbore temperatures used. Locations of regions of interest for comparing measured and modelled temperatures are bound in white.* ***b)*** *Comparison between measured wellbore temperatures (red) and modelled temperatures for the same points (black) plotted against depth for the whole model.*

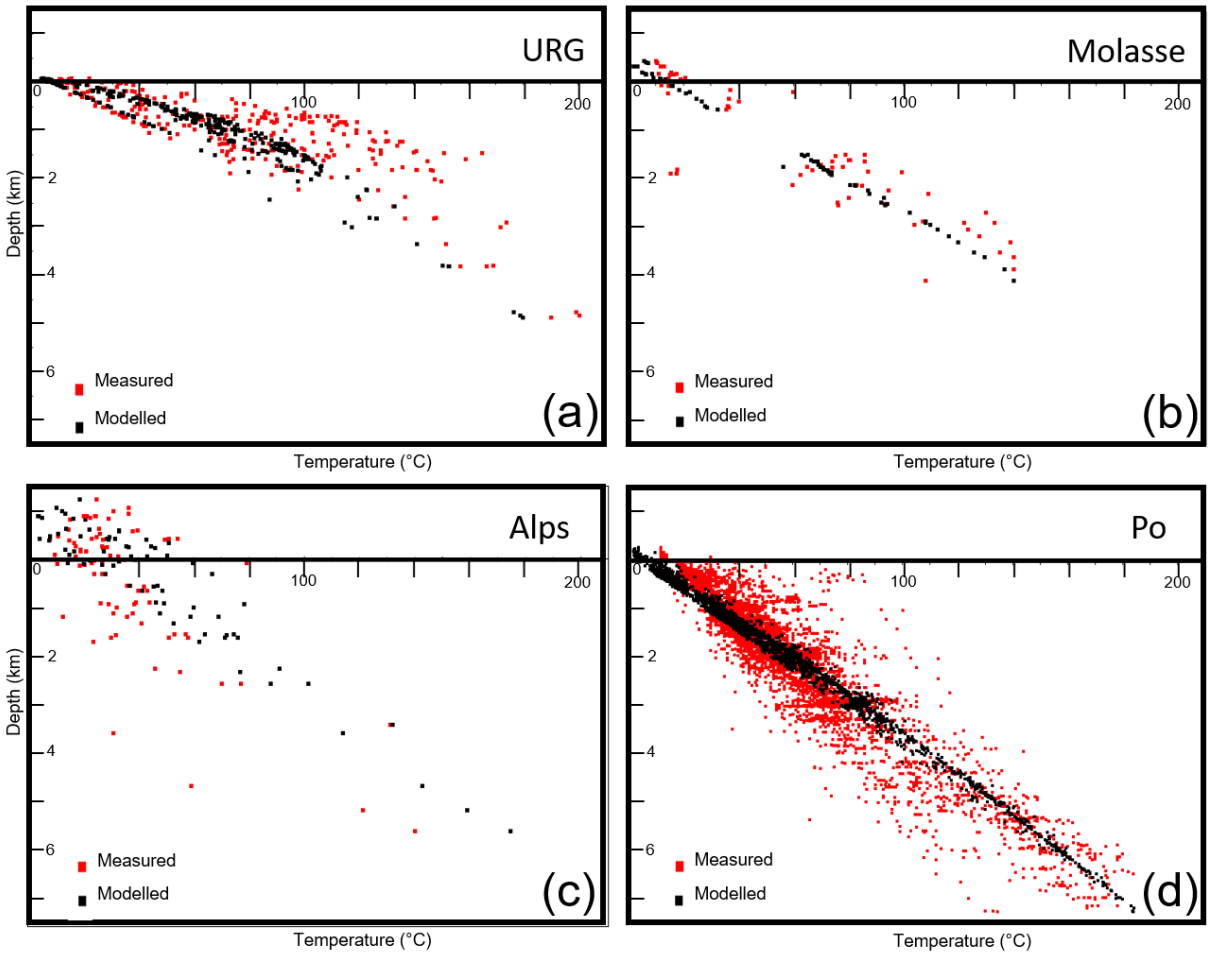

Figure 3.8. *Comparison between measured wellbore temperatures (red) and modelled temperatures at those points (black) plotted against depth for locations of interest:* ***a)*** *Upper Rhine Graben;* ***b)*** *Molasse Basin;* ***c)*** *the Alps;* ***d)*** *Po Basin. Boundaries of locations of interest are shown in Figure 3.7a.*

On the Adriatic plate, geotherms are found to be significantly lower with the Po Basin showing a temperature gradient of 0.025 K/m. Covering the largest area and containing the largest amounts of measured points, the Po Basin shows a larger spread of temperatures at each depth level, however despite this, the average modelled geotherm matches the majority of measured values well, the latter not displaying any systematic deviation from the average geotherm.

The geothermal gradient found to best fit the Alpine region was equally low (0.025 K/m), like the Po Basin. The larger variation of the observed thermal gradient in the Alpine domain results from the low spatial resolution and lower accuracy of Alpine measurements.

These derive from a thermal spring wellbore dataset (Luijendijk et al., 2020), which due to heat loss during transport of thermal fluids in the well represent minimum temperatures. This explains why our modelled temperatures are slightly higher than observed. Moreover, thermal springs are expressions of advective and convective heat transport - mechanisms that are not considered in our approach. Thus we aim to reproduce the overall trend of the "observed" geotherm but not its details.

3.3.3. Distribution of Seismicity

The locations of all seismic events used are shown in Figure 3.9a, with events separated into different regions (Europe, East Alps, West Alps, Adria and Apennine) to compare their relationships with modelled temperatures. Key isotherms representing temperatures in the brittle ductile transition of the dominant crustal minerals are also shown: 275 °C for wet quartz; 450 °C for feldspar; and 600 °C for wet pyroxene (Evans et al., 1990; Simpson, 1999). In the European Plate and western Alps, the majority of seismic events occur between the 275 °C and 450 °C isotherms, with most seismicity ceasing at 475 °C. However, a few isolated events occur deeper, at hotter temperatures. In the Adriatic plate and eastern Alps the correlation between seismicity and temperature is less distinct, with the majority of seismicity also occurring between the 275 °C and 450 °C isotherms, however many more events are found to temperatures of 600 °C. In the Apennine region, seismicity begins at a higher temperature (>100 °C) and events are continuous down to the 600 °C isotherm. In both the Adriatic and Apennine regions, isolated seismicity can be seen to around 70 km depth.

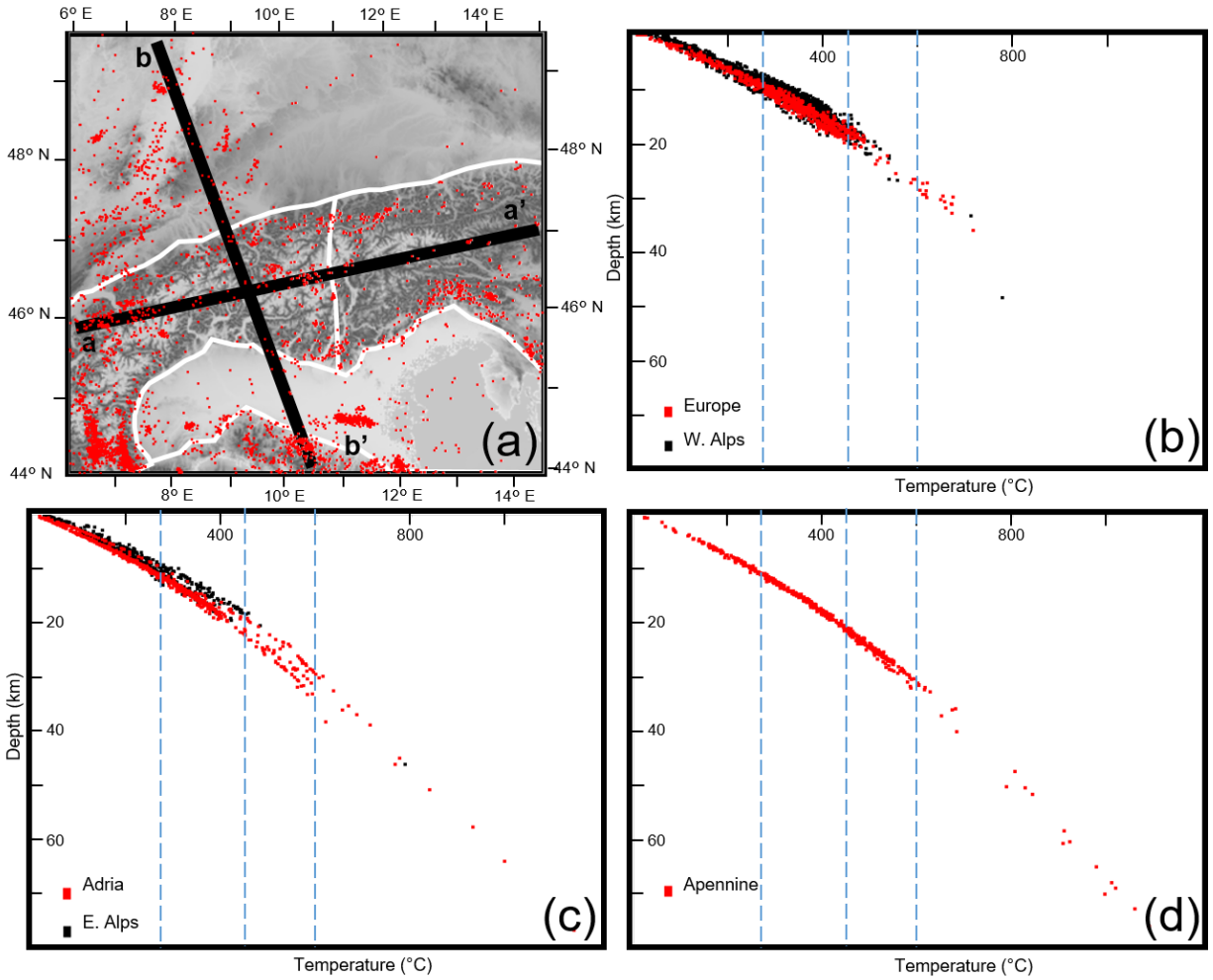

Figure 3.9. *Overview of seismicity data.* ***a)*** *Location of all seismic events used from the International Seismological Centre (International Seismological centre, 2020) between Jan 2000 and Jan 2018 with a magnitude larger than 2 shown in red dots. a-a' represents the cross section in Figure 3.10, b-b' represents the cross section in Figure 3.11. The white polygons delimit regions of interest, where the depth and modelled temperature of each seismic event have been shown in following panels:* ***b)*** *the European plate and West Alps,* ***c)*** *The Adriatic plate and East Alps,* ***d)*** *the Apennine plate. Isotherms for 275 °C, 450 °C and 600 °C are overlain as dashed blue lines.*

Two cross sections through the structural model are shown to further illustrate the relationship between local seismicity and temperature. An East to West running section through the middle of the orogen (a-a', Figure 3.10) and a North to South cross section from one foreland to the other through the orogen (b-b', Figure 3.11) are marked on the map of the study area in Figure 3.9a. The sediments, upper crust, lower crust and lithospheric mantle of the structural model are displayed along with all seismological epicentres that lay within a 20

km distance of the cross section. Cross section a-a' shows that in the Alps all seismicity is localised in the upper crust or Alpine nappes (shown as sediments in the cross section), with a largely aseismic lower crust also in the western Alps, where it is shallowest. Seismicity is centred around the 275 °C isotherm and does not occur at temperatures above 450 °C. Little difference can be discerned between the pattern of seismicity in the Western and Eastern Alps.

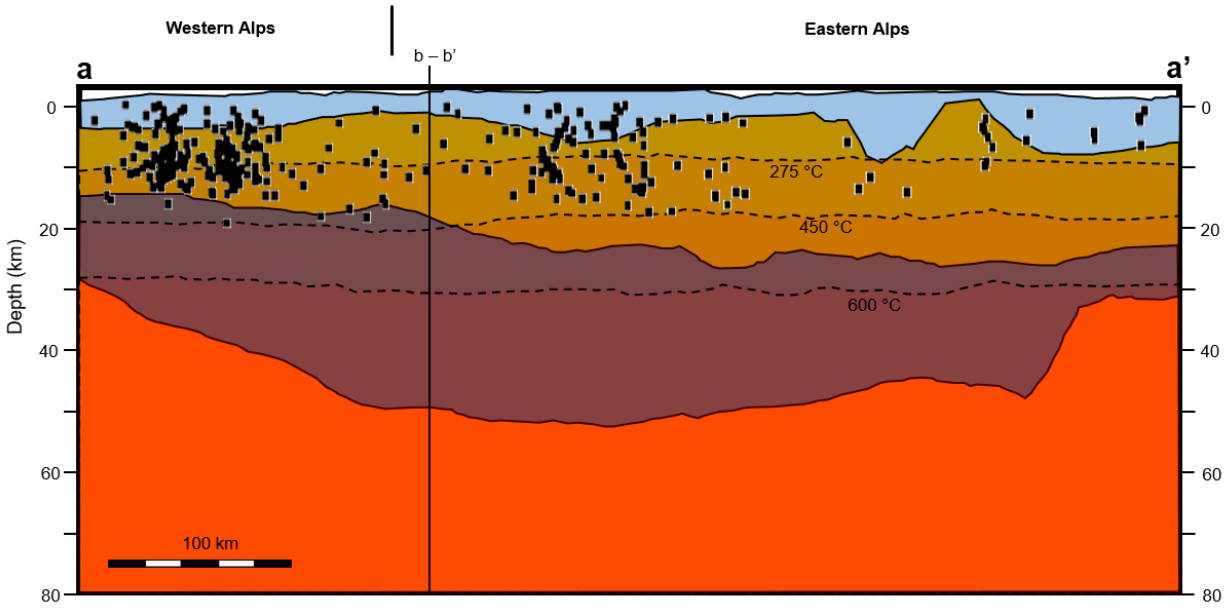

Figure 3.10. *A West to East cross section (a-a' in Figure 3.9) through the structural model. Thickness of model layers is shown: lithospheric mantle (red), lower crust (grey), upper crust (brown) and consolidated and unconsolidated sediments (blue). Isotherms for 275 °C, 450 °C and 600 °C are overlain as dashed black lines and seismicity from the International Seismological Centre (International Seismological centre, 2020) that lay within 20 km distance of the section has been marked as black dots.*

Cross section b-b' sheds light onto regional differences in the maximum depths of seismicity between different tectonic domains. As already mentioned, most seismicity within Europe and the Alps occurs at temperatures from 275 °C to 450 °C, corresponding mostly to the upper crust. With the exception of a couple of seismic events corresponding to the 600 °C isotherm at the base of the lower crust, all seismicity in Europe and the Alps terminates at the 450 °C isotherm. On the European plate, the maximum depth of seismicity is 20 km however

due to raised isotherms beneath the centre of the orogen the maximum depth below the Alps is 15 km. In the Adriatic and Apennine domains, seismicity is present uniformly throughout the upper and lower crusts from 275 °C down to temperatures of 600 °C and a depth of 25 km. Additionally, the location of known subduction interfaces within the model are also overlain to show that all seismicity recorded at temperatures higher than 600 °C corresponds to known subduction interfaces (e.g. Piana Agostinetti and Faccenna, 2018; Kästle et al., 2019).

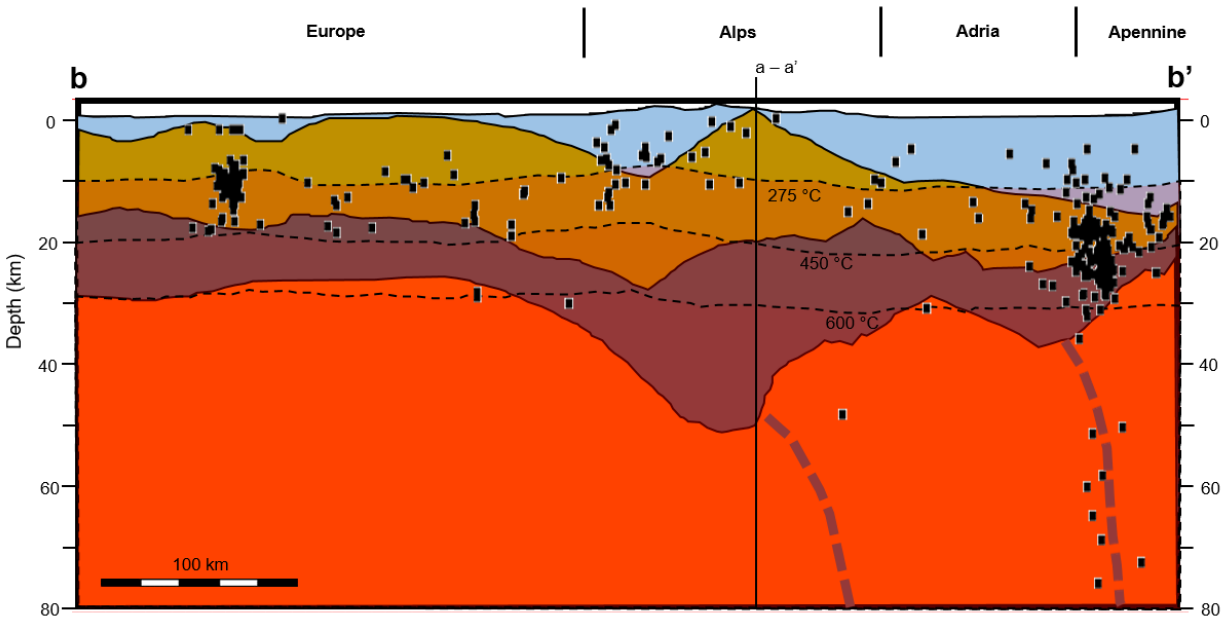

Figure 3.11. *A North to South cross section (b-b' in Figure 3.9) through the structural model. Thickness of model layers is shown: lithospheric mantle (red), lower crust (grey), upper crust (brown) and consolidated and unconsolidated sediments (blue). The location of unmodelled subduction interfaces have been marked as thick grey dashed lines. Isotherms for 275 °C, 450 °C and 600 °C are overlain as dashed black lines and seismicity from the International Seismological Centre (International Seismological centre, 2020) that lay within 20 km distance of the section has been marked as black dots.*

3.4. Discussion

3.4.1. Thermal Field

In line with previous studies (e.g. Lucazeau and Le Douaran, 1985; Stephenson et al., 2009; Scheck-Wenderoth et al., 2014; Sippel et al., 2014), results from the sedimentary depocentres of our model show that the shallow thermal field is largely controlled by the insulating effects of sedimentary blanketing. In the 5 km below sea level depth slice (Figure 3.5), temperatures are elevated by 20 °C in the Upper Rhine Graben and Molasse Basin with sedimentary thicknesses of 4 km and 5 km respectively. However, the effect of thicker sediments is less prominent in the temperature field at a crustal depth of 20 km suggesting that other factors control the temperature distribution at these crustal depths.

All main depocentres of the study area display different geothermal gradients, largely independent of their sedimentary thickness, however correlating closely with the depth of the LAB. The thermal gradient is highest in the Upper Rhine Graben (0.04 K/m) which also lies above the shallowest LAB (75 km). The higher thermal gradient in the Molasse Basin than the Po Basin, appears not solely related to the depth of the LAB as that is similar in both cases, however the upper crust below the Molasse Basin is significantly thicker than in the Po Basin, indicating radiogenic heating from the upper crust also plays a significant role. Our results demonstrate that the shallow thermal field in basins is primarily controlled by sedimentary blanketing, whilst the crustal thermal field is mostly influenced by the depth of the LAB and thickness of the radiogenic upper crust.

Outside of the basins, in regions of higher relief, the topographic effect is found to play a significantly larger role than sedimentary blanketing. In the 2 km below sea level depth slice (Figure 3.5), the Alps appear ~80 °C warmer than their forelands, with locally up to 140 °C predicted. This results from the higher relief since 2 km below sea level translates to 5-6 km below surface in the Alps. Accordingly, even for an average thermal gradient of 0.03 K/m, temperatures in the predicted range are to be expected. In contrast, below the forelands, that are elevated less than 600 m above sea level, relatively lower temperatures are reached. To further interrogate the effect of relief on the thermal field, temperatures from 2 and 20 km below sea level and below surface were extracted from the model and the resulting temperature difference visualised in Figure 3.12. The difference maps demonstrate that the topographic effect is indeed responsible for the largest part of the temperature difference between the orogen and forelands at shallow depths (around 80 °C at 2 km below sea level). The effect decreases

with increasing depth, but is still evident at a depth of 20 km below sea level with a difference of around 55 °C.

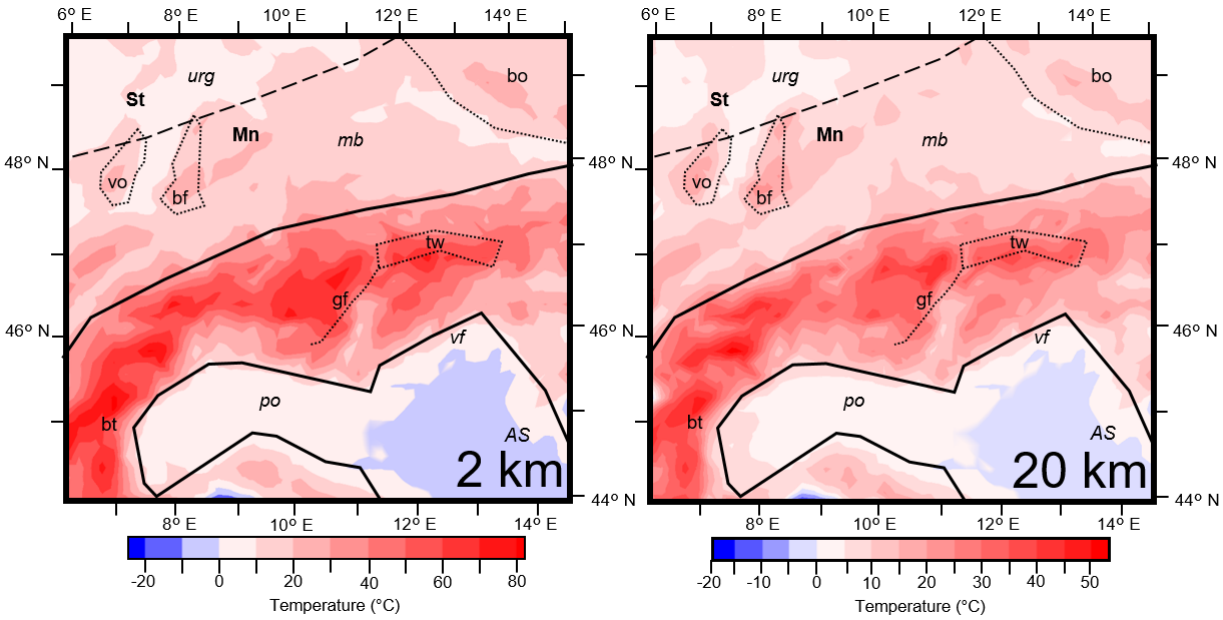

Figure 3.12. *Difference maps between temperature slices below sea and below surface at depths of 2 km and 20 km, showing the effect of topographic relief at either depth. Locations of key tectonic features are overlain (abbreviations shown in Figure 3.1 caption).*

The lessening impact of the topographic effect with depth is also mirrored by the increasing impact of upper crustal thickness on temperatures as depth increases. Areas of thicker Alpine upper crust that appear warmer than their surroundings include the Brianconnais terrane and the Tauern Window, with it also being the primary cause of the Alpine West to East cooling transition noted to correspond with the Guidicarie fault line seen in Figure 3.5. In the northern Alpine foreland, the Bohemian Massif is characterised by both thick upper crust and elevated relief. However, in accordance with the results by Przybycin et al. (2015), temperatures are not particularly elevated there since the exhumed Variscan basement acts as a heat chimney in the absence of insulating sediments.

The presence of European crust thicker (27.5 km) than Adriatic crust (22.5 km) explains why the northern foreland is warmer than the southern at all depth levels. However, these temperatures also correlate with the LAB depth. The LAB deepens southwestwards, shallowest

below the Upper Rhine Graben in the European domain (70 km) and deepest below the Adriatic Sea (140 km). LAB depth is also a primary driver of the observed West to East cooling of both the northern and southern forelands visible at all depth levels, and this effect also manifests in the nearby crustal blocks, with higher temperatures below the Vosges Massif compared to the adjacent Black Forest, both of which are represented by the same thermal parameters, relief and upper crustal thickness.

3.4.2. Lithological Inferences from Seismicity

Different minerals undergo brittle to ductile transition at different temperatures, (see Distribution of Seismicity section) which also act as the lower bound to the seismogenic zone. In polymineralic rocks, i.e. almost all crustal rocks, the brittle ductile transition for different minerals in the rock is reached at different temperatures (Evans et al., 1990) allowing approximate bulk lithological assumptions to be made based on the depths seismicity is present to in the different regions of the model. Across the European and Alpine domains, the upper crust shows a cut off in seismicity across the 450 °C isotherm, with seismicity centered around the 275 °C isotherm suggesting a bulk quartz-feldspathic lithology whilst the lower crust remains largely aseismic. Such lithology would also be consistent with observed seismic velocities and modelled densities in these domains (Spooner et al., 2019 and references therein). Seismicity is only present in the European foreland lower crust under 2 conditions: either (1) at temperatures cooler than 450 °C, suggesting a less mafic lithology than would be expected, which is supported with the results of previous work (Spooner et al., 2019), where the European lower crust is shown to have lower density (2800 kg/m3) than typical lower crust; or (2) related to European slab rollback under the Central Alps (Singer et al., 2014)

Expected limitations of the steady state methodology are observed through overestimated temperatures at subduction interfaces in the region. Although seismicity is known to terminate around 600 °C in these settings (Emmerson and McKenzie, 2007), we observe events occurring at modelled temperatures in excess of 1000 °C, where the Adriatic crust subducts below the northern Apennines. This is due to the crust being subducted faster than it can reach thermal equilibrium with the surrounding warmer mantle, requiring in the region of 1.6 ma after subduction has ended to achieve equilibrium (Fairley, 2016). However, as this effect is not accounted for in the steady state model, seismicity appears to occur at higher temperatures than would be expected.

Outside of subduction interfaces, seismicity occurs to the 600 °C isotherm in the Adriatic and Apennine upper and lower crusts, indicating a bulk lithology with higher pyroxene content for both than the European crusts. This is also consistent with the results of density modelling, where the southern foreland Adriatic crust is shown to be in general denser (2800 kg/m3) than the European crust (2750 kg/m3). Due to the topographic effect and the radiogenic heating of the thickened upper crust below the orogen, much of the alpine lower crust is hotter than 600 °C and seismicity is predominantly absent.

We find that in general the Adriatic upper crustal domain requires lower radiogenic heat production (1.30E-06 W/m3) and thermal conductivity (2.4 W/mK) than the European upper crustal domains (1.3- 2.6E-06 W/m3 and 2.4-3 W/mK), a trend visible even though each region is parameterised by multiple domains. The radiogenic heat values required to fit observations also indicate a more mafic (e.g. Hasterok and Webb, 2017) composition for the Adriatic crust than the European, which is consistent with the bulk lithology derived from density modelling or seismic velocities.

Indications that the Adriatic crust is more mafic in composition than the European crust are therefore supported by: 1) seismicity distribution relative to the thermal field and the brittle ductile transition of crustal minerals; 2) thermal properties necessary to fit measured wellbore temperatures; and 3) densities necessary to fit the measured gravity field. These bulk lithological observations in conjunction with the calculated temperatures and the previous 3D density-structural model of the region, can be used to shed light on the lateral changes in crustal strength within the Alps and their forelands, helping to explain the observed patterns of deformation and to create more accurate strength profiles throughout the region.

3.4.3. Importance of Limitations

The local mismatch of observed shallow temperatures with those predicted by a conductive heat transport simulation suggests that hydrothermal convection in the Upper Rhine Graben significantly effects the shallow thermal field of the region. This is in line with other works (e.g. Bächler et al., 2003; Freymark et al., 2017; Koltzer et al., 2019) that also suggested these effects are negligible below 10 km depth. Thus our findings for the relationships between observed crustal seismicity and the deep thermal field are robust. However, none of the other thermal effects unaccounted for in a steady state thermal model (examples listed in the Methodological Limitations section) are noticed during an interrogation of our results. Whilst

their impact is likely present, they are not of a magnitude that could result in visible systematic offset between measured and modelled temperatures.

Whilst an increase in resolution of 3D structural model, is nevertheless desirable, the largest limiting factor to the thermal field generated is the availability of measured temperature data. Even with a course 20 km x 20 km structural model resolution, as can be seen in Figure 3.7a, large portions of the orogen and either foreland lack any measured temperatures. Therefore, without an increase in coverage of measured temperatures an increase of model resolution would not result in a more accurate thermal field. To interrogate this, work is underway to quantify the sensitivity of thermal parameters used in this model in relation to the spacing of measured temperatures available.

3.4.4. Global Applicability

Observations made during this study of physical controls on the modelled thermal field remain applicable to a wide array of tectonic settings worldwide. We find that in central mountain belt settings, the thickness of the radiogenic upper crust, depth to the LAB and topographic effect have the largest impact on the thermal field, with a relief of 4 km raising temperatures by 50 °C at 20 km depth. In conjunction with associated upper crustal thickening resulting from orogenesis these raised temperatures result in maximum depths of seismicity more than 5 km shallower than in the forelands.

In basin settings, we find that in the absence of relief, the thickness of sedimentary deposits, the depth to the LAB and the magnitude of crustal thinning have the largest impact on the thermal field. The results also suggest that the advection of hot fluids and associated influence of localised faults in these regions are an important factor unaccounted for in this study. Similarly, in subduction zones we see that it is crucial to consider the transient thermal effects, such as the time taken for the downgoing crust to thermally equilibrate.

Inferences on lithology from the maximum observed depths of seismicity, align well with previous observations on bulk densities from gravity modelling, an indication that seismicity distribution in conjunction with a 3D thermal field can be used to gain a rough first order estimate of the bulk lithology of a region. These findings are not region specific and as seismicity represents a global issue, the techniques this study utilises can be applied worldwide in order to interrogate the relationship between seismicity and the lithospheric thermal field as a first step to quantifying seismic hazard.

3.5. Summary

By creating the first 3D steady state thermal field of the Alps and their forelands, validated with wellbore temperature measurements, that uses different thermal parameters for different tectonic domains, insights were gained into the controlling factors on the thermal field and lithological indications of each crustal block. The findings suggest that the shallow thermal field (0 - 10 km) is largely controlled by sedimentary blanketing or topographic effects, with the central orogen appearing 80 °C warmer than its forelands at a depth of 2 km below sea level and temperatures in the centre of the Molasse Basin 20 °C warmer than at the edges. We also show how the deeper thermal field (10 - 20 km) appears controlled by the LAB depth and the radiogenic contribution of the upper crust, with thickness and lithology (magnitude of radiogenic heat production) important influencing factors at crustal depths.

The European upper crustal domains require higher radiogenic heat productions and thermal conductivities (1.3-2.6E-06 W/m3 and 2.4-3 W/mK) than the Adriatic upper crust (1.30E-06 W/m3 and 2.4 W/mK). In conjunction with density observations, we use these thermal parameters to suggest the Adriatic crust is more mafic than the European. This is strengthened by observed differences in the clustering of seismicity at suspected brittle ductile transitions, with the Adriatic and Apennine plates demonstrating seismicity to higher temperatures, indicating a larger percentage of pyroxene than in the European crust.

Chapter 4. How biased are our models? – A Case Study of the Alpine Region

4.1. Introduction

Understanding the physical processes occurring within the subsurface is as important in the field of Geosciences as understanding climatic processes. In this paper, we focus on the understanding of the subsurface temperature field, which is of major importance for geothermal applications. Here, we focus on numerical process simulations to improve our understanding of the subsurface. These simulations are based on both geological and physical models, however in this paper, we will further investigate primarily the latter. The physical model has two major sources of uncertainties arising from the physical processes itself (i.e neglected processes, generalizations) (i.e. Houghton et al., 2001; Murphy et al., 2004; Refsgaard et al., 2007) and from the physical parameters (i.e. thermal conductivity, radiogenic heat production) in terms of ranges (i.e. Freymark et al., 2017; Lehmann et al., 1998; Vogt et al., 2010; Wagner and Clauser, 2005) and their distribution (i.e. Feyen and Caers, 2006; Floris et al., 2001).

To compensate for both sources of uncertainties, one commonly performs model calibrations, either deterministically (i.e. Doherty and Hunt, 2010; Fuchs and Balling, 2016; Hill and Tiedeman, 2006; Wellmann and Reid, 2014) or stochastically (i.e. Elison et al., 2019; Linde et al., 2017). Model calibrations aim to compensate for existing model error by adjusting the model parameters to a given data set. Naturally, the data set itself is subject to uncertainties. However, if we perform, for instance, stochastic model calibrations as Markov Chain Monte Carlo (Iglesias and Stuart, 2014), we are able to take these uncertainties into account. Nonetheless, there is another problem related to the data set and this is the data distribution. Note that in the following, we introduce the problems arising from data distribution through the example of temperature measurements. Still, many of the presented problems are generalizable for other geophysical data sources.

The first problem related to the data distribution is the depth location of the individual measurements. Our geothermal models have a depth in the magnitude of 100 km. In contrast, our deepest thermal measurements are commonly at a depth of 5 km to 7 km. The second problem is related to data density. Focusing on the horizontal data distribution, we face the problem of data sparsity and unequal data distribution. In certain model areas, we have very few temperature measurements and in other areas, we have a much larger data density. This inequality can be compensated by using data weighting schemes (i.e. Degen et al., 2020a;

Lerch, 1991). However, we also have areas where no temperature measurements exist. Data weighting cannot compensate for these non-existent measurements. The problem is further enlarged by the data source. Most of our temperature measurements come from the hydrocarbon industry, however, their targets and those of the geothermal industry are not the same in every region. This means that we can face the problem of lower data resolution in areas of interest whilst possessing higher data resolution in areas that are not of primary interest.

The problem of data sparsity is long and widely recognized (i.e. Cherpeau and Caumon, 2015; Zehner et al., 2010). However, there are no studies systematically investigating the bias we introduce due to temperature measurements in a geothermal setting. Studies for the measurement bias are common in the field of remote sensing (i.e. Feng et al., 2016; Schwarz et al., 2020), however, their focus is entirely different. In remote sensing, the location of the measurements is subjected to uncertainties. In contrast, our problems do not arise from imprecise measurement locations but their distribution. Naturally, our locations are also associated with uncertainties, however, in basin-scale applications they are of minor importance.

In this paper, we aim to provide a systematic investigation of the bias induced by measurement distribution. Therefore, we perform global sensitivity analyses to determine the influence of the model parameters (i.e. thermal conductivity, radiogenic heat production) on the model response (i.e. temperature). Sensitivity analyses can be subdivided into local and global analyses. We choose a global sensitivity analysis to investigate not only the influence of the parameters itself but also the parameter correlations. Note that a local sensitivity analysis assumes that all parameters are independent of each other (Degen et al., 2020a; Saltelli, 2002; Saltelli et al., 2010; Sobol, 2001; Wainwright et al., 2014). Furthermore, we want to avoid a possible overestimation of the influences. A previous model study showed that the local sensitivity analysis can overestimate the influences (Degen et al., 2020a). Global sensitivity analyses have been performed before in, for example, Baroni and Tarantola (2014); Cannavó (2012); Cloke et al. (2008); Degen et al. (2020a); Fernández et al. (2017); van Griensven et al. (2006); Song et al. (2015); Tang et al. (2007); Wainwright et al. (2014); Zhan et al. (2013), however, they are either in a different geophysical setting and or with a different focus of interest.

Global sensitivity analyses have the disadvantage of being computationally very demanding since they require several thousand to several hundred-thousands forward simulations. This makes these analyses infeasible even for state-of-the-art finite element

problems. To compensate for the expensive nature of the method, we employ the reduced basis method to construct suitable surrogate models. The principle idea is to replace the original high dimensional model with a low dimensional model while keeping the key characteristic of the problem (Benner et al., 2015; Hesthaven et al., 2016; Prud'homme et al., 2001; Quarteroni et al., 2015). In this paper, we do not focus on the observation space alone but also investigate the entire temperature state. Hence, we need a surrogate model for the entire state. The reduced basis method is able to provide us with this, in contrast to many other surrogate model techniques (Ba¸s and Boyacı, 2007; Bezerra et al., 2008; Frangos et al., 2010; Khuri and Mukhopadhyay, 2010; Miao et al., 2018; Mo et al., 2019; Myers et al., 2016; Navarro et al., 2018). The reduced basis method is widely known in mathematical applications (i.e. Benner et al., 2015; Grepl, 2005; Hesthaven et al., 2016; Aretz-Nellesen et al., 2019; Kärcher et al., 2018; Prud'homme et al., 2001; Quarteroni et al., 2015; Rozza et al., 2007), however only few geoscientific applications exist (Degen et al., 2019). Nevertheless, some studies do use comparable approaches (Ghasemi and Gildin, 2015; Gosses et al., 2018; Rizzo et al., 2017; Rousset et al., 2013; Zlotnik et al., 2015).

In this paper, we investigate the problems related to the data distribution for the case study of the Alpine Region. The geological model, covering the Alpine orogen and its forelands, is taken from a previous study (Spooner et al., 2020). Thermal studies of the Alpine Region are of interest to understand how the present-day deformation is linked to the thermal field. Therefore, we want to illustrate how the interpretation of the temperature field might be biased.

4.2. Materials and Methods

In the following, we briefly introduce the concepts of global sensitivity analyses and the reduced basis method. Furthermore, we introduce the physical model and the temperature data used throughout this study.

4.2.1. Global Sensitivity Analysis

In this study, we investigate the measurement bias and therefore require knowledge of which parameters the temperature distribution is sensitive to. Therefore, we employ a sensitivity analysis (SA). We distinguish two types of sensitivity analyses: local and global. The local sensitivity analysis investigates the influence of the model parameters with respect

to a user-defined reference parameter set. All parameter variations are considered independent of each other and only the vicinity of the input parameters is explored (Sobol, 2001; Wainwright et al., 2014). In contrast, the global sensitivity analysis explores the entire parameter space and also investigates the parameter correlations (Sobol, 2001). In this paper, we use a global sensitivity analysis with the Saltelli sampler (Saltelli, 2002; Saltelli et al., 2010), and we investigate two types of sensitivity indices: the first- and total order indices. First-order indices describe the influence arising from the model parameter itself. Total-order indices additionally contain information about the parameter correlation (Sobol, 2001). We perform the SA with the Python library SALib (Herman and Usher, 2017) and 100,000 realizations per parameter to reduce the statistical error. For further information regarding the global sensitivity analysis refer to Sobol (2001); Saltelli (2002); Saltelli et al. (2010), and for a comparison between local and global sensitivity analysis to Wainwright et al. (2014) and Degen et al. (2020a).

4.2.2. Forward Problem

For this case study, we are using a conductive heat transfer problem (Turcotte and Schubert, 2002). To ensure that we investigate the relative importance of the parameters and for better efficiency, we use the following non-dimensional form:

$$\frac{\lambda}{\lambda_{ref}\, S_{ref}} \frac{\nabla^2}{l_{ref}^2} \left(\frac{T - T_{ref}}{T_{ref}} \right) + \frac{S}{S_{ref}\, T_{ref}\, \lambda_{ref}} \tag{4.1}$$

where λ is the thermal conductivity, S the radiogenic heat production, and T the temperature. The subscript "ref" denotes the respective reference parameters and l_{ref} the reference length. Note that the Laplace-operator acts on the normalized space.

4.2.3. Reduced Order Modelling

In this work, we require a surrogate model that is representative of the entire temperature state to ensure the feasibility of the study. Therefore, we use the reduced basis (RB) method for the surrogate model construction, a projection based model order reduction technique. It aims to replace the original high dimensional model with a low dimensional representation while keeping the input-output relationship the same. Hence, the method

preserves the underlying physics. One limitation of the RB method is that it is restricted to underlying low dimensional parameter spaces. With higher dimensional parameter spaces the complexity of the parameter space tends to increase, leading to longer construction times and surrogate model dimensions that are too large. The RB method destroys the sparsity pattern of the system, meaning that a large surrogate model will require a longer execution time than the original finite element model due to its dense nature. To overcome this issue, we use a hierarchical sensitivity study as we will discuss in Section 4.3.1.

The RB method compromises two parts: the offline and online stages. During the offline stage, we construct our surrogate model. This stage is computationally expensive but needs to be performed only once. In the online stage, we use the low dimensional surrogate model. This stage is computationally fast and therefore ideal for expensive outer loop processes such as the global sensitivity analysis. In previous studies, we showed that the RB method yields a speed-up of several orders of magnitude for the here described physical problem (Degen et al., 2019, 2020a).

All reduced models are generated with the software package DwarfElephant (Degen et al., 2019). Degen et al. (2019) also contains a detailed description of the reduced order model construction, which is omitted here for the sake of clarity. For further information regarding the RB method refer to Hesthaven et al. (2016); Prud'homme et al. (2001); Quarteroni et al. (2015) and a detailed overview of various model order reduction techniques is provided in Benner et al. (2015). Further information regarding the RB method in the field of Geosciences is presented by Degen et al. (2019) and specifically for basin-scale thermal applications in (Degen et al., 2020a).

4.2.4. Temperature Data

We present the temperature data set in form of a histogram in Figure 4.1, and illustrate the spatial distribution in Figure 4.2. This temperature data is identical to the one presented in Spooner et al. (2020). The entire data set compromises 8120 measurements with a maximum depth of 7.3 km and a mean depth of 1.8 km. The Italian National Geothermal Database (Trumpy and Manzella, 2017) provides the data for the southern foreland. For the northern foreland, the data is derived from the Upper Rhine Graben data base provided in Freymark et al. (2017) and references therein. The data of the Molasse Basin is retrieved from Przybycin et

al. (2015) and references therein, whereas the data from the Alps is compiled from Luijendijk et al. (2020).

The spatial distribution of measurements varies widely across the region, sparse in the Molasse Basin (103) and Alps (83) to dense in the Po Basin (7,619). In an effort to alleviate a significant bias and to improve the efficiency of the presented methods, the dataset was filtered to give a more uniform measurement density across the region, with a significant reduction in the Po Basin (2,028) whilst retaining those in the Molasse Basin (103) and Alps (83). Deeper measurements (> 2 km) were preferentially maintained throughout the region as they better indicate crustal temperatures, a particular focus of the work undertaken here. This resulted in a filtered dataset of 2,388 wellbore temperatures measurements with a mean depth of 2.3 km.

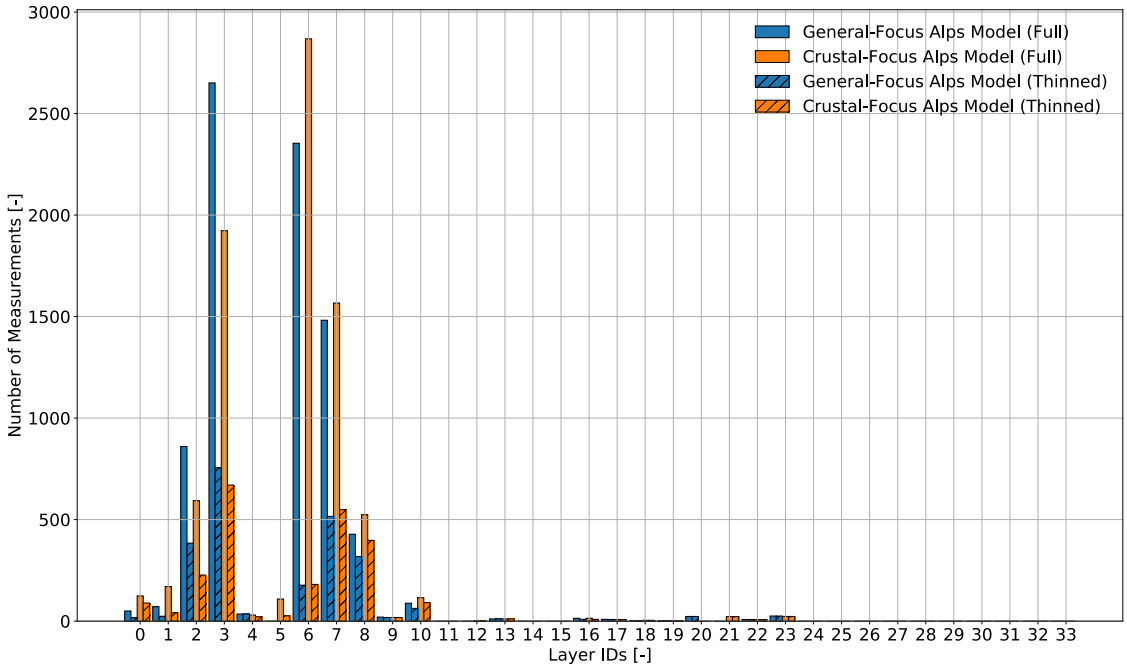

Figure 4.1. *Distribution of the measurements according to the geological layers. For the Layer IDs please refer to Table 4.1.*

Layer	Layer ID	Property	Acronym
Unconsolidated Sediments URG (top 1km)	0	Thermal Conductivity Radiogenic Heat Production	λ_0 S_0
Unconsolidated Sediments URG (below 1km)	1	Thermal Conductivity Radiogenic Heat Production	λ_1 S_1
Unconsolidated Sediments Rest (top 1km)	2	Thermal Conductivity Radiogenic Heat Production	λ_2 S_2
Unconsolidated Sediments Rest (below 1km)	3	Thermal Conductivity Radiogenic Heat Production	λ_3 S_3
General-Focus Model: Unconsolidated Sediments Molasse	4	Thermal Conductivity Radiogenic Heat Production	λ_4 S_4
Crustal-Focus Model: Unconsolidated Sediments Molasse (top 1km)	4	Thermal Conductivity Radiogenic Heat Production	λ_4 S_4
Unconsolidated Sediments Molasse (below 1km)	5	Thermal Conductivity Radiogenic Heat Production	λ_4 S_4
Unconsolidated Sediments Po Basin (top 2km)	6	Thermal Conductivity Radiogenic Heat Production	λ_6 S_6
Unconsolidated Sediments Po Basin (below 2km)	7	Thermal Conductivity Radiogenic Heat Production	λ_7 S_7
Consolidated Sediments	8	Thermal Conductivity Radiogenic Heat Production	λ_8 S_8
Consolidated Sediments Molasse	9	Thermal Conductivity Radiogenic Heat Production	λ_9 S_9
Consolidated Sediments Po Basin	10	Thermal Conductivity Radiogenic Heat Production	λ_{10} S_{10}
Upper Crust Apennine	11	Thermal Conductivity Radiogenic Heat Production	λ_{11} S_{11}
Upper Crust Istrea	12	Thermal Conductivity Radiogenic Heat Production	λ_{12} S_{12}
Upper Crust Moldanubia	13	Thermal Conductivity Radiogenic Heat Production	λ_{13} S_{13}
General-Focus Model: Upper Crust Bohemia	14	Thermal Conductivity Radiogenic Heat Production	λ_{14} S_{14}
Crustal-Focus Model: Upper Crust Bohemia	14	Thermal Conductivity Radiogenic Heat Production	λ_{14} S_{14}
Upper Crust Bohemia Volcanics	15	Thermal Conductivity Radiogenic Heat Production	λ_{14} S_{14}
Upper Crust Saxothuringia	16	Thermal Conductivity Radiogenic Heat Production	λ_{16} S_{16}
Upper Crust Vosges	17	Thermal Conductivity Radiogenic Heat Production	λ_{17} S_{17}
Upper Crust Molasse	18	Thermal Conductivity Radiogenic Heat Production	λ_{18} S_{18}
Upper Crust East Alps	19	Thermal Conductivity Radiogenic Heat Production	λ_{19} S_{19}
General-Focus Model: Upper Crust West Alps	20	Thermal Conductivity Radiogenic Heat Production	λ_{20} S_{20}
Crustal-Focus Model: Upper Crust West Jura	20	Thermal Conductivity Radiogenic Heat Production	λ_{20} S_{20}
Upper Crust West Alps	21	Thermal Conductivity Radiogenic Heat Production	λ_{20} S_{20}
Upper Crust Po Basin	22	Thermal Conductivity Radiogenic Heat Production	λ_{22} S_{22}
Upper Crust North East Adria	23	Thermal Conductivity Radiogenic Heat Production	λ_{23} S_{23}
Upper Crust Ivrea	24	Thermal Conductivity Radiogenic Heat Production	λ_{24} S_{24}
Upper Crust South East Adria	25	Thermal Conductivity Radiogenic Heat Production	λ_{25} S_{25}
Lower Crust Saxothuringia	26	Thermal Conductivity Radiogenic Heat Production	λ_{26} S_{26}
Lower Crust Moldanubia	27	Thermal Conductivity Radiogenic Heat Production	λ_{27} S_{27}
Lower Crust Alps	28	Thermal Conductivity Radiogenic Heat Production	λ_{28} S_{28}
Lower Crust Ivrea	29	Thermal Conductivity Radiogenic Heat Production	λ_{29} S_{29}
Lower Crust Liguria and Apennine	30	Thermal Conductivity Radiogenic Heat Production	λ_{30} S_{30}
Lower Crust Adria	31	Thermal Conductivity Radiogenic Heat Production	λ_{31} S_{31}
Lithospheric Mantle North West	32	Thermal Conductivity Radiogenic Heat Production	λ_{32} S_{32}
Lithospheric Mantle South East	33	Thermal Conductivity Radiogenic Heat Production	λ_{33} S_{33}

Table 4.1. *Acronyms and Layer IDs for both the General-Focus and Crustal-Focus Model*

4.2.4.1 Weighting

A common issue of the temperature data for the calibration of thermal models is their unequal distribution. To compensate for this inequality, we introduce a weighting scheme in this paper. There are different possibilities to weight the measurement data. In this paper, we use a regional weighting scheme that combines quantitative measures and our knowledge about the geophysical settings and the data quality. As previously mentioned the data set was reduced to 2,388 data points in total. We subdivide the model into four regions:

- the Alps with 83 measurements,
- the URG with 177 measurements,
- the Molasse with 103 measurements,
- and the Po Basin with 2028 measurements.

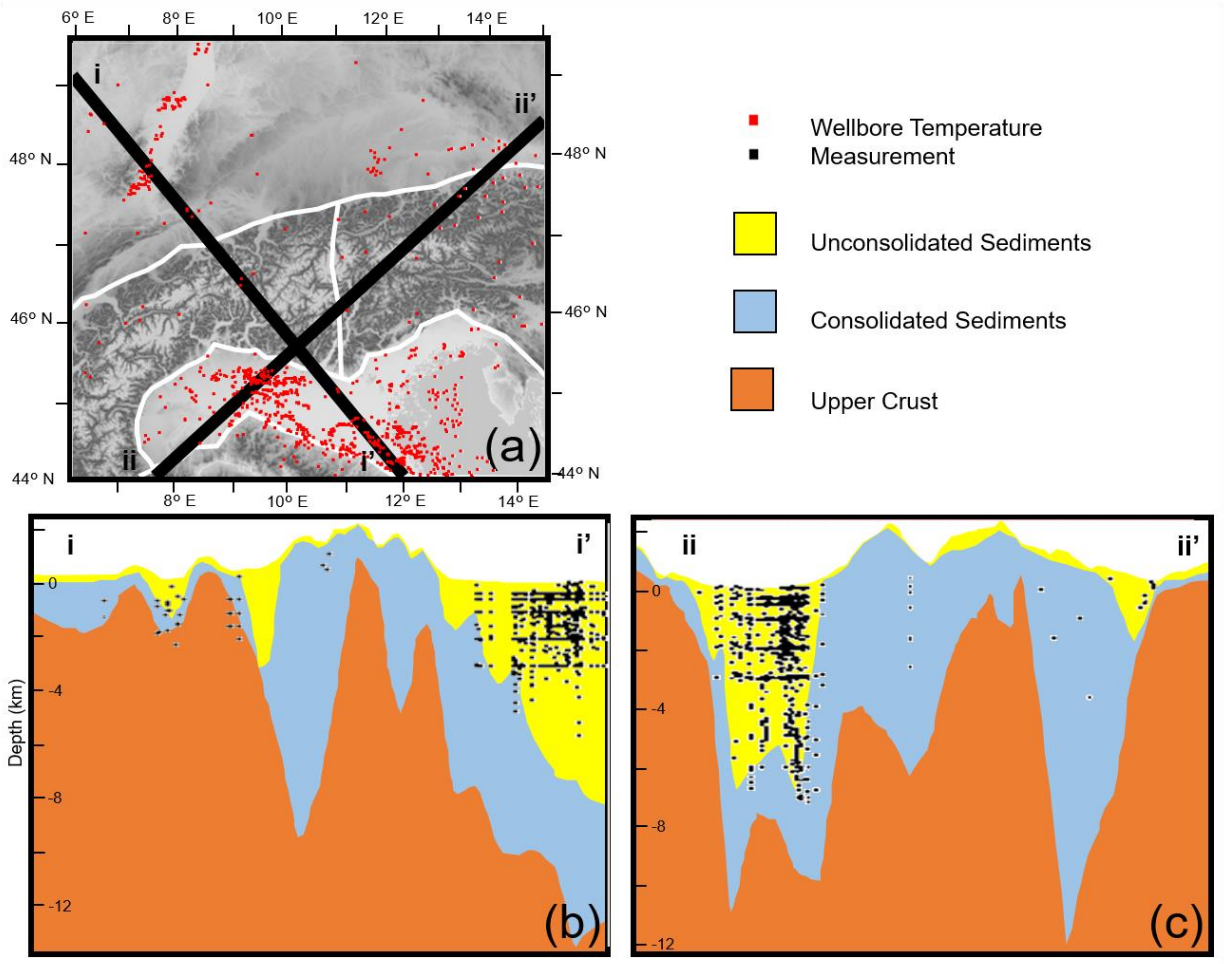

Figure 4.2. *Spatial distribution of the temperature measurements a) projected on the surface, b) along the crossection i, and c) along the crossection ii.*

As we can see, the Po Basin contains many more temperature measurements than the other regions. Additionally, we need to take into account that the temperature measurements of the Alps are non-robust since they are minimum temperature values. Also, the data from the Upper Rhine Graben needs to be treated carefully since we do not account for convective processes in this paper. These aspects yield the following weighting scheme:

- the Po Basin is not weighted,
- the Molasse is weighted by a factor of 20 since the Po Basin contains 20 times more data points,
- and the Upper Rhine Graben and the Alps are weighted by a factor 0.5.

4.3. Alpine Region

In this paper, we study two versions of the Alps Model:

1. The first one focuses on the Sediments and the Lithospheric Mantle. This model has been presented in Spooner et al. (2020) and is from here on denoted as the "General-Focus Alps" model. It consists of 31 geological layers. Each layer has a homogeneous and isotropic thermal conductivity and radiogenic heat production.
2. The second model concentrates on the Upper Crust and is denoted as the "Crustal-Focus Alps" model. This model contains 34 geological layers, again each layer has a homogeneous and isotropic thermal conductivity and radiogenic heat production.

Both models have an extent of 640 km in the x-direction and 600 km in the y-direction. In the vertical direction, both models extend down to the Lithosphere-Asthenosphere Boundary (LAB). The models are discretized using hexahedrons with a horizontal resolution of about 21.33 km × 19.35 km.

At the top of both models we apply a Dirichlet boundary condition representing the annual average surface temperatures (Böhm et al., 2009; Fan and Van den Dool, 2008; Locarnini et al., 2013) varying from -10 °C (Alps) to 16 °C (Adriatic Sea). Additionally, at the base of the model, we assign a Dirichlet boundary condition varying between 1250 °C below the Vosges massif and 1400 °C below the Bohemian massif (Schaeffer and Lebedev, 2013). For further information regarding the physical and geological setting of the General-Focus Alps model refer to Spooner et al. (2020).

For the reference thermal conductivity, we use a value of 3.0 W m^{-1} K^{-1} (corresponding to the largest thermal conductivity). Analogously, the reference length is 640,000 m (corresponding to the maximum model extent), and the reference radiogenic heat production 2.6 µW m-3 (corresponding to the largest radiogenic heat production). The reference parameters are the same for both models.

In this paper, in addition to the General-Focus Alps model, already presented in Spooner et al. (2020) we use the Crustal-Focus Alps model, where the Upper Crust below the Po Basin was thinned (with requisite thickening of the Lower Crust carried out in order to compensate) in order to better fit temperature observations from the previous thermal modelling work (Spooner et al., 2020). Inconsistencies in the original classification of Unconsolidated Sediments and Consolidated Sediments were also rectified, specifically in the region of the Southern Alps. Small alterations to the depth of the Moho were also made as a result of more recent observations (Magrin and Rossi, 2020). The gravity residual of the newly generated structural model was then re-minimised using the same methodology described in Spooner et al. (2019), achieving a misfit as good as the original model.

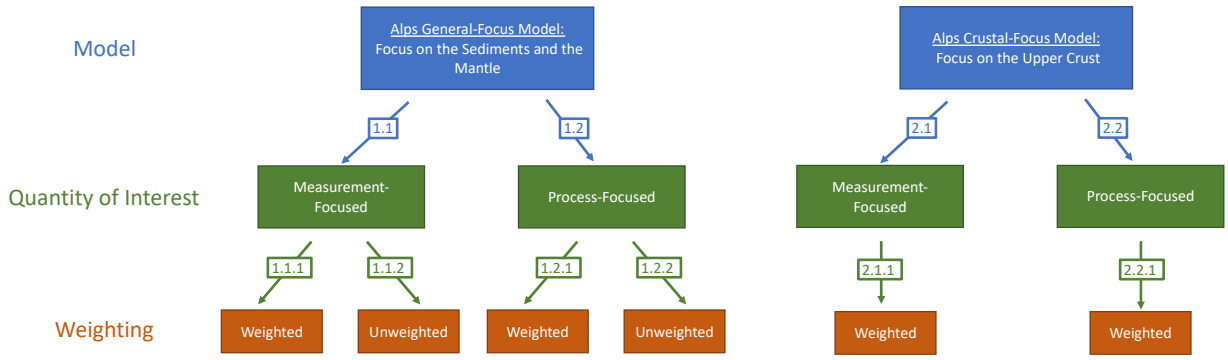

Figure 4.3. *Schematic overview of the models used in this paper.*

4.3.1. Thermal Model

To avoid the problem of the parameter space dimension becoming too large, we perform a hierarchical global sensitivity analysis. The setup for both the General-Focus and Crustal-Focus Alps model is the same. Therefore, we explain the hierarchical sensitivity analysis using the General-Focus Alps model. For the top level sensitivity analysis, we separately combine layers with equal thermal conductivities and radiogenic heat productions, reducing the number of thermal parameters from 62 to 19. This top level sensitivity analysis investigates the influences of the thermal properties in the entire model region. However, the investigated properties combine several entities, so in order to isolate the thermal properties that are influencing the temperature distribution, we perform additional sensitivity analysis for those properties that exceed our threshold of 1·10-2. This threshold was chosen at a level, where we observed a significant decrease in the sensitivity indices. In total, we perform three additional sensitivity analysis for the:

1. Unconsolidated Sediments and the Lower Crust (red rectangle of Figure 4.4 and Peak 1 of Figure 4.5),
2. Unconsolidated and Consolidated Sediments (gray rectangle of Figure 4.4 and Peak 2 of Figure 4.5),
3. and the Upper Crust (blue rectangles of Figure 4.4 and Peak 3 of Figure 4.5).

Each of these additional sensitivity analyses also contains a thermal parameter from the top level sensitivity analysis to enable a comparison between all analyses. We investigate all thermal properties of the Upper Crust and not only those that are above the threshold since the Upper Crust has been the primary interest in previous studies (Spooner et al., 2020). The setup of the hierarchical sensitivity analysis is shown in Figure 4.4 and 4.5. Note that in this section we only present the setup of the hierarchical sensitivity analysis. A detailed presentation of the individual analyses follows in the next sections.

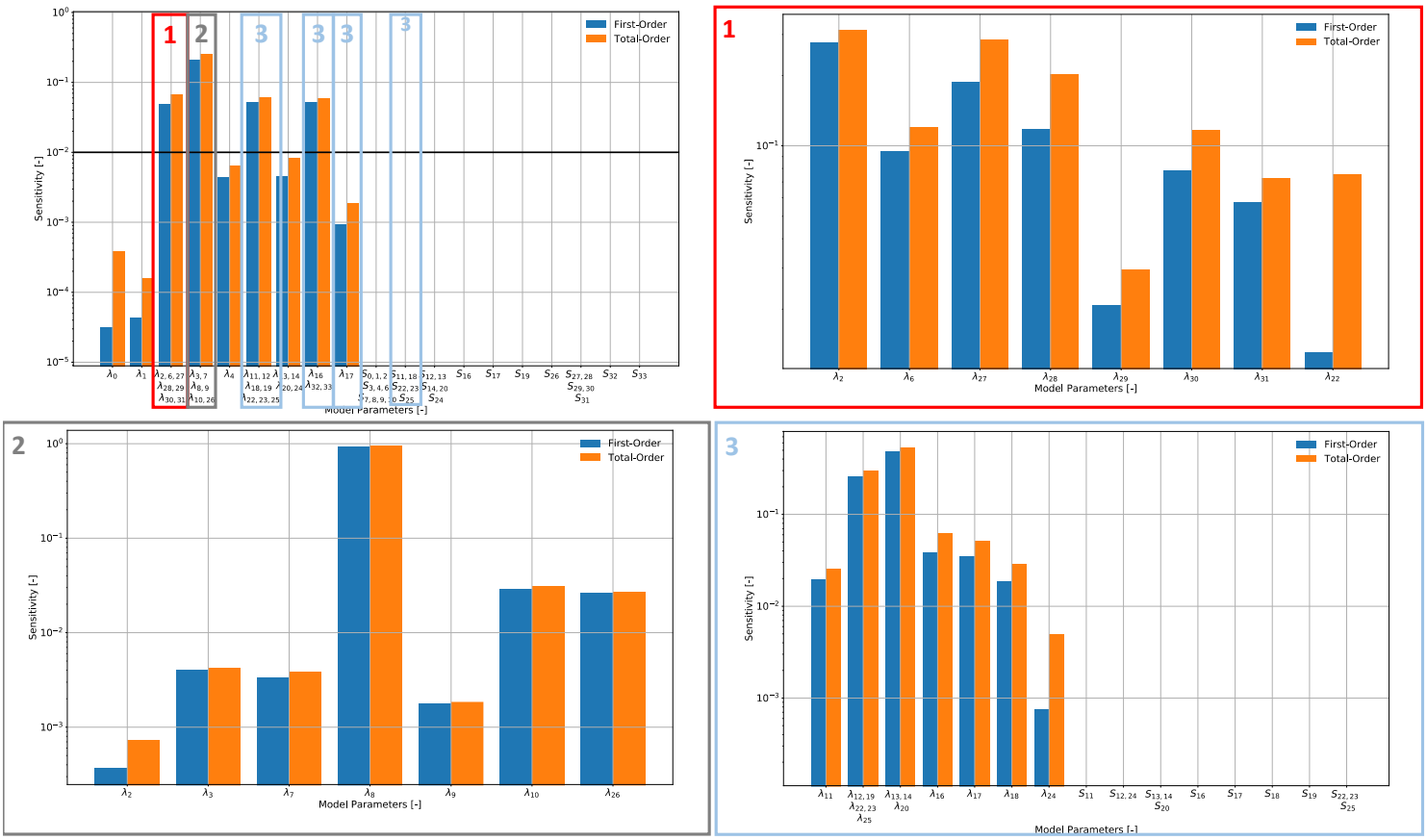

Figure 4.4. *Representation of the hierarchical process-focused sensitivity analysis of the General-Focus Alps model. For the Layer IDs and acronyms please refer to Table 4.1.*

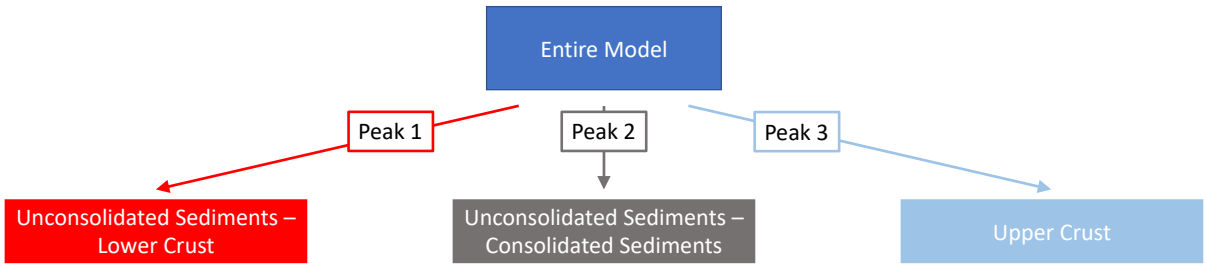

Figure 4.5. *Schematic representation of the hierarchical global sensitivity analysis.*

4.3.2. Influence of the Quantity of Interest

In this paper, we want to investigate how much our analyses are influenced by focusing on measurements. This is important since we calibrate and validate our analyses with, for instance, temperature measurements. The sensitivity analysis investigates the relative changes that are induced by changes in the model parameters (i.e. thermal conductivity and radiogenic heat production). For the sensitivity analysis, we need to define a quantity of interest, which allows us to define with respect to what measure the changes are investigated. To investigate the influence of the measurements, we perform the hierarchical sensitivity analyses with two different quantities of interest for the General-Focus Alps model (branch 1.1 and 1.2 of Figure 4.3):

1. The first quantity of interest is defined as the sum of the absolute temperature values of the entire model. This results in a sensitivity analysis that is representative of the physical processes since all regions in the model are treated equally.
2. The second quantity of interest is defined as the absolute misfit between the simulated and measured temperature values. Hence, the resulting sensitivity analysis is focused on the temperature measurements.

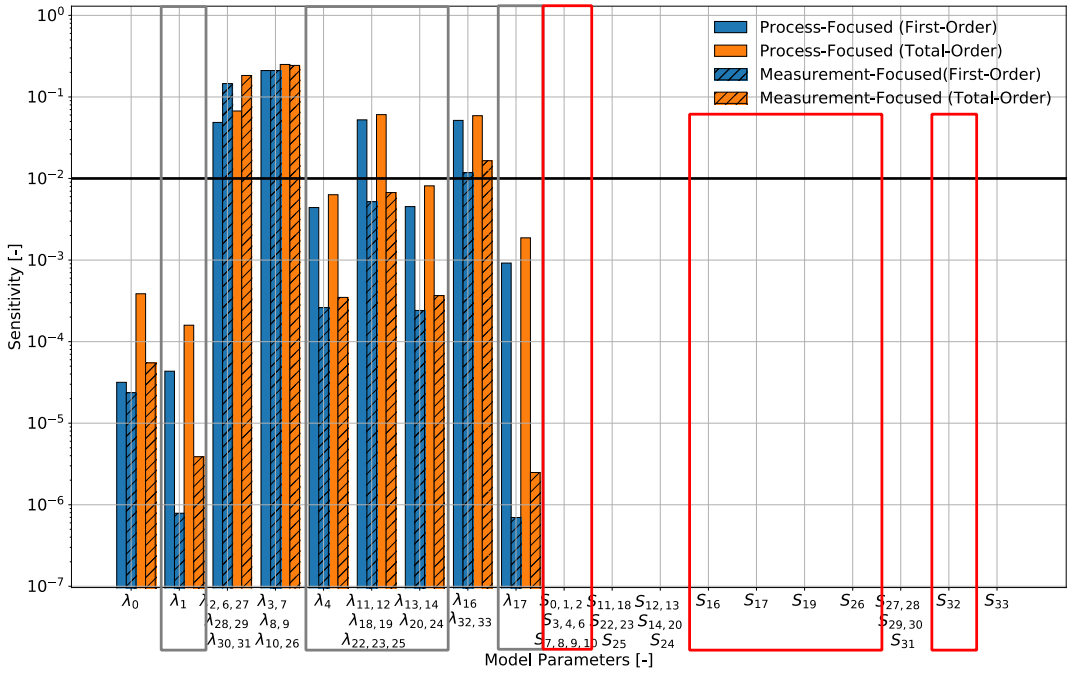

Figure 4.6. *Top level sensitivity analysis (focusing on the entire Alps model) with different quantities of interest of the hierarchical global sensitivity analysis for the General-Focus Alps model. For the Layer IDs and acronyms please refer to Table 4.1.*

In the following, we focus on the difference in the total order sensitivity indices between those two hierarchical sensitivity analyses (branch 1.1 and 1.2 of Figure 4.3) to present the bias introduced by the measurements and the consequences of using temperature data from the hydrocarbon industry for the calibration of geothermal models. In this study, we use only the General-Focus Alps model to avoid any influence from factors other than the measurements. Focusing on the difference between the hierarchical sensitivity analyses, we make two key observations:

1. We observe tendentiously higher difference for the thermal conductivities of deeper geological layers. This is highlighted in Figure 4.6 with gray rectangles. Here, we observe the highest differences for:
   - λ_1 being the thermal conductivity of the Unconsolidated Sediments of the Upper Rhine Graben below 1 km,
   - λ_4 being the thermal conductivity of the Unconsolidated Sediments of the Molasse Basin,
   - λ_{11},λ_{12}, λ_{18}, λ_{19}, λ_{22}, λ_{23}, and λ_{25} compromising the thermal conductivities of the Appennine, Istrea, Molasse, East Alps, Po, and the North East and South East Adria Upper Crust,
   - λ_{13}, λ_{14}, λ_{20}, and λ_{24} compromising the thermal conductivities of the Moldanubia, Bohemia, West Alps, and Ivrea Upper Crust,
   - λ_{17} being the thermal conductivity of the Vosges Upper Crust.

   Furthermore, this can be confirmed by looking at the additional sensitivity analysis of the Unconsolidated Sediments–Lower Crust (Figure 4.7), where we observe higher differences for the Lower Crust thermal conductivities.

2. The difference in the sensitivity indices tend to be larger for the radiogenic heat production than for the thermal conductivity. This is highlighted in Figures 4.6 and 4.9 with red rectangles.

Furthermore, in the case of the process-focused analyses, the model is sensitive to more parameters and we obtain a slightly higher parameter correlation.

Now, we focus on the difference observable for the analysis of the Unconsolidated and Consolidated Sediments. For both sediment types, we obtain huge differences in the sensitivities. For the thermal conductivities of the Unconsolidated Sediments, the measurement-focused analysis returns tendentiously higher influences, whereas for the

Consolidated Sediments the process-focused analysis results in tendentiously higher influences of the thermal conductivities.

Finally, we switch our focus to the analysis of the Upper Crust. For the Upper Crust, we observe six thermal conductivities with a significant difference in the sensitivity indices:

- λ_{13}, λ_{14}, and λ_{20} compromising the thermal conductivities of the Moldanubia, Bohemia, and West Alps Upper Crust,
- λ_{16} being the thermal conductivity of the Saxothuringia Upper Crust,
- λ_{17} being the thermal conductivity of the Vosges Upper Crust,
- λ_{18} being the thermal conductivity of the Molasse Upper Crust,
- λ_{24} and being the thermal conductivity of the Ivrea Upper Crust.

The differences for the radiogenic heat production are the highest for:

- S_{12} and S_{24} compromising the radiogenic heat production of the Istrea and Ivrea Upper Crust,
- S_{22}, S_{23}, and S_{25} compromising the radiogenic heat production of the Po, North East, and South East Adria Upper Crust.

Note that we do not present the results of the Upper Crust sensitivities in Figure 4.7 and the Lower Crust sensitivities in Figure 4.8. Both are properties from the top level sensitivity analysis and are required to enable a comparison between the different analyses. However, they represent only one property from the lithological unit. Therefore, they are not representative for any kind of trend analysis.

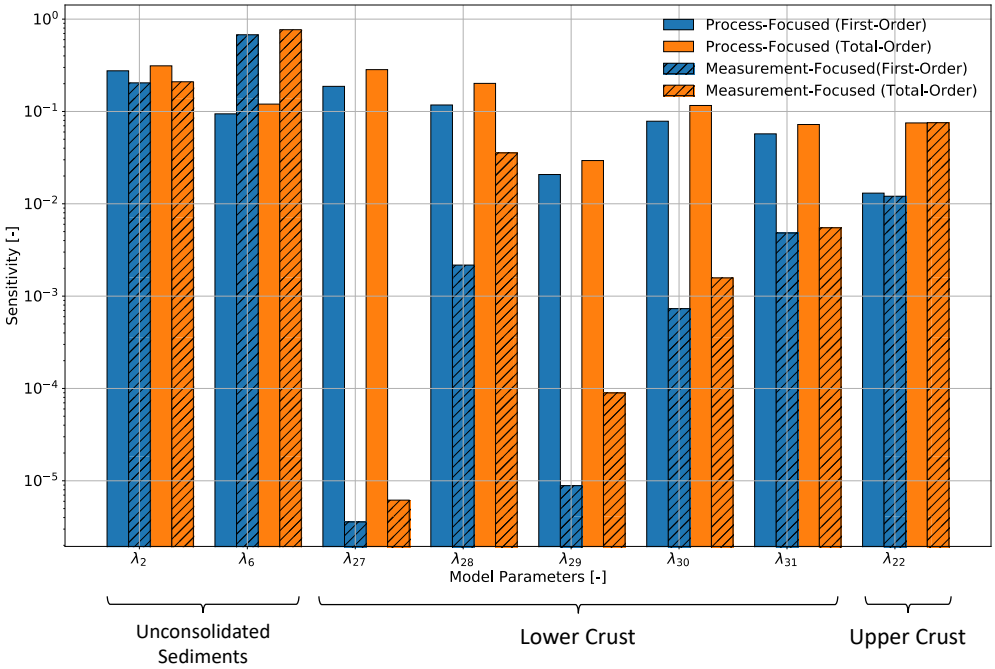

Figure 4.7. *Sensitivity analysis of the Unconsolidated Sediments and Lower Crust with different quantities of interest of the hierarchical global sensitivity analysis for the General-Focus Alps model. For the Layer IDs and acronyms please refer to Table 4.1.*

4.3.3. Influence of the Weighting

The consequences of introducing a weighting scheme have been already partly addressed in Degen et al. (2020a). However, there the authors focused on the consequences for the process of model calibrations. Here, we want to investigate how we can compensate for the measurement bias by applying weights.

Analogous to the previous section, we focus on the differences in the total order sensitivity indices. For all analyses, we can observe that the weighted scenario tends to be closer to the process-focused analysis than the non-weighted scenario for the thermal conductivities. This is highlighted by the gray rectangles in Figures 4.10 and 4.13. The behavior is very prominent for the thermal conductivity of the Moldanubia Lower Crust (gray rectangle of Figure 4.11).

In contrast, we observe for the thermal conductivities of the Upper Rhine Graben layers a closer resemblance of the non-weighted scenario to the process-focused analysis (blue rectangle of Figure 4.10).

We also observe, for the radiogenic heat production, that for most layers the indices of the weighted case are closer to the process-focused analysis than the non-weighted (red rectangles of Figure 4.10). Differing from this trend is the radiogenic heat production of the Istrea and Ivrea Upper Crust. Furthermore, we observe that the weighted analysis overestimates the influence of the Molasse Upper Crust (Figure 4.13).

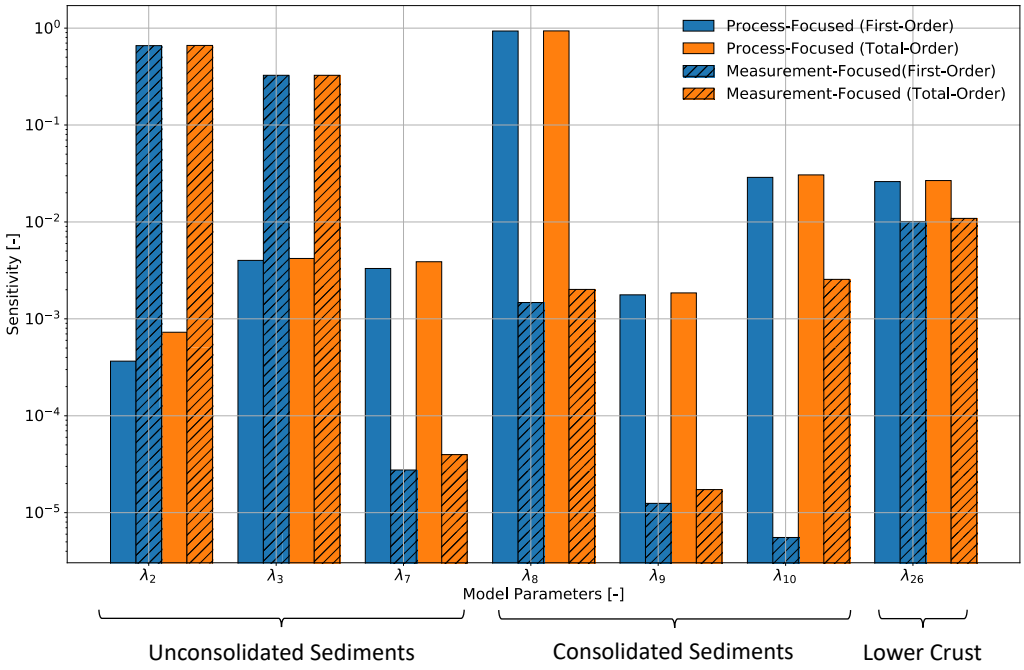

Figure 4.8. *Sensitivity analysis of the Unconsolidated and Consolidated Sediments with different quantities of interest of the hierarchical global sensitivity analysis for the General-Focus Alps model. For the Layer IDs and acronyms please refer to Table 4.1.*

4.4. Discussion

In the following, we discuss the consequences of focusing a study on measurements. Therefore, we discuss the changes in the sensitivities for the different quantities of interest and weighting schemes. Furthermore, we demonstrate the consequences through a deterministic model calibration example.

4.4.1. Influence of the Quantity of Interest

The different quantities of interest represent the bias introduced by the unequal distribution of the measurement locations. Hence, we can use the difference in the sensitivity analysis to discuss the bias that is induced by the temperature measurements. So far, we had two key observations for the study of the different quantities of interest:

1. the difference in the indices for the thermal conductivities are higher for deeper layers,
2. the differences are higher for the radiogenic heat productions than for the thermal conductivities.

Both of these observations can be explained by having a closer look at the depth distribution of the temperature measurements (Figure 4.14). We can see that most measurements are located in a depth of up to 2 km. The deepest measurement is at depth of about 7.3 km, whereas the model extends to a maximum depth of about 140.5 km. Hence, most measurements are located in shallower geological layers, and in the deepest layers, we find no measurements at all (Figure 4.1). Therefore, the measurement focused analysis tends to underestimate the influences of the deeper geological layers and overestimates the influences of shallower. This is true for both thermal conductivity and radiogenic heat production.

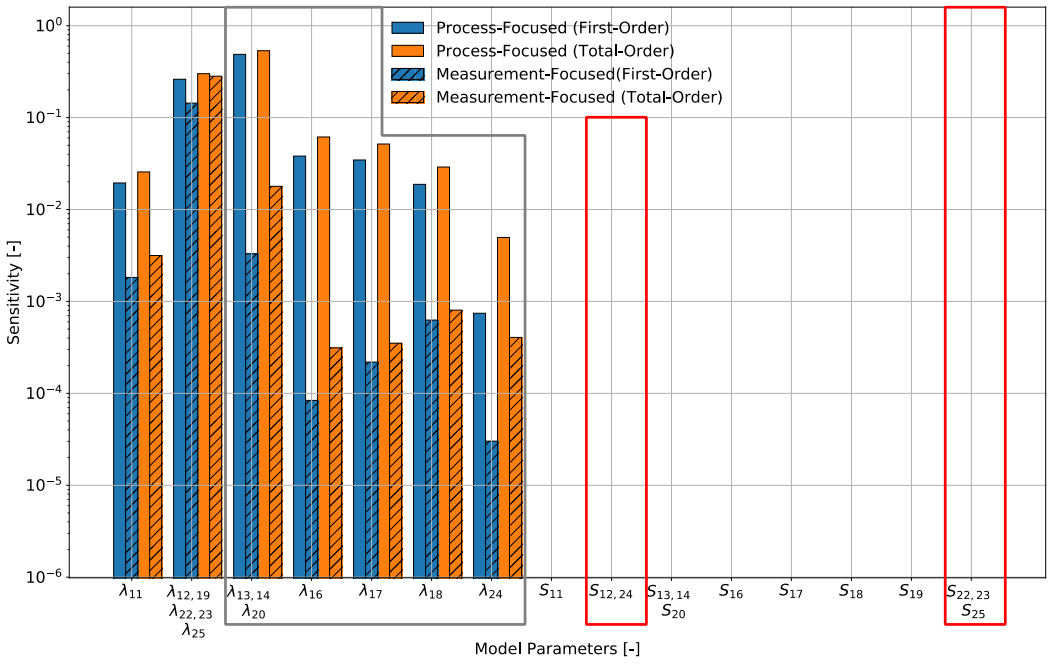

Figure 4.9. *Sensitivity analysis of the Upper Crust with different quantities of interest of the hierarchical global sensitivity analysis for the General-Focus Alps model. For the Layer IDs and acronyms please refer to Table 4.1.*

We investigate the phenomenon closer for the analysis of the Unconsolidated and Consolidated Sediments. Here, we have a prominent overestimation of the influences of the Unconsolidated Sediments and an underestimation of the Consolidated Sediments. We have:

- 384 data points in the Unconsolidated Sediments of the Upper Rhine Graben above 1 km (λ_0 in Figure 4.6),
- 755 data points in the Unconsolidated Sediments of the Upper Rhine Graben below 1 km (λ_1 in Figure 4.6),
- 516 data points in the Unconsolidated Sediments of the Po Basin below 2 km (λ_7 in Figure 4.6),
- 318 data points in the Consolidated Sediments outside of sedimentary basins (λ_8 in Figure 4.6),
- 18 data points in the Consolidated Sediments of the Molasse Basin (λ_9 in Figure 4.6),
- and 63 data points in the Consolidated Sediments of the Po Basin (λ_{10} in Figure 4.6).

The much higher data density in the Unconsolidated Sediments explains the high influence of the thermal conductivities of the Unconsolidated Sediments for the measurement-focused analysis. The only remaining question is why the influence of the thermal conductivity of the Unconsolidated Sediments Po below two kilometers is underestimated although containing 516 data points. This might be a bias introduced by the high data density of 755 data points in the Unconsolidated Sediments (λ_3).

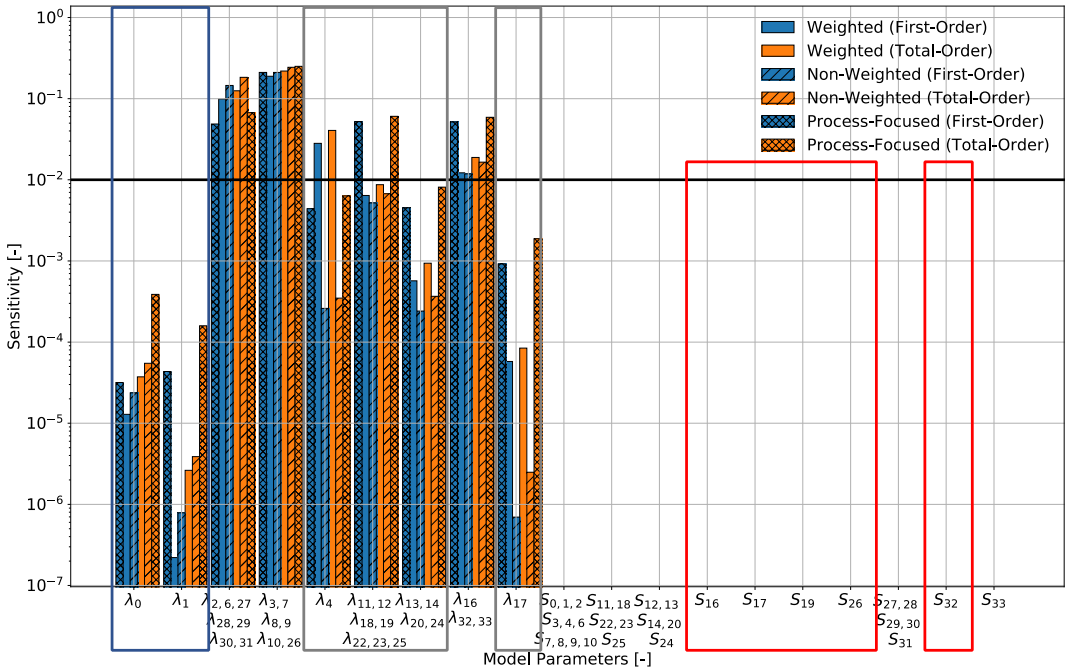

Figure 4.10. *Top level sensitivity analysis (focusing on the entire Alps model) with different weighting schemes of the hierarchical global sensitivity analysis for the General-Focus Alps model. For the Layer IDs and acronyms please refer to Table 4.1.*

The behavior is more pronounced for the radiogenic heat production for lithological reasons. The highest influences of the radiogenic heat productions arise from the Upper Crust (Figure 4.6), meaning that the radiogenic heat production is more prominent in deeper parts of the model. However, these parts of the model are further away from our measurement locations. Hence, the measurement-focused analysis highly underestimates the influence of the radiogenic heat production. The same effect can be observed for the thermal conductivity of the Upper Crust (λ_5 in Figure 4.6). For the measurement-focused analysis, the influence of the thermal conductivity is below the threshold, whereas for the process-focused analysis it is above.

The consequence of the data distribution becomes obvious once we look at the analysis of the Unconsolidated Sediments and Lower Crust (Figure 4.7). For all lower crustal layers, the influence is significantly underestimated in the measurement-focused scenario. Consequently, by focusing on the measurement in the further analysis we would lose all information related to the Lower Crust, although the layer might be important for the physical understanding of the subsurface.

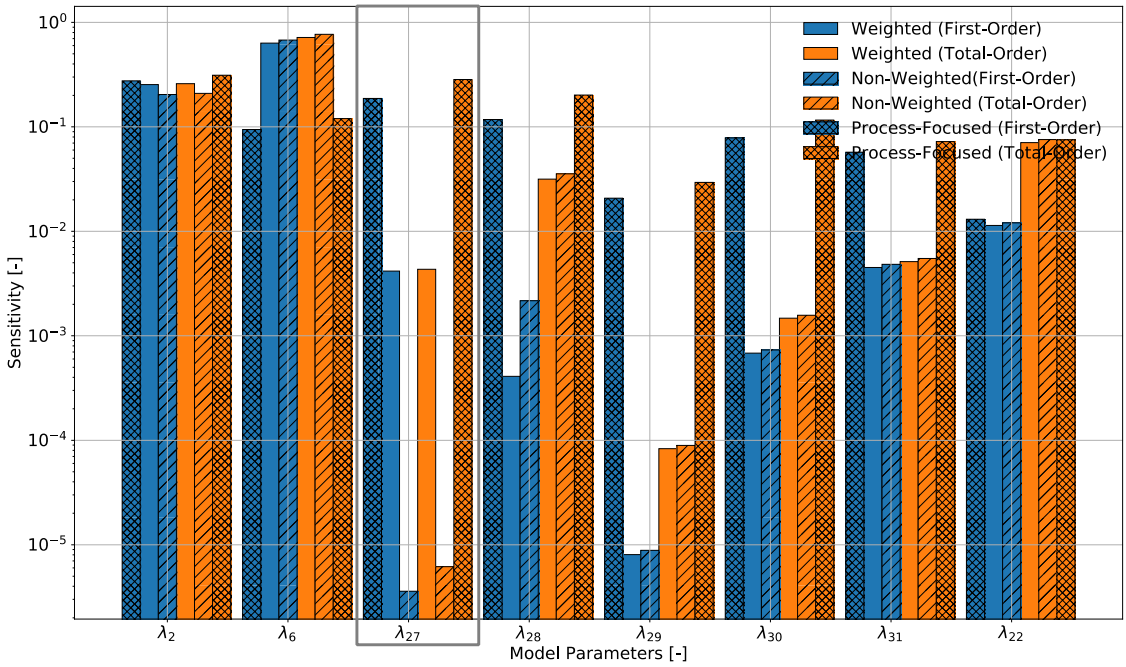

Figure 4.11. *Sensitivity analysis of the Unconsolidated Sediments and Lower Crust with different weighting schemes of the hierarchical global sensitivity analysis for the General-Focus Alps model. For the Layer IDs and acronyms please refer to Table 4.1.*

Also, for the analysis of the Upper Crust (Figure 4.9), we are confronted with the consequences of the unequal data distribution. The huge difference in the influences of the thermal conductivities of the Saxothuringia, Vosges, Molasse, and Ivrea Upper Crust is caused by a very low or zero data density. Also, the influence of the Moldanubia, Bohemia, and West Alps Upper Crust is underestimated. We have data in the Moldanubia and West Alps Upper Crust but no data in the Bohemia Upper Crust yielding this discrepancy.

The influence of the radiogenic heat production of the Istrea and Ivrea Upper Crust is underestimated in the measurement focused study due to the lack of data. Whereas the influence of the radiogenic heat production of the Po, North East Adria, and South East Adria Upper Crust is overestimated. This is likely caused by the measurements available for both the Po and North East Adria Upper Crust layers.

We also observed slightly higher parameter correlations for the process-focused analysis. This is probably related to the fact that the model is sensitive to more parameters.

4.4.2. Influence of the Weighting

We observed that the weighted measurement-focused analysis tends to be closer to the process-focused analysis. This becomes understandable by looking at the applied weighting scheme. We applied a regional weighting scheme to compensate for the unequal data distribution in the four regions of our model. Hence, we can compensate partly for the measurement bias. However, we are not able to fully compensate for the data sparsity. The main reason for this is that we can compensate for fewer data points but not for regions without data points since no measurements are available to which we could apply a higher weight. This can be observed, for instance, in the properties related to the layers of the Molasse.

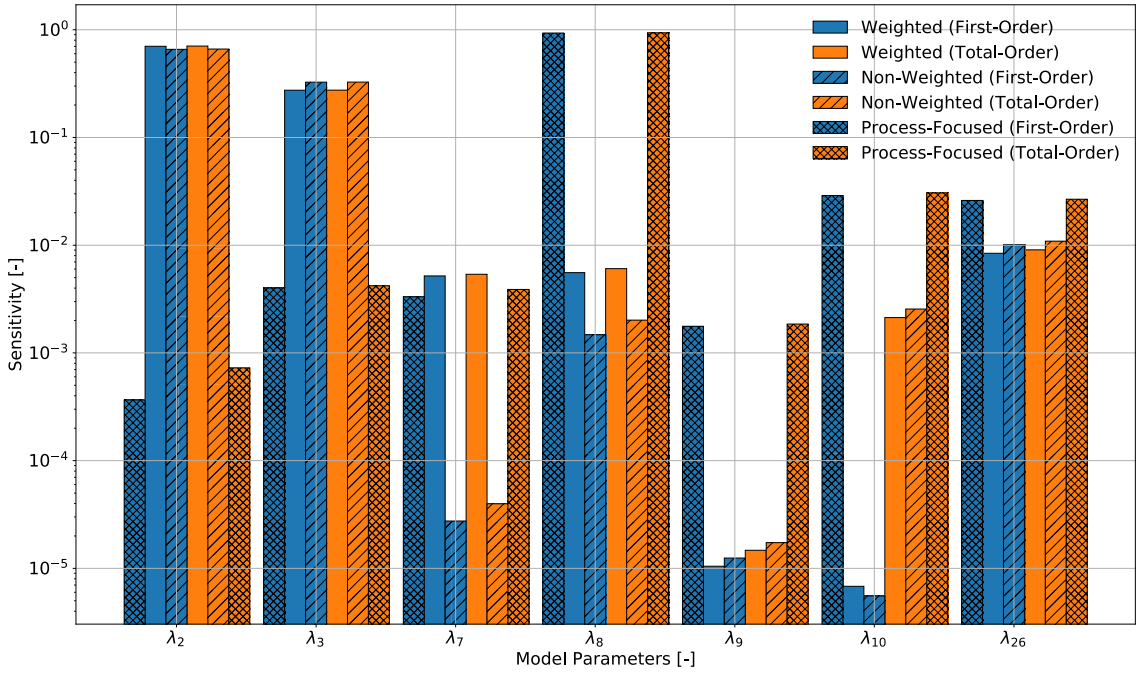

Figure 4.12. *Sensitivity analysis of the Unconsolidated and Consolidated Sediments with different weighting schemes of the hierarchical global sensitivity analysis for the General-Focus Alps model. For the Layer IDs and acronyms please refer to Table 4.1.*

We observed that the sensitivity indices of the thermal properties related to the layers inside the Upper Rhine Graben are further apart for the weighted and process-focused comparison than for the non-weighted process-focused one. This is related to the choice of the weighting scheme. We chose to put less weight on the temperature data from the Upper Rhine

Graben since we do not account for convective effects in this paper. Analogously, the properties of the Apennine Upper Crust layers also have a too small influence for the weighted scenario. As a reminder, we downgraded the importance of the temperature data in this region since the data consists of minimum temperature data.

Through the weighting we are able to compensate for the underestimation of the Unconsolidated Sediments of the Po Basin. Hence, the bias most likely induced by the high data density of the other layers can be removed.

For the thermal conductivities of the Saxothuringia, Vosges, Molasse Upper Crust (gray rectangle of Figure 4.13), we are again able to remove parts of the data bias caused by the data sparsity of these layers. The same phenomenon is observable for the radiogenic heat production of the Upper Crust (red rectangles of Figure 4.13).

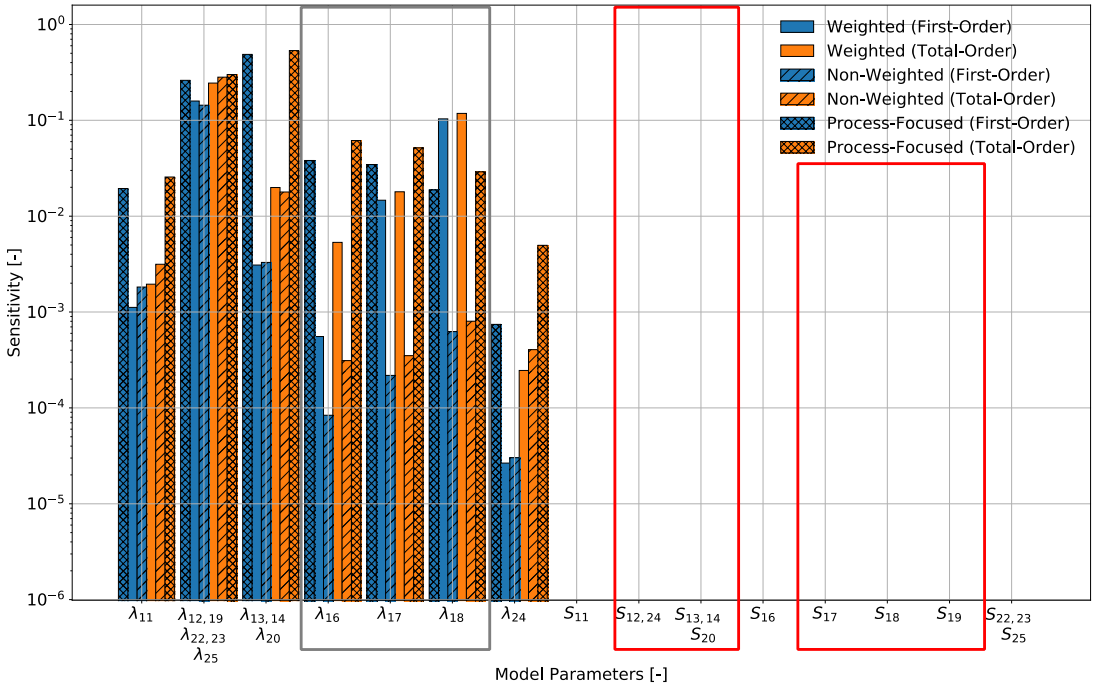

Figure 4.13. *Sensitivity analysis of the Upper Crust with different weighting schemes of the hierarchical global sensitivity analysis for the General-Focus Alps model. For the Layer IDs and acronyms please refer to Table 4.1.*

Note that the weighting scheme is case study and aim specific. Depending on our knowledge about data quality, regions of interest, and other aspects the weighting scheme can be case-specifically designed. In this paper, we do not aim to provide "the ideal" weighting scheme for the Alpine Region. Instead, we demonstrate the impact of a weighting scheme for thermal modeling.

4.4.3. Calibration Example

So far, we have presented that we obtain significantly differing sensitivities for the process-focused and measurement-focused study. In the following, we demonstrate the consequences of this difference through a deterministic model calibration. We choose the example of a model calibration because this is a typical inverse process that relies on observation data.

Model calibration aims to compensate for existing model errors by adjusting the model parameters in accordance with our temperature measurements. Analogous to Degen et al. (2020a), we use a sensitivity-driven model calibration for more robust results. In this study, we performed various sensitivity analyses. For the model calibration, we require the measurement-focused sensitivity analyses (branch 1.1 and 2.1 of Figure 4.3). We need these sensitivity analyses because they represent the information content that can be derived from the temperature data. In the case of the General-Focus Model, five thermal parameters that can be calibrated are yielded (Table 4.2). The data is insensitive to the remaining parameters. Hence, we cannot calibrate these values. We are left with mostly shallow layers to calibrate. The exception is the Lithospheric Mantle which is influential due to its large volume.

Parameter	Initial Value	Calibrated Values		
		General-Focus - Unweighted	General-Focus - Weighted	Crustal-Focus - Weighted
λ_2 [W m^{-1} K^{-1}]	2.0	1.53	1.70	2.02
λ_3 [W m^{-1} K^{-1}]	2.3	1.33	2.04	3.45
$\lambda_{4,5}$ [W m^{-1} K^{-1}]	1.8	n/a	1.62	1.53
λ_6 [W m^{-1} K^{-1}]	2.0	1.86	2.02	2.03
$\lambda_{32,33}$ [W m^{-1} K^{-1}]	3.0	3.71	3.18	2.5
$S_{22,23,25}$ [μW m^3]	1.3	0.2	0.8	1.3

Table 4.2. *Comparison of the initial thermal properties and the calibrated thermal properties for different geological models and different weighting schemes.*

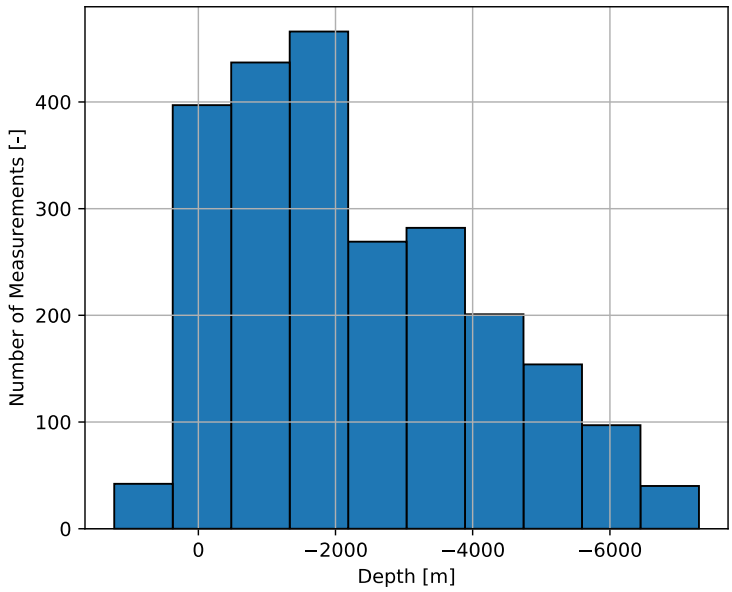

Figure 4.14. *Distribution of the measurements according to the depth*

In the following, we discuss the results of the automated model calibration and its consequences. Note that in this work, we use the model calibration in a slightly different way. Usually, it is used to compensate for model errors. That means of course that it also identifies the problematic model areas. In this work, we employ the model calibration as an identification tool for model errors. Therefore, we use as initial values the calibrated values by Spooner et al. (2020), which have been obtained through a "trial-and-error" model calibration. Then, large discrepancies between our initial values and calibrated values identify model problems.

The first model problem that we can identify is the measurement bias through an unequal data distribution (General-Focus – Unweighted). This can be at least partly removed through data weighting (General-Focus – Weighted) yielding smaller differences between initial and calibrated values. Nonetheless, we observe a low radiogenic heat production of the Upper Crust, meaning that our model is non-ideal in the description of the Upper Crust. This also leads to thermal conductivities that are too low in the Sediments and too high in the Lithospheric Mantle.

Therefore, we introduce a second model, the Crustal-Focus Model. For this model, we obtain a good agreement for the Upper Crust but greater discrepancies in Unconsolidated Sediments (below 1 km) and the Lithospheric Mantle. Hence, we can remove the error of the Upper Crust but at the same time introduce new error sources.

Note that we do not aim to present the "optimal" model in this paper. Instead, we want to demonstrate various components that influence the model. Generating an optimal model is not possible since all models are per definition wrong (Box, 1979). We present here two models that fulfill different purposes. The General-Focus Model is better if we are interested in the entire model domain. In the case that our area of interest is only the Upper Crust, the Crustal-Focus Model is preferable.

4.4.4. Influence of the Model

We have discussed the consequences of the model change for the calibrated thermal conductivities. Now, we want to briefly discuss the consequences for the sensitivities. Therefore, we repeat the process-focused and measurement-focused sensitivity analysis for the Crustal-Focused model. Note that we consider only the weighted scenario (branch 2.1.1 and 2.2.1 of Figure 4.3).

For the Crustal-Focused model, we thinned the Upper Crust. This can be clearly observed, in the decreased sensitivities of the model to the Upper Crust layers (red box of Figure 4.15). However, this change is only visible in the process-focused analysis. The measurement-focused analysis mostly fails to resolve these changes due to the data sparsity in the Upper Crust (red box of Figure 4.16). Underestimated changes are observable for the Saxothuringia Upper Crust. This highlights again the information loss of measurement-focused studies and the dangers associated with calibrations.

The radiogenic heat production of the most of the Lower Crust is more influencial for the Crustal-Focused model since the Upper Crust was thinned by thickening the Lower Crust. The only exception is the Saxothuringia Lower Crust (λ_{26}). For the process-focused analysis (Figure 4.15) it loses importance and for the measurement-focused analysis (Figure 4.16) it gains importance. For both models, we apply a Dirichlet boundary condition at the top and the bottom of the model. Hence, the temperature distribution is determined by the ratio of the thermal properties. Therefore, the difference in the Saxothuringia Lower Crust likely arising from the changes of other geological layers. The same is likely for the changes of the thermal conductivity of the Unconsolidated Sediments in the Molasse Basin. Also, the changes of the influences arising from the radiogenic heat production of the Lithospheric Mantle are caused by other layers, especially considering the very low values of these layers.

Furthermore, we observer a higher influence of the Unconsolidated Sediments in the Upper Rhine Graben (gray box of Figure 4.15) although the model has not been changed around the Upper Rhine Graben. However, this might be an effect of the reclassification in the Unconsolidated and Consolidated Sediments. These changes are more pronounced for the measurement focused (gray box of Figure 4.16) than for the process-focused analysis. This is again caused by the data distribution since we have more measurements at a shallower depth.

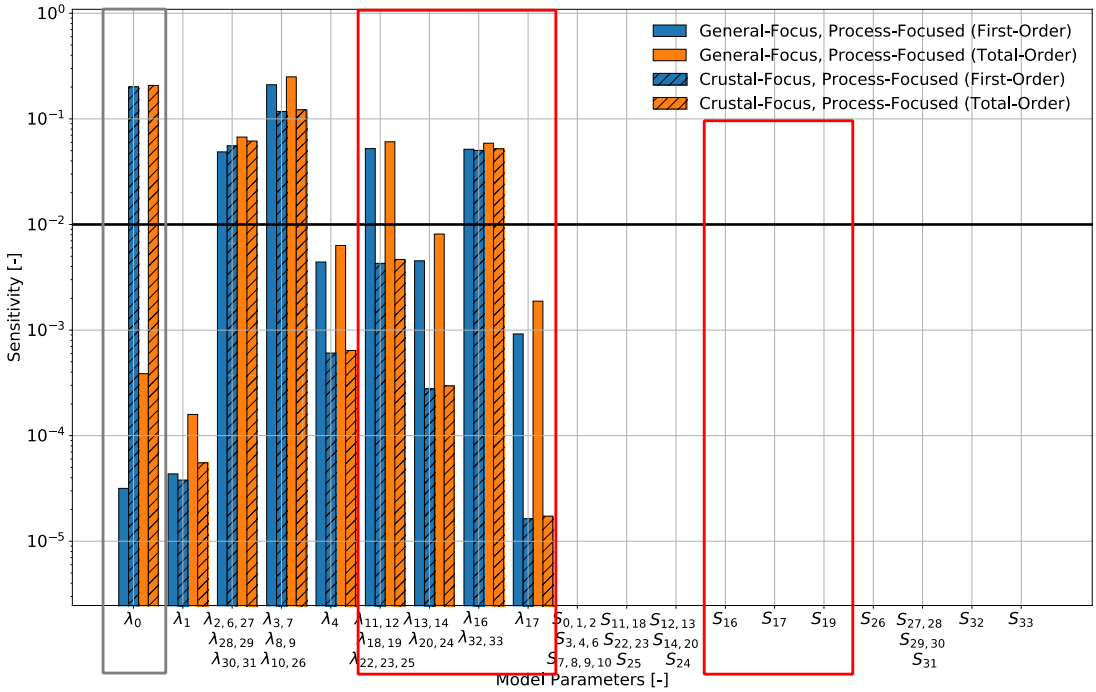

***Figure 4.15**. Comparison of the sensitivities of the process-focused study for both the General-Focus and Crustal-Focus Alps Model. For the Layer IDs and acronyms please refer to Table 4.1.*

4.4.5. Gravity Model

The model change is observable in both the model calibration for the thermal properties and the corresponding sensitivities. However, if we look at the gravity residuals (Figure 4.17), we do not observe any significant changes. This highlights a general point for the construction of geological models. We have different data sources available for the construction of a geological model. It is crucial to incorporate multiple data sources and not rely on a single data source. If we would have constructed a model of the Alps purely based on gravity, we would not have been able to identify the problem of the thickness of the Upper Crust.

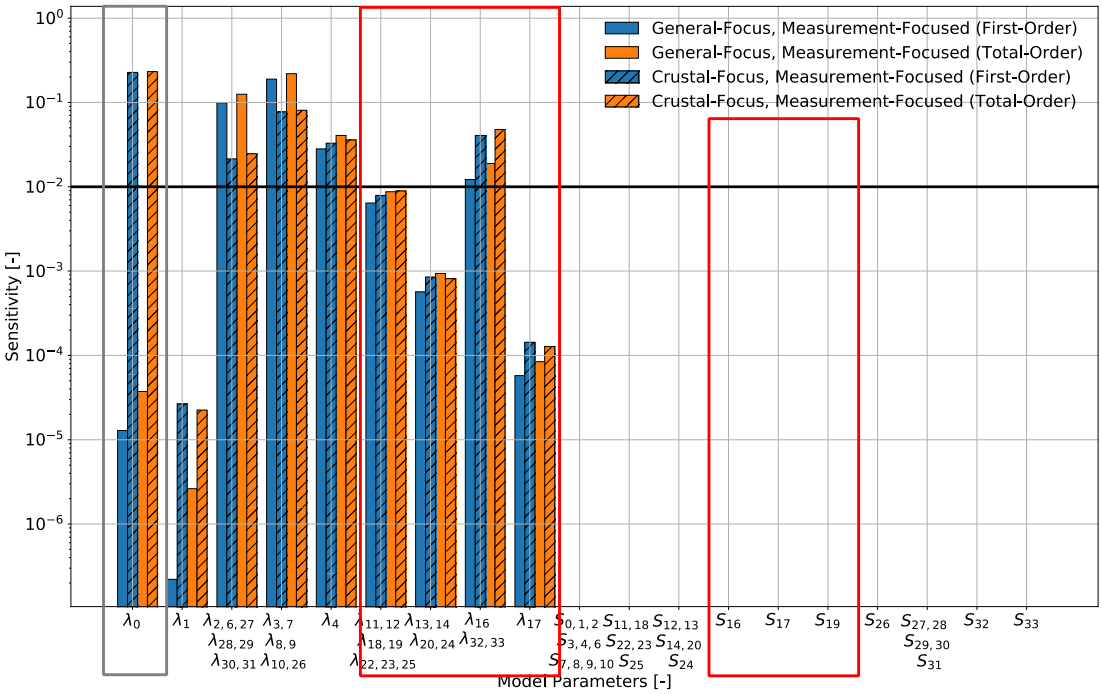

Figure 4.16. *Comparison of the sensitivities of the measurement-focused study for both the General-Focus and Crustal-Focus Alps Model. For the Layer IDs and acronyms please refer to Table 4.1.*

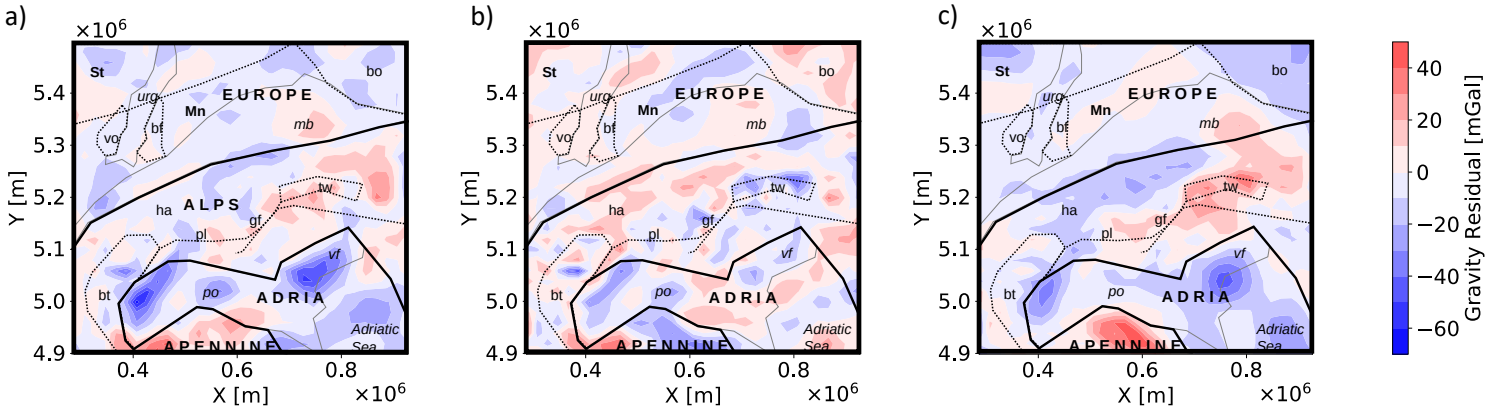

Figure 4.17. *Gravity residual of* ***a)*** *the General-Focus Model,* ***b)*** *the Crustal Focus Model, and* ***c)*** *the difference between the General-Focus and Crustal-Focus Model. Acronyms - St - Saxothuringian Zone; Mn – Moldanubian Zone; Ha – Helvetic Alps; bo – Bohemian Massif; vo – Vosges Massif; bf – Black Forest Massif; tw –Tauern Window; bt – Briançonnais Terrane; pl – Periadriatic Lineament; gf – Guidicarie Fault; urg – Upper Rhine Graben; mb – Molasse Basin; po – Po Basin; vf – Veneto–Friuli plain.*

4.4.6. Outlook

In this paper, we have seen that the measurements induced a significant bias. This opens the discussion of subsequent projects. Therefore, we would like to investigate how we can decrease this bias by incorporating further data sources that give us only an indirect measure of the temperature. Furthermore, it would be interesting to further explore the field of joint inversion to incorporate various geophysical data sources already used during model construction.

4.5. Conclusion

Throughout the entire paper, we have demonstrated the bias that a measurement-focused study can cause. This bias can be partly removed through automated and customized data weighting schemes. However, as typical for geoscientific applications, many areas of the model do not have any associated data. Unfortunately, it is not possible to compensate for the bias arising from these areas. This shows the importance of focusing on regions where data is present, whenever possible.

However, many inverse processes such as deterministic and stochastic model calibrations are dependent on measurement data. Here, this bias is unavoidable. Nonetheless, we need to be aware of which kind of bias we are introducing through this procedure to take the effects for all further analyses into account. We need to be aware that the data is often only informative towards the shallower layers. Hence, we lose the information about deeper layers and at the same time overestimate the influence of the shallower layers. This also means that we are unable to calibrate and validate the lower parts of our geological models. Nonetheless, these parts are important to avoid influences from, for instance, the lower boundary condition.

We have also seen the importance of considering various data sources. The model changes from the General-Focus to the Crustal-Focus model were only visible in the thermal studies but not in the gravity residuals.

Note that although we performed the analyses for the case study of the Alps these aspects hold in general since the data distribution shown here is typical for geoscientific applications.

Chapter 5. How Alpine seismicity relates to lithospheric strength

5.1. Introduction

The present-day seismicity distribution is still poorly understood and presently debated in the Alpine orogen and its northern and southern forelands (Deichmann, 1992; Bonjer, 1997; Cattaneo et al., 1999; Singer et al., 2014; Eva et al., 2015). Therefore, any additional constraints on the controlling factors affecting event localisation are of interest. Local models have been used with some success to assess the stress regime on individual faults thereby offering important insights into the local dynamics driving the observed localisation of seismicity (e.g. Bonjer, 1997). However, and despite its relevance in the current ongoing scientific debate, the cross-correlation between monitored seismicity and its localisation in space with respect to the long-term stress state of the whole lithosphere is still lacking.

Previous works in the region have attempted a quantification of the long-term mechanical state of the lithosphere mainly relying on 2D sections across the Alpine chain such as the EGT (Okaya et al., 1996) and Transalp (Willingshofer and Cloetingh, 2003) profiles. Relatively few models exist that try to compute lithospheric strength variations across the entire orogen (e.g. Tesauro et al., 2011; Marotta and Splendore, 2014). In this contribution we propose a revision of the current understanding of the long-term lithospheric strength of the lithosphere in the Alpine area in light of higher resolution, region specific 3D geophysical models. To this end, we make use of recently published results derived from a gravity and seismically constrained structural and density model of the region (Spooner et al., 2019) that has been verified by secondary sources (Magrin and Rossi, 2020) along with a wellbore measurement constrained thermal field (Spooner et al., 2020) to arrive at an updated model of the rheological configuration of the study area.

After a detailed summary of the methodology used to calculate lithospheric strength, we dedicate the second part of the manuscript to a critical discussion of the correlation between modelled lithospheric strength variations and a comprehensive dataset of regional seismicity in order to investigate the potential role that lithospheric heterogeneity plays in shaping the observed localisation of seismicity throughout the Alps and their forelands. In depth analysis leads us to partially revise the main conclusions derived from recent numerical work that attributes the seismicity depth distribution across the region solely to the relatively low plate convergence rate, with negligible influence from tectonic inheritance (Dal Zilio et al., 2018).

We also quantify the role of viscosity contrasts caused by the presence of a laterally heterogeneous lithospheric configuration in limiting the maximum depth of seismicity through dissipation creep mechanisms. As a result, the 3D distribution of effective viscosities calculated within this work, are able to complement the ongoing debate on the relative impact of glacial isostatic adjustment versus tectonic and mantle dynamic processes as causes of the observed present-day kinematic state of the Alpine region (e.g. Norton and Hampel, 2010; Chéry et al., 2016; Mey et al., 2017; Sternai et al., 2019).

5.1.1. Geological History

Large scale crustal differentiation within the northern foreland of the Alps (the European plate) primarily results from the Carboniferous age Variscan orogeny (Franke, 2000), such as the juxtaposition of the Moldanubian and Saxothuringian terrains (Babuška and Plomerová, 1992; Freymark at al., 2017) and the assemblage of crystalline basement presently exposed in the Vosges, Black Forest and Bohemian massifs. Heterogeneity within the Alpine orogen, largely stems from the ongoing collision of the Adriatic plate with the European plate from the Cretaceous to present-day (Handy et al., 2010). Traditionally, the Alpine crust is split up according to its plate of origin prior to orogenesis, such as the European derived Helvetic Alps and the Adriatic derived Southern Alps, that both represent the proximal domains of their respective plate (Schmid et al., 1989; Schmid et al., 2004). At the surface the present-day boundary of the European and Adriatic derived crust within the Alps broadly occurs at the East-West running Periadriatic Lineament. Ongoing deformation is primarily driven by the convergence of the European and Adriatic plates in northeast Italy (Restivo et al., 2016), where the Adriatic plate is considered to act as a rigid (mechanically stiff) indenter, moving northwards with a radial counter-clockwise rotation against the weaker European plate (Nocquet and Calais, 2004; Vrabec and Fodor, 2006; Serpelloni et al., 2016). The foreland basins related to the orogen, forming as a result of flexure, are the Po Basin and Veneto-Friuli Plain of the southern foreland and the Molasse Basin of the northern foreland. Also in the northern foreland the Upper Rhine Graben formed as part of the European Cenozoic Rift System in the Eocene (Dèzes at el., 2004). The locations of all relevant tectonic features within the region can be found in Figure 5.1.

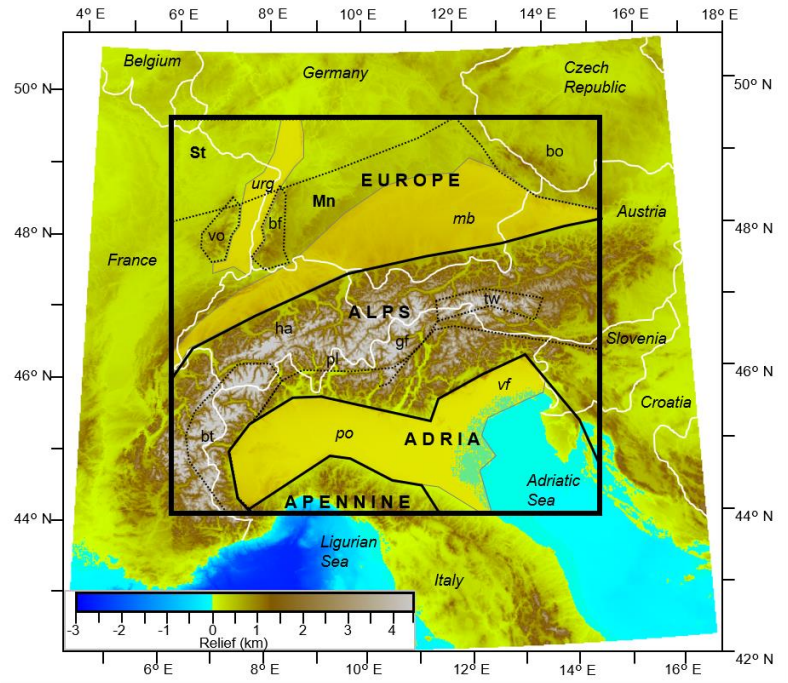

Figure 5.1. *Topography and bathymetry from ETOPO 1 (Amante and Eakins, 2009) shown across the Alpine region with the key tectonic features overlain. Study area is indicated with a black box. Solid black lines demark the boundaries of the weakly deformed European and Adriatic plates, the location of the Apennine plate is also marked. Yellow areas bound by a solid grey line indicate the extent of sedimentary basins (urg – Upper Rhine Graben; mb – Molasse Basin; po – Po Basin; vf – Veneto-Friuli Plain). Dotted black lines indicate the extent of other tectonic features within the model (St – Saxothuringian Variscan domain; Mn – Moldanubian Variscan domain; bo – Bohemian Massif; vo – Vosges Massif; bf – Black Forest Massif; ha – Helvetic Alps; tw – Tauern Window; gf – Giudicarie Fault; pl – Periadriatic Lineament; bt – Brianconnais Terrane). The Adriatic Sea is marked as (AS) in further figures.*

5.2. Method

Lithospheric structural geometries and densities were sourced from an integration of previous geoscientific datasets in the region by Spooner et al. (2019). Topography and bathymetry (Figure 5.1) comes from ETOPO1 (Amante and Eakins, 2009), and the seismically derived lithosphere-asthenosphere boundary (referred to as LAB hereon) originates from Geissler et al (2010). Other sub-surface lithospheric depths were constrained from the use of numerous published deep seismic surveys (e.g. Brückl et al., 2007; Hetényi et al., 2018a), existing structural models of smaller subsets of the study area (e.g. Ebbing, 2002; Przybycin et al., 2014; Freymark et al., 2017) and European plate crustal models (Tesauro et al., 2008; Molinari and Morelli, 2011). Densities were constrained using forward 3D gravity modelling

in IGMAS+ (Schmidt et al., 2010, Schmidt et al., 2020) and the global satellite gravity model EIGEN-6C4 (Förste et al., 2014), with the lithospheric layers split into domains of different density to account for lateral heterogeneity.

The resulting structural and density model (Spooner et al., 2019), with dimensions of 660 km x 620 km (Figure 5.1) and a horizontal grid resolution of 20 km x 20 km, represents a 3D structural model of the Alps and foreland regions with the highest spatial resolution among available models and conforms to both seismic and gravity-based observations. Five model layers that represent key lithospheric structural and density contrasts were used for the rheological calculations: (1) unconsolidated sediments (mostly Quaternary strata); (2) consolidated sediments (mostly Mesozoic strata); (3) upper crystalline crust; (4) lower crystalline crust; and (5) lithospheric mantle. Layer thicknesses and the domains of different density that comprise them are shown in Figures 5.2 and 5.3c. Slabs and subduction interfaces are not considered within this work as no consistent model of their geometry or polarity is available for the study area at present (Kästle et al., 2019).

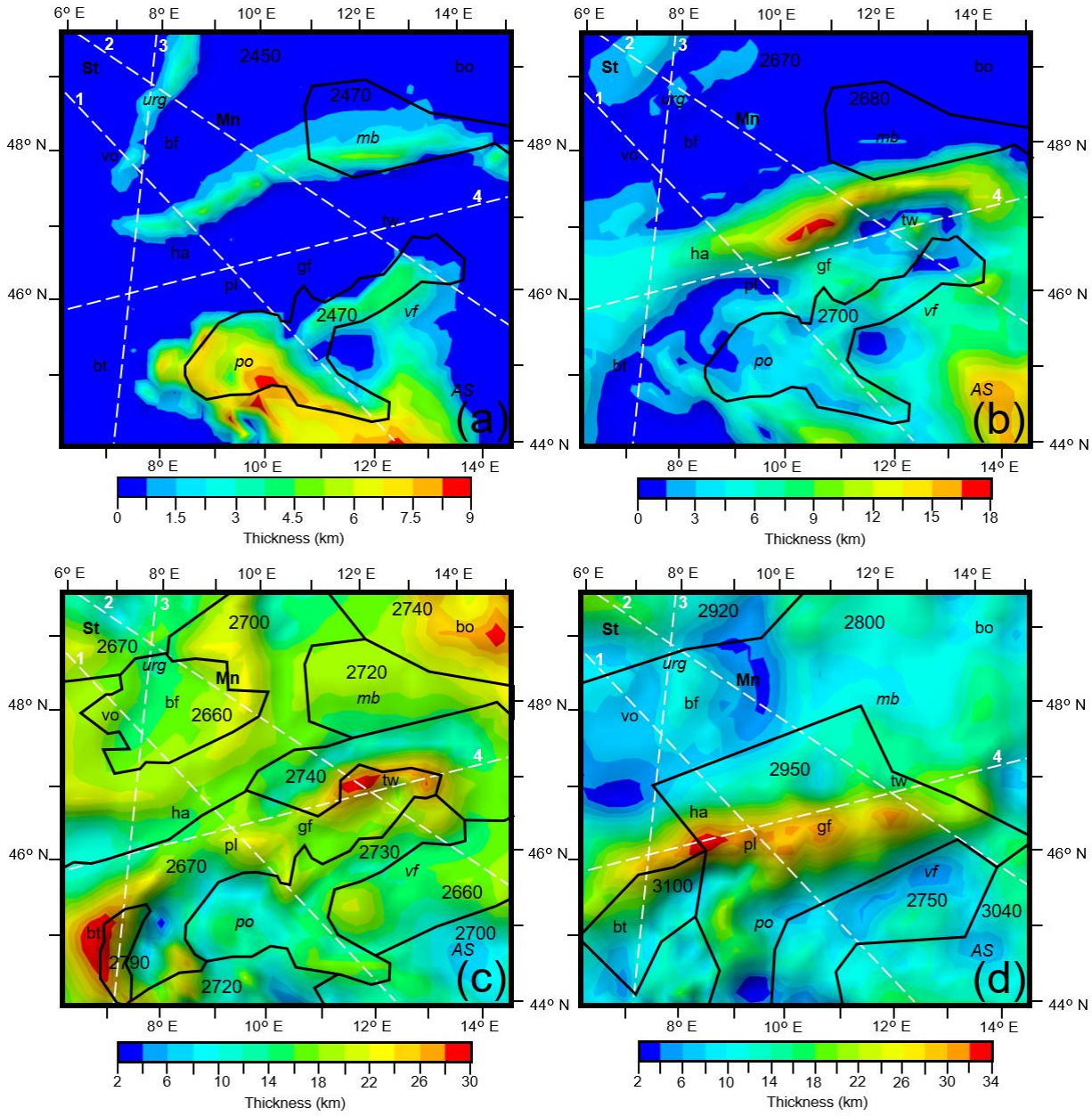

Figure 5.2. *Thickness of* ***a)*** *unconsolidated sediments,* ***b)*** *consolidated sediments,* ***c)*** *the upper crust and* ***d)*** *the lower crust across the modelled area. Density domains required during modelling are outlined in black with the density used for each (in* $kg\,m^{-3}$*) shown within. Locations of key tectonic features are overlain (abbreviations shown in Figure 5.1a caption). Cross sections 1, 2, 3 and 4 from Figures 5.6 and 5.8 are marked with white dashed lines.*

The temperature distribution input to the rheological calculations was obtained from a thermal model of the Alps and their forelands (Spooner et al., 2020) generated from the same structural model utilised here (Spooner et al., 2019). The 3D conductive steady state thermal field was computed using the numerical simulator GOLEM, that can calculate coupled thermal-hydraulic-mechanical processes (Cacace and Jacquey, 2017). Therefore, steady state

conductive heat transport was assumed as the main mechanism and specific thermal parameters were assigned to domains of the structural model, to fit a compiled dataset of measured sub-surface temperatures (Przybycin et al., 2015 and references therein; Freymark et al., 2017 and references; Trumpy and Manzella, 2017). Depth maps of the calculated 200 °C, 400 °C, 600 °C, and 800 °C isotherms are plotted in Figure 5.4.

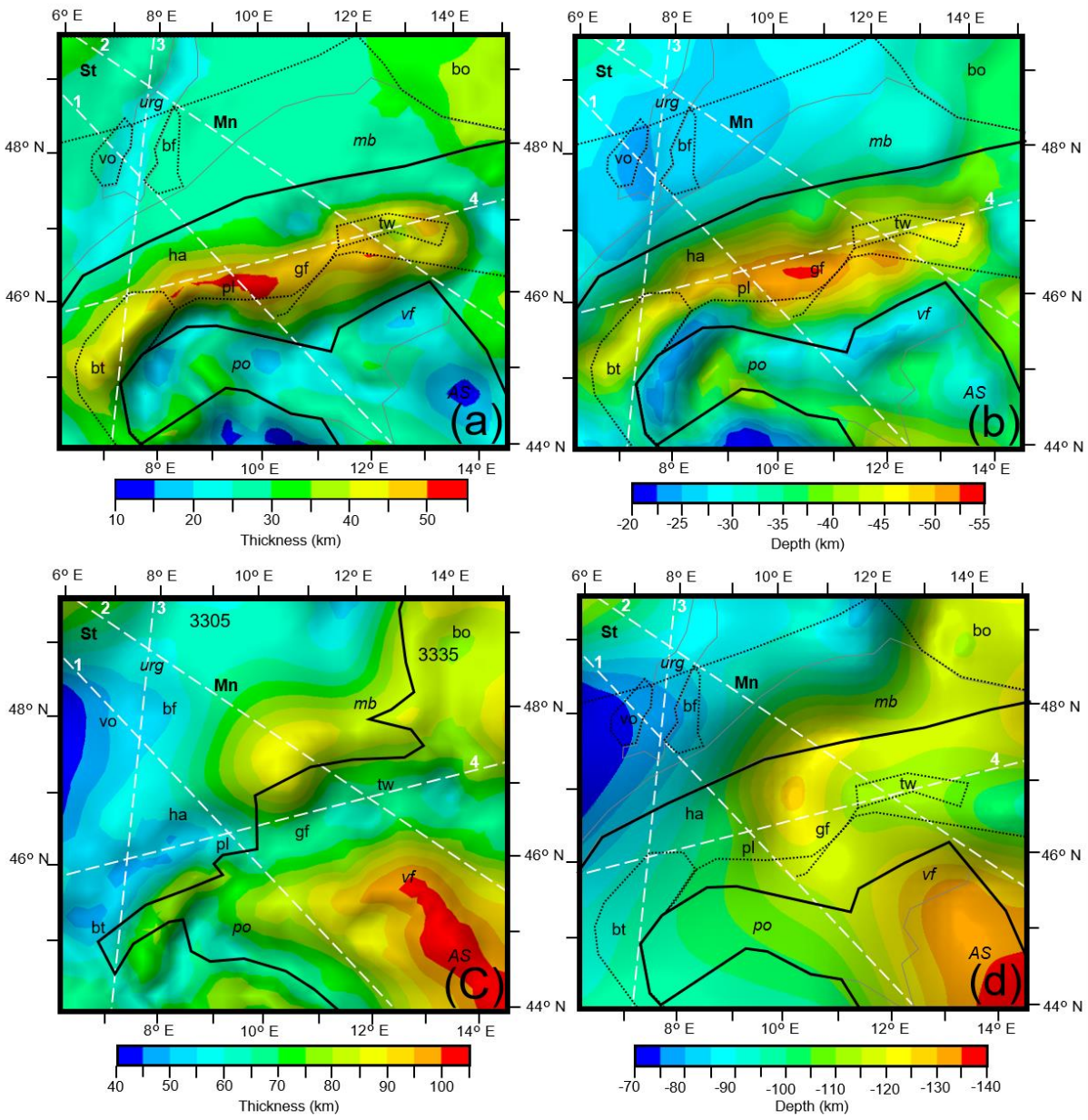

Figure 5.3. a) *Thickness of the entire crust.* ***b)*** *Moho depth.* ***c)*** *Thickness of the lithospheric mantle. Density domains required during modelling are outlined in black with the density used for each (in kg m^{-3}) shown within.* ***d)*** *LAB depth (from Geissler et al., 2010). Locations of key tectonic features are overlain (abbreviations shown in Figure 5.1a caption). Cross sections 1, 2, 3 and 4 from Figures 5.6 and 5.8 are marked with white dashed lines.*

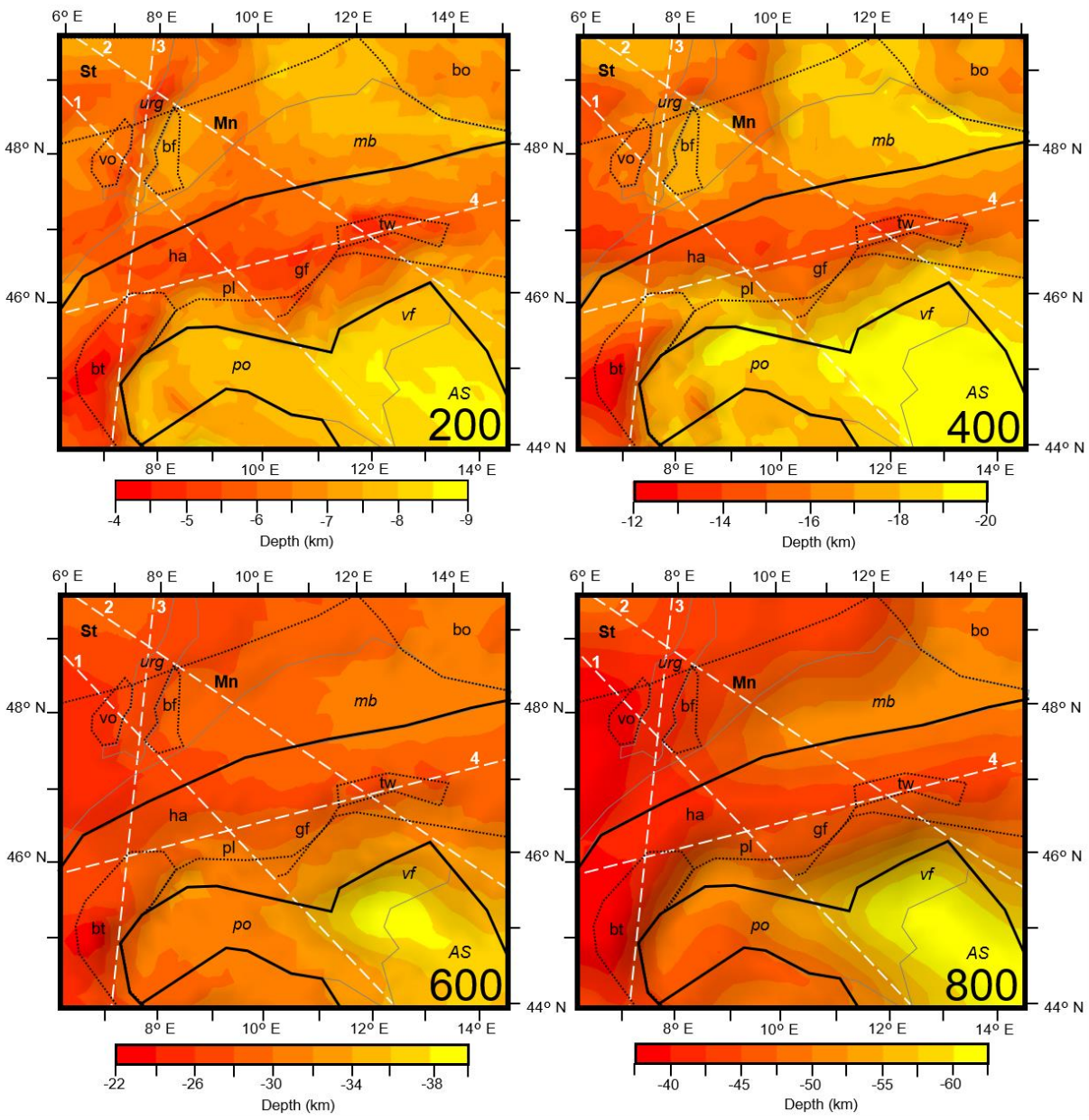

Figure 5.4. *Depths to the 200 °C, 400 °C, 600 °C and 800 °C isotherms across the modelled area. Locations of key tectonic features are overlain (abbreviations shown in Figure 5.1a caption). Cross sections 1, 2, 3 and 4 from Figures 5.6 and 5.8 are marked with white dashed lines.*

The yield strength of the lithosphere (maximum differential stress achievable prior to failure [Goetze and Evans, 1979]) was calculated, taking into account the 3D temperature and pressure state of the system as derived from the structural and thermal models (Spooner et al., 2019; Spooner et al., 2020). Rheological parameters, also used to calculate structural model layer strengths, were assigned based on the compilation of laboratory measurements (Ranalli

and Murphy, 1987) for the dominant lithology interpreted for each layer from observed seismic velocities as well as the modelled density and thermal properties. Parameters used can be found in Table 5.1. Long term lithospheric strength of the Alps and either forelands were then calculated with a vertical resolution of 100 m, assuming steady state - secondary creep as the dominant mode of viscous deformation and frictional plastic brittle behaviour following Byerlee's law, using the same methodology described in Cacace and Scheck-Wenderoth (2016).

Model layer and representative rheology used	Power-law strain rate A (Pa^{-n} s^{-1})	Power-law Exponent n -	activation enthalpy Q (J mol^{-1})
Sediments (Granite, wet)	7.94E-16	1.9	1.37E+05
Upper Crust (Quartzite)	2.51E-24	2.4	1.56E+05
Lower Crust (Diabase)	8.04E-25	3.4	2.60E+05
Mantle (Olivine)	4.00E-12	3	5.40E+05

Table 5.1. *Representative lithologies and rheological parameters (from Ranalli and Murphy, 1987) used for modelling the layers of the structural model.*

Byerlee's law (equation 5.1), a temperature-independent function of confining pressure resulting from increasing density and depth (Byerlee, 1978; Ranalli, 1995) was used to calculate the brittle portion of the yield strength ($\Delta\sigma_b$):

$$\Delta\sigma_b = f_f \, \rho_b g z (1 - f_p) \tag{5.1}$$

where Δf_f is the static friction coefficient (set to a constant value of 3 to represent lithospheric stress as per Brace and Kohlstedt [1980]), ρ_b is the bulk rock density, g is the gravitational acceleration, z is the depth (below surface) and f_p is the pore factor (the ratio of the pore

pressure to the lithostatic pressure, set here to a constant value of 0.36, representing a fluid density of ~1000 kg m^{-3} and a rock density of ~2750 kg m^{-3}).

Power law creep (equation 5.2), representing non-Newtonian, temperature activated deformation of rocks at increasing depth (Karato and Wu, 1993; Burov, 2011), was used to calculate ductile strength ($\Delta\sigma_d$):

$$\Delta\sigma_d = \left(\frac{\dot{\varepsilon}}{A}\right)^{\frac{1}{n}} \exp\left(\frac{Q}{nRT}\right) \tag{5.2}$$

where $\dot{\varepsilon}$ is the strain rate (set to a constant $10^{-15}s^{-1}$, consistent with observed GPS measurements from the region [Houlié et al., 2018]), A is the power-law strain rate, n is the power-law exponent, Q is the activation enthalpy, R is the gas constant, T is the temperature. Tests were made to account for the onset of low temperature crystal plasticity in the lithospheric mantle layer (Peierls creep mechanism [Katayama and Karato, 2008]), however this was found to not affect the ductile strength of the plate.

For the visualisation of maximum rock strength under a constant strain rate at every point in the model, yield strength envelopes (referred to as YSE hereon) showing the differential stress envelope (minimum between $\Delta\sigma_b - \Delta\sigma_d$) versus depth were calculated (Brace and Kohlstedt, 1980). The modelled strengths of both the crust and the entire lithosphere were then vertically integrated over their entire thicknesses in order to compare lateral changes in strength throughout the region.

From the above stated relationships, it follows that rates of viscous dissipation in our model can be expressed in terms of a non-linear with temperature effective solid viscosity as (η_{eff}):

$$\eta_{eff} = \frac{2^{\frac{1-n}{n}}}{3^{\frac{1+n}{2n}}} A^{-\frac{1}{n}} \dot{\varepsilon}^{\frac{1}{n}-1} \exp\left(\frac{Q}{nRT}\right) \tag{5.3}$$

The calculated lithospheric strengths and viscosities were then compared to the seismic event catalogue of the International Seismological Centre (International Seismological Centre, 2020) for the study area. The catalogue was filtered to remove events where fixed depths were assigned, where depth error estimates were absent or where the depth error was in excess of 20

% of the event's hypocentre depth (allowing errors of <3 km at a depth of 15 km), to both maximise the accuracy and number of useable events. The catalogue was further filtered to remove events smaller than magnitude 2 in an effort to remove the effects of smaller events 'clustering' around seismic stations observed in similar seismic catalogues (e.g. González, 2016), whilst maintaining coverage across the entire study area. The events used ranged from March 1964 to November 2017, providing a dataset of 4,405 seismic events (shown in Figures 5.5, 5.7 and 5.9) that were then used to interrogate the relationships between lithospheric strength and seismicity throughout the region.

5.3. Results

Across the Alps and their forelands, the pattern of variations in integrated strength of the entire lithosphere (shown in Figure 5.5a) corresponds closely to the pattern of Moho depth (Figure 5.3b). The weakest lithosphere (13 $\log_{10}$ Pa m) occurs at the deepest portion of the Alpine crustal root, the largest Moho depth in the study area (55 km), West of the Guidicarie Line. Similarly, the eastern Alps are characterised by both a shallower Moho (45 km) and higher strength (13.2 $\log_{10}$ Pa m). In agreement with this correlation, both forelands exhibit significantly shallower Moho depths and higher lithospheric strength than within the orogen. The lithosphere of the southern foreland was also found to be stronger than the northern foreland, with the highest strength in the study area exhibited on the Apennine plate (13.8 $\log_{10}$ Pa m) and the Adriatic indenter (13.9 $\log_{10}$ Pa m). Similar results have been observed by previous works modelling the lithospheric strength of the eastern Alps along the Transalp profile (Willingshofer and Cloetingh, 2003) and in the central Alps along the EGT profile (Okaya et al., 1996) and the entire orogen (Marotta and Splendore, 2014).

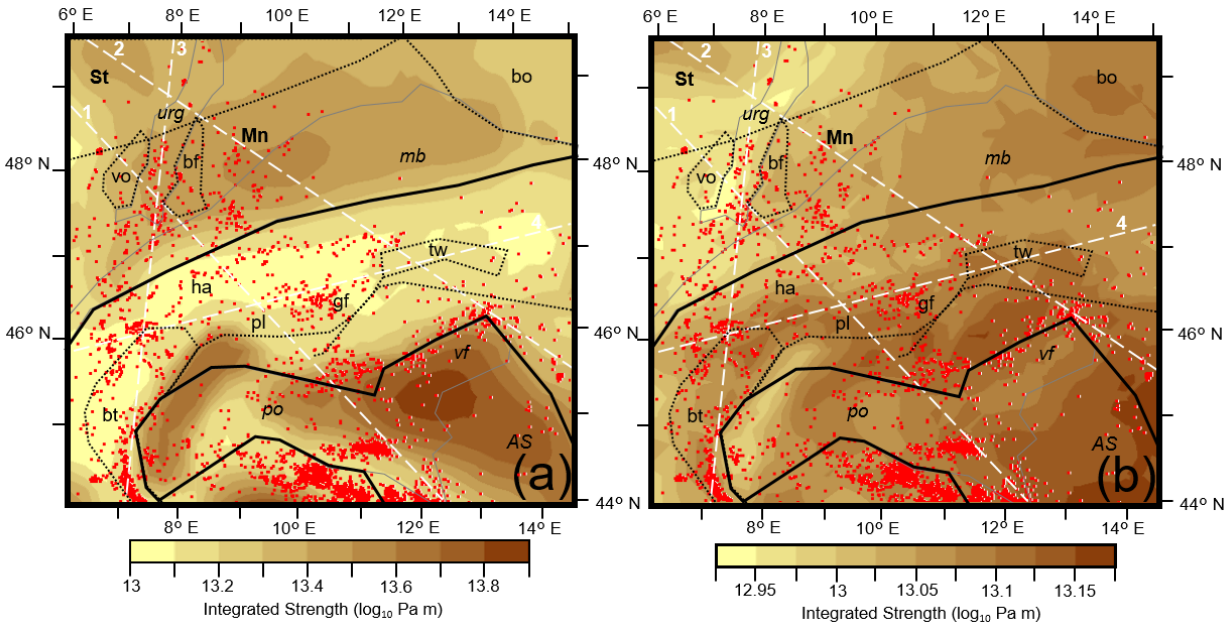

Figure 5.5. *Integrated strength of* ***a)*** *the lithosphere and* ***b)*** *the crust across the modelled area with seismicity > M2 shown in red dots. Locations of key tectonic features are overlain (abbreviations shown in Figure 5.1a caption). Cross sections 1, 2, 3 and 4 from Figures 5.6 and 5.8 are marked with white dashed lines.*

Not all zones of high strength observed in the southern foreland correspond to shallow Moho depths. Whilst the mechanically strong portions of the Apennine plate occur at the location of the shallowest Moho depth (20 km, below the Ligurian Sea), the strong Adriatic indenter has some of the largest Moho depths encountered in either foreland (40 km, south of the Veneto-Friuli plane). Instead the strong indenter is observed to correspond to the deepest portion of the LAB (140 km, shown in Figure 5.3d) and to a region of significantly colder lithospheric temperatures in the Adriatic plate (shown in Figure 5.4).

The integrated crustal strength (shown in Figure 5.5b) also positively correlates with temperature, being highest (13.175 $\log_{10}$ Pa m) in the South East of the Adriatic indenter where all isotherms are deepest (Figure 5.4). North of the Periadriatic lineament and West of the Guidicarie Line, isotherm depths are consistently shallower than in the southern and eastern Alps. Consequently, the northern and western Alps feature lower crustal strengths (13 $\log_{10}$ Pa m) than the Alpine crust in the south and east (13.125 $\log_{10}$ Pa m) a finding also observed by Marotta and Splendore (2014). Where isotherms are raised below the URG, crustal strength is also the lowest (12.925 $\log_{10}$ Pa m).

The distribution of seismic event epicentres in the southern foreland strongly correlates spatially with the computed integrated lithospheric strength (Figure 5.5a) and not with crustal strength, as most events occur in the weak lithosphere surrounding the more rigid Adriatic indenter or Ivrea body. Within the northern foreland no correlation is observable between seismicity localisation and lithospheric strength, with epicentres instead corresponding closely to the weaker portions of the crust (Figure 5.5b) around the URG in the west of the Moldanubian domain. Both integrated lithospheric and crustal strength maps portray lower strength within the Alps proper, North and West of the Guidicarie Line, corresponding to the location of the majority of Alpine seismicity.

Cross sections showing variations in differential strength (minimum between brittle strength and ductile strength) with depth and the relation to seismicity are plotted in Figure 5.6. In line with previous works (Okaya et al., 1996; Willingshofer and Cloetingh, 2003; Marotta and Splendore, 2014), all cross sections show that the majority of seismicity occurs within the strongest region of the upper crust (~ 1 GPa), between 200 °C and 400 °C, with a largely aseismic and weaker lower crust mechanically decoupling the crust from the lithospheric mantle. Seismicity deeper than the upper crust is however present in regions where the upper lithospheric mantle is cooler than 600 °C and strong (> 2 GPa), as shown in cross sections 1 and 3. Regions seen in Section 1 and 2 characterised by a stronger lower crust (~ 1 GPa) also show seismicity to a greater depth. Section 4, which runs West to East through the centre of the orogen, does not portray a strong lower crust or upper lithospheric mantle, and shows Moho temperatures consistently higher than 600 °C, exhibiting no seismicity outside of the upper crust.

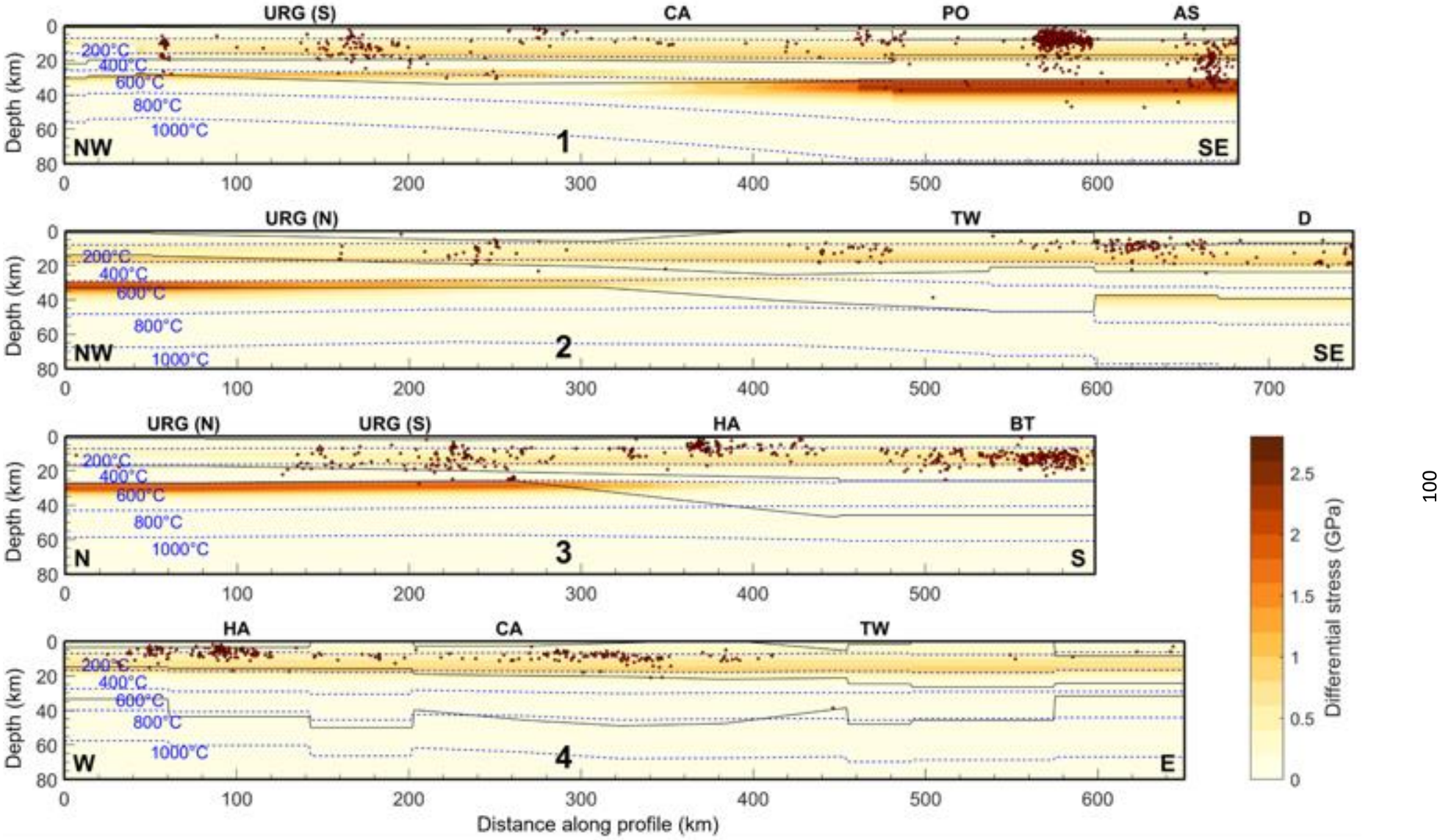

Figure 5.6. *Cross sections 1, 2, 3 and 4 (Locations shown in Figures 5.2, 5.3, 5.5 and 5.7) showing the variation of differential stress with depth throughout the lithosphere. The top of the upper crust, lower crust and Moho are shown as solid black lines. Isotherms up to 1000 °C are overlain as dashed blue lines and seismicity > M2 that lay within 20 km distance of the section has been marked as red dots.*

The pattern of variations in integrated effective viscosity of the lithospheric mantle (shown in Figure 5.7) are the same as the integrated strength distribution of the whole lithosphere (Figure 5.5a), with higher strengths analogous to higher viscosities, corresponding closely to the Moho depth (Figure 5.3b). Seismicity is therefore observed in the orogen and southern foreland to spatially correlate to regions of lower viscosity such as the Alpine root (20.6 $\log_{10}$ Pa s) that surround the higher viscosity blocks such as the Ivrea Zone, Adriatic Indenter and Apennine plate (22.2 $\log_{10}$ Pa s). In the Northern Foreland the opposite is observed, with seismicity occurring in the region of highest viscosity surrounding the URG (20.8 $\log_{10}$ Pa s). Similar results, showing that viscosities below the crustal root must be lower than below the forelands have also been modelled by Chéry et al. (2016), in order to fit the observed trends of glacial rebound.

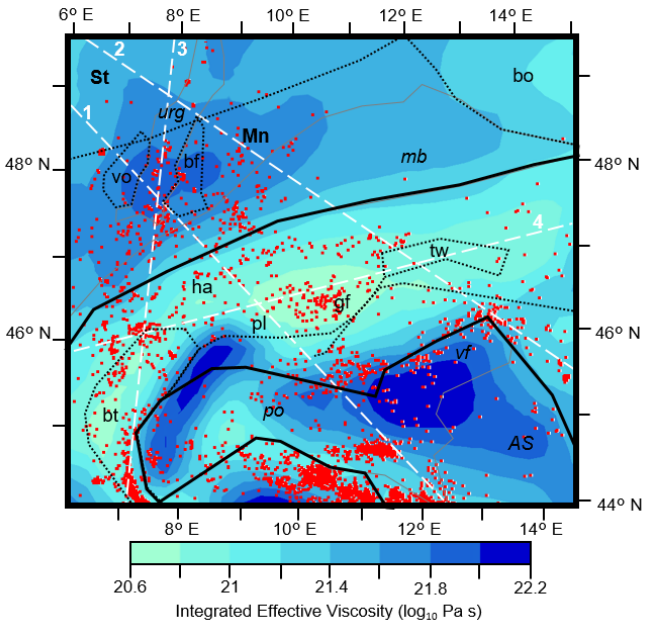

Figure 5.7. *Integrated effective viscosity of the lithospheric mantle across the modelled area with seismicity > M2 shown in red dots. Locations of key tectonic features are overlain (abbreviations shown in Figure 5.1a caption). Cross sections 1, 2, 3 and 4 from Figures 5.6 and 5.8 are marked with white dashed lines.*

Variations of effective viscosity with depth in relation to seismicity are shown in the cross sections on Figure 5.8. As previously observed, the majority of seismicity occurs in the upper crust, which largely corresponds here to effective viscosities of 23.5 $\log_{10}$ Pa s or higher. Viscosities for the lithospheric mantle tend to be between 19 – 23 $\log_{10}$ Pa s and for the lower crust between 21 – 23 $\log_{10}$ Pa s with both largely aseismic across the region. Regions where seismicity does occur deeper than the upper crust also correspond to regions of the lower crust or lithospheric mantle where effective viscosities are also in excess of 23.5 $\log_{10}$ Pa s, such as in the South East of Section 1 and the North of Section 3.

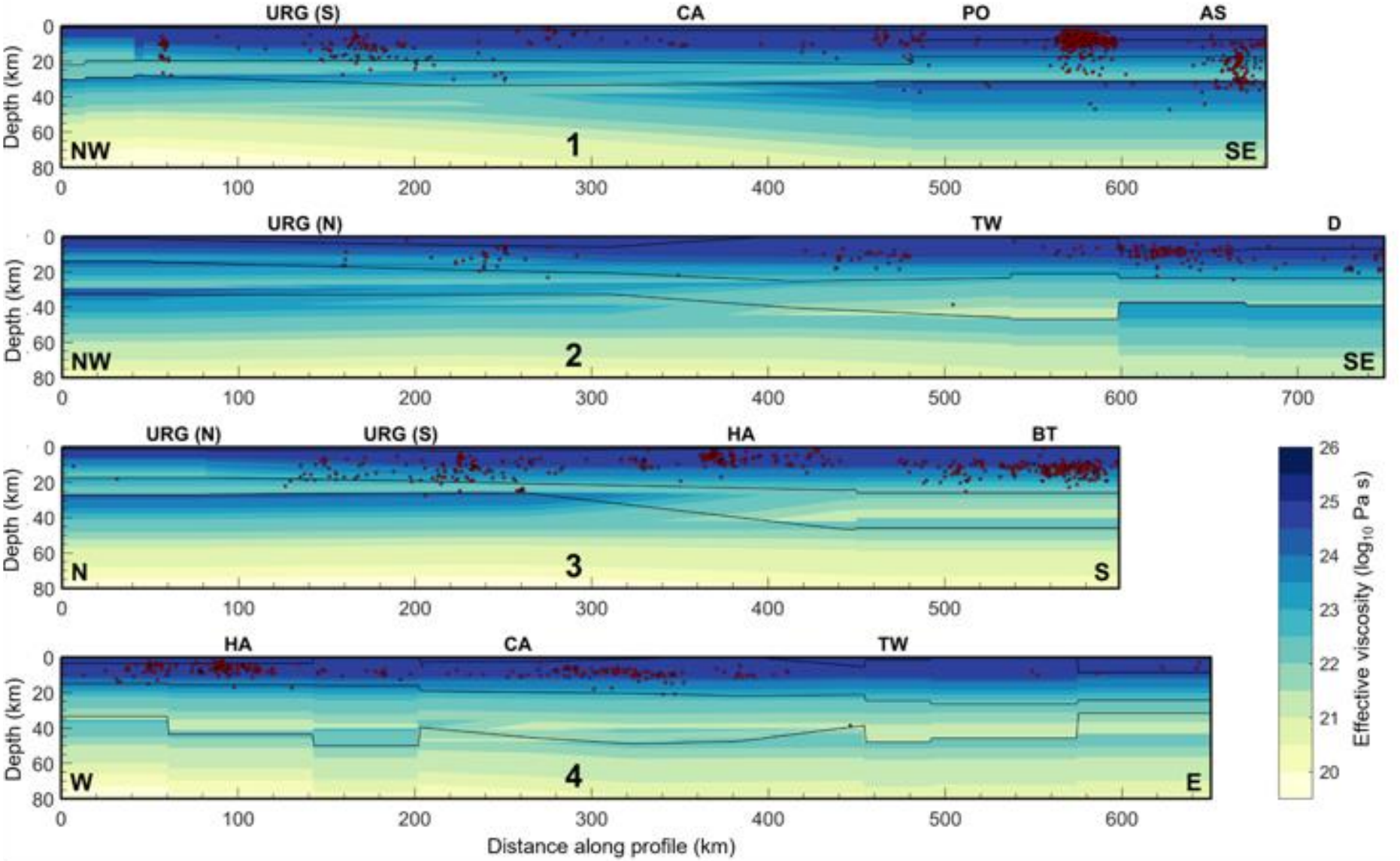

Figure 5.8. *Cross sections 1, 2, 3 and 4 (Locations shown in Figures 5.2, 5.3, 5.5 and 5.7) showing the variation of effective viscosity with depth throughout the lithosphere. The top of the upper crust, lower crust and Moho are shown as solid black lines. Seismicity > M2 that lay within 20 km distance of the section has been marked as red dots.*

5.4. Discussion

5.4.1. Mechanical Strength

The strongest regions at depth in the study area correlate with the 600 °C isotherms within the upper lithospheric mantle, corresponding to a phase change in mantle rocks (Boettcher et al., 2007, McKenzie et al., 2005). Additionally, the map of the integrated lithospheric strength (Figure 5.5a) portrays a positive inverse correlation with respect to the Moho depth (Figure 5.3b), allowing Moho depth throughout the region to be used as a first order estimate for the relative strength of the whole lithosphere. Based on these findings we can conclude that the lithospheric mantle is both the largest contributor to the overall computed lithospheric strength variations and is also highly influenced by the temperature configuration across the entire orogen foreland system, thereby expanding upon previous findings derived from, but limited to, the central Alps (Okaya et al., 1996).

The integrated crustal strength (Figure 5.5b) amounts only to a small portion of the total lithospheric strength (Figure 5.5a) except in locations where the crust is at its thickest such as the crustal root of the orogen (Figure 5.3a). Under this area, the pattern of crustal strength distribution equals the whole plate strength distribution. The presence of a weak and thick crust North of the Periadriatic lineament contributes to a significant weakening of the lithosphere underneath this domain, a feature that was also noticed by previous work (Marotta and Splendore, 2014). To further deepen the discussion about the implications derived from the thermo-rheological model on the seismicity distribution within the area we also note that Alpine events mostly occur beneath this domain, North and West of the Guidicarie fault, consisting mainly of the Helvetic nappes, where the crust is both warmer and weaker. This is part of a broader observed trend of West to East mechanical strengthening within the Alpine crust, that results in significantly less seismicity in the Eastern Alps, explained by a deepening of LAB topography (Figure 5.3d) and therefore a lower geothermal gradient.

The temperature distribution throughout the region is primarily a function of lithospheric composition, with the relative contribution of model layers to the heat budget varying in response to their specific thermal properties and relative volume. Features such as a shallow thermal LAB, here derived from a global tomographic model (Schaeffer and Lebedev, 2013), a higher percentage of felsic (radiogenic) upper crust to mafic lower crust or the presence of thick insulating sediment deposits have been previously shown to raise the geothermal gradient within the study area (Spooner et al., 2020). We therefore expect that these

specific features would also exert a first-order control on the resulting mechanical configuration of the lithosphere and thereof to the seismicity distribution.

5.4.2. Relation to Seismicity

The northern and southern forelands of the Alps display a markedly different pattern of seismicity in terms of their epicentre locations, potentially reflecting the different tectonic settings and driving mechanisms at play within each foreland. In the southern foreland seismicity primarily occurs at the boundaries of the European, Adriatic and Apenninic plates (e.g. Chiarabba et al., 2005). These locations mark a relatively sharp gradient in modelled lithospheric strength and effective viscosities from 13.9 $\log_{10}$ Pa m and 22.2 $\log_{10}$ Pa s within the plate to 13.2 $\log_{10}$ Pa m and 20.8 $\log_{10}$ Pa s along its edges, respectively. These mechanically stiff and rheologically strong lithospheric blocks move independent of one another (e.g. Nocquet and Calais, 2004). Therefore, it stands to reason that seismicity in such a setting would localise at the boundaries of these rigid lithospheric blocks (Figure 5.5a and Figure 5.7). The situation differs in the northern foreland, where seismicity occurs within an intraplate setting (e.g. Bonjer, 1997) of the European plate and where the upper mantle is not seismogenic. It therefore seems logical to assume that under these tectono-thermal conditions the weaker regions of the crust would accommodate the majority of seismicity as depicted in Figure 5.5b, where the lithospheric mantle remains relatively stable throughout the northern foreland.

It is nowadays established that temperature is an important variable for determining the depth of the lithospheric seismogenic domain. This was noted in the seminal study of Sibson (1982) that demonstrated a correlation between intraplate seismicity focal depths and surface heat flow distribution, with shallow seismicity in areas of high surface heat flow and vice versa. The existence of an inverse correlation between heat flow and focal depth is easy to explain when considering the homogeneous configuration of oceanic plates. However, it is challenging to extrapolate these results to continental intraplate regions where the log-linear age-temperature relationship does not apply and the thermal state is a complex function of the history of a heterogeneous plate over geological times. In such cases, a conservative estimate for the lower bound of the seismogenic zone can be derived based on a quasi-static thermodynamic description of the continental plate characterized by a non-Newtonian fluid-like rheology descriptive of its most abundant constitutive minerals. By relying on such a description, a maximum in the static strength would correspond to a particular value of the

system's internal energy, which can then be described by the temperature at its maximum dissipation potential. Under this assumption, one would expect that to a first-order, within the study area the 600 °C isotherm, which represents this transition for olivine rich lower crustal and mantle rocks (Boettcher et al., 2007, McKenzie et al., 2005), would both represent a maximum lower bound to seismicity and also the highest strength in the lower crust and upper lithospheric mantle.

The majority of observed seismicity occurs between the 200 °C and 400 °C isotherms, representing the strongest portion of the upper crust (up to ~1 GPa). Deeper in the crust, higher temperatures result in a gradual decrease in the plate strength and subsequent aseismic behaviour. These observations can be taken as indicative of the brittle-ductile transition within the crust, that provides a conservative estimate to the lower bound of the seismogenic zone in that area. Willingshofer and Cloetingh (2003) performed an end-member sensitive analysis for the lithospheric strength along the Transalp section of the eastern Alps in terms of considering either a strong or a weak crust. The main conclusion derived from their study was that a model portraying a strong crust provides a better fit with the seismicity. From their analysis they determine that the brittle-ductile transition occurs between 9 and 14 km. By plotting the depth level above which 95% of seismic events occur (Figure 5.9), our results, based on more up-to-date 3D structural and thermal model, estimate that the brittle-ductile boundary within the Alps occurs at ~ 20 km depth, providing a better fit with the depths of recorded seismicity and adding validity to the model setup utilised here.

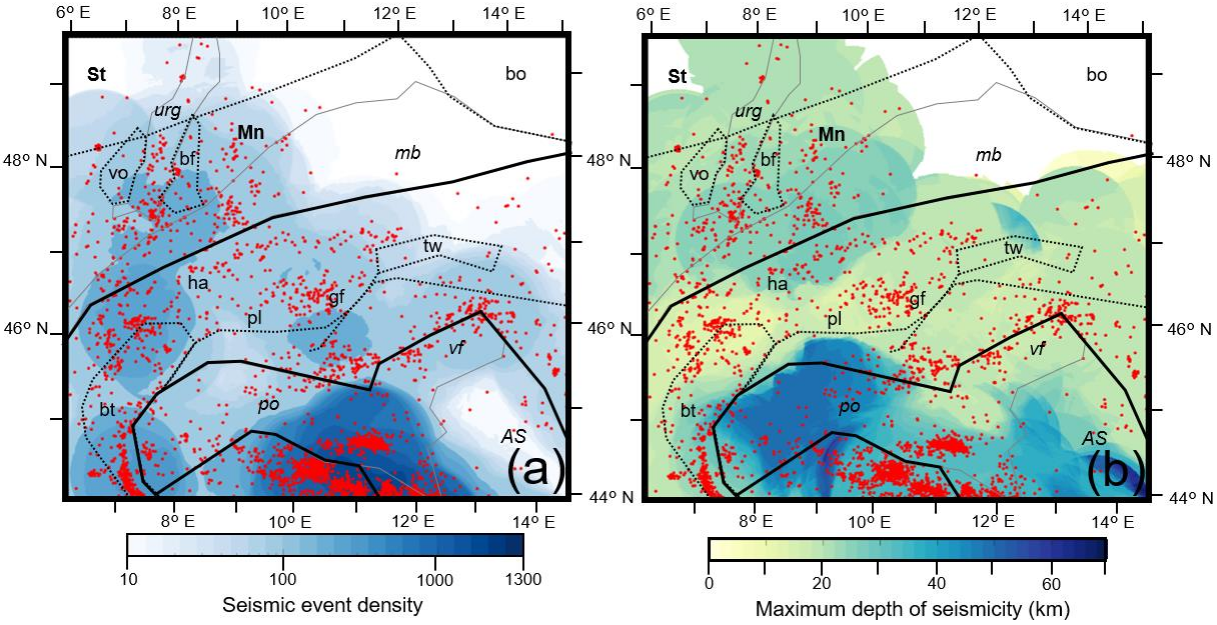

Figure 5.9. a) *Seismic event density and* ***b)*** *Maximum depth of seismicity (depth above which 95% of events occur) for events > M2 within a radius of 75 km of each grid point. Locations of key tectonic features are overlain (abbreviations shown in Figure 5.1a caption).*

Additionally, whilst the majority of seismicity occurs in the upper crust, observations also show that seismicity in deeper layers occurs in both the northern and southern forelands (e.g. Bonjer 1995; Chiarabba et al., 2005). From the differential stress cross sections shown here (Figure 5.6), it can be discerned that hypocentre depths of deeper seismicity vary with temperature, occurring where upper lithospheric mantle temperatures are ~ 600 °C or cooler. This thermal configuration leads to the presence of a relative weak lower crust, mechanically decoupled from and sandwiched between the upper crust and a strong upper mantle (more than 2 GPa), thus providing a first-order explanation to the deepening of seismicity in the area. Seismicity within the lower crust is found to only occur in domains of higher strength (~ 1.4 GPa), though within the majority of the region the lower crust is observed to be largely weak and therefore aseismic. This is particularly evident from the effective viscosity cross sections (Figure 5.8) depicting how the lower crust mechanically decouples the upper crust from the lithospheric mantle, with effective viscosity values (22.5 $\log_{10}$ Pa s) indicative of a ductile regime and fitting well with the general lack of observed lower crustal seismicity.

The unimodal pattern of seismicity beneath the Alps being limited to the upper crust contrasts to the bimodal (crust and upper mantle) seismicity pattern found in other orogens worldwide, such as the Himalaya. Based on this observation, a recent modelling study by Dal Zilio et al. (2018) advanced the hypothesis of a structural correlation between plate convergence rates and seismicity distribution alone. The analysis of Dal Zilio and co-authors is based on a linear correlation between convergence rates and the resulting thermal configuration of the orogen, with faster rates resulting in a colder orogen and therefore in a more widespread seismogenic brittle domain. A major limitation of this reasoning is that it does not take into account the role of crustal inheritance. Whilst results presented here mostly agree with the unimodal nature of seismicity throughout the crust, they also suggest that the lithospheric makeup of the region such as crustal, and lithospheric thickness have a first-order effect on the location of seismicity in the region via their control on the lithospheric thermal field. In addition, relating the overall distribution of seismicity within the Alpine region to the background tectonic convergence rates cannot reconcile the diversity in the observed seismic style across the whole orogen. While the eastern Alps are characterized by seismicity showing mainly dilatational faulting, the western and central Alps portray mainly compressional seismicity. Therefore, it would be difficult to relate this difference in style to a common geodynamic process. Indeed, there is evidence from present day uplift rates that the seismicity in the western Alpine domain could be instead related to still ongoing viscous relaxation from the waning of the last ice cap (e.g. Norton and Hampel, 2010; Chéry et al., 2016; Mey et al.,

2017; Sternai et al., 2019). In this regard a word of caution comes from the uncertainty in the mantle and (lower) crustal viscosities input in these studies. Past works have adopted values as low as ~20 $\log_{10}$ Pa s for mantle viscosity (Norton and Hampel, 2010; Chéry et al., 2016; Mey et al., 2017) whilst more recent work has made use of higher values ~22 $\log_{10}$ Pa s for the Alpine lithospheric mantle (Sternai et al., 2019). The values derived in the present study, ranging from ~21 $\log_{10}$ Pa s beneath the orogen to ~22 $\log_{10}$ Pa s in the forelands compare favourably to those estimates. In addition, our model favours the presence of lower viscosities below the orogen domain proper in comparison to below the forelands, a result that agrees with the main conclusions derived from Chéry et al. (2016). This last result confirms how the pattern and style of seismicity within the complex Alpine area cannot be related to a single geodynamic parameter, such as convergence rates, but should be considered as a natural outcome of a rather complex crustal structure developed during the whole orogenic cycle in an ongoing plate tectonic setting.

5.4.3. Slab Influence

The temperature present at the maximum depth of seismicity (Figure 5.9) is plotted in Figure 5.10a, showing that most mechanically strong portions of the plate, whether within the crust or the upper lithospheric mantle, are effectively bounded by the depth of the 600 °C isotherm previously discussed to represent the maximum temperature of seismicity. This trend also visible in the various cross sections through the region (Figure 5.6). In thick felsic crustal regions that also lie above a weak lithospheric mantle, such as the crustal root of the orogen, maximum depths of seismicity are significantly shallower than on the forelands and as such maximum temperatures of seismicity are also significantly lower at ~ 350 °C. We do however note regions where the maximum temperature of seismicity greatly exceeds 600 °C, corresponding to the presence of both actively subducting and previously subducted slabs, shown as high velocity features at a depth of 100km (Figure 5.10b) from a recent shear wave velocity model of the region (El-Sharkawy et al., 2020). As the thermal field utilised here (Spooner et al., 2020) is calculated as static and steady state, the cooling effect of subduction zones, which is still largely unquantified, is not incorporated. Therefore, the possibility of seismicity occurring in these regions at higher temperatures than expected is anticipated, as previously discussed in Spooner et al., (2020). This effect is most pronounced at the location of the active Apennine subduction zone where maximum temperatures of seismicity appear to approach 1000 °C, however regions where seismicity above 600 °C are also noticed below the

Alps, corresponding to the location of Alpine slabs, indicating that these frozen in subduction zones may still be having a thermal effect on the lithosphere.

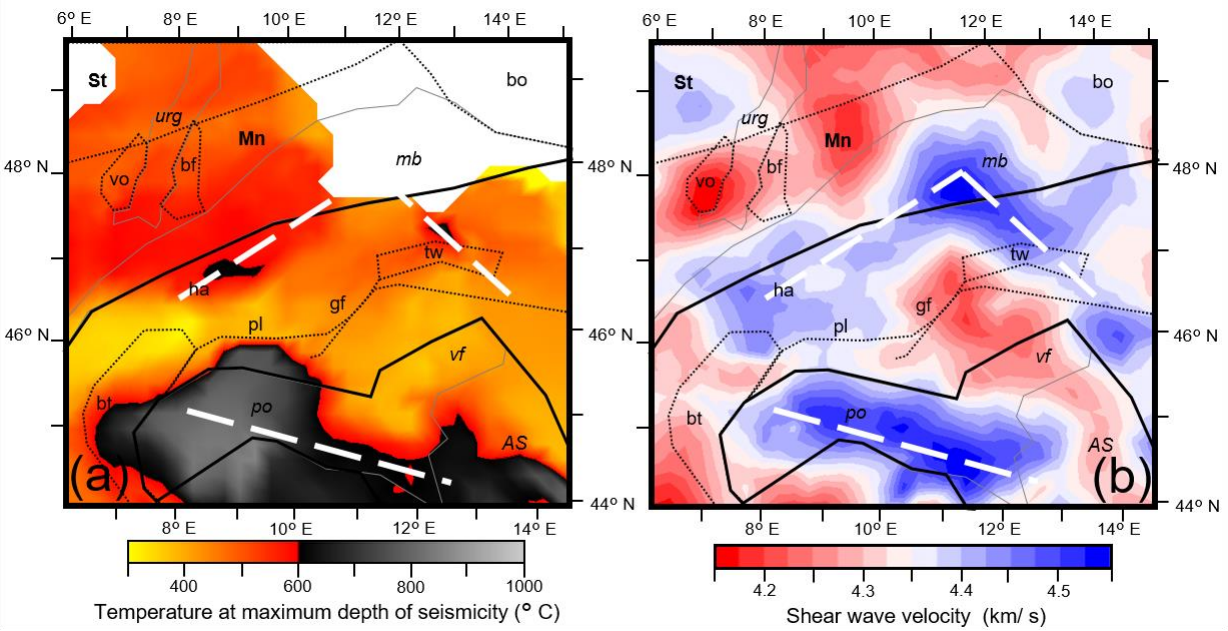

Figure 5.10. a) *Temperatures that correspond to the maximum depth of seismicity (Figure 5.9b).* ***b)*** *Shear wave velocity model at 100 km depth from El-Sharkawy et al. (2020). Locations of slabs are highlighted with white dashed line. Locations of key tectonic features are overlain (abbreviations shown in Figure 5.1a caption).*

5.5. Summary

In this work we have computed the long-term lithospheric yield strength for the Alpine regions and its forelands by using available up to date structural, density and thermal input data. Variations in the strength of the upper lithospheric mantle exert the largest influence on the strength of the whole lithospheric column, with crustal strength only contributing significantly to the whole plate integrated strength beneath the orogen proper, where the crust is thickest (55 km). The strength, whether in the crust or mantle, is largely temperature dependant, with upper lithospheric mantle temperatures controlled by Moho depth and crustal temperatures by thermal LAB depth, thickness of the radiogenic felsic upper crust and thickness and distribution of insulating sediments and.

The results from the thermos-rheological modelling exercise has shed light on the relationship between background seismicity and resolved lithospheric strength variations in the region. We

have been able to demonstrate how the occurrence of crustal seismicity in the study area is influenced by several factors acting at different scales with inherited geological crustal and upper mantle structures exerting a primary control in the seismicity distribution and style. The highest yield strength within the crust (~ 1 GPa) and upper mantle (> 2 GPa) occur at temperatures interpreted as phase transitions (crust: 200 – 400 °C; mantle: ~ 600 °C) with almost all seismicity occurring in these regions. We also note the presence of a weak lower crust (< 1 GPa) that mechanically decouples the upper crust and lithospheric mantle across the entire region. Therefore, the lower crust appears largely aseismic, likely due to seismic energy being dissipated by ongoing creep in regions where effective viscosities are lower. Both active present day and frozen-in subducting slabs are also shown to significantly influence the maximum depth of seismicity possible above them, furthering the argument that lithospheric inheritance and heterogeneity within the region, are key components to explain the regional distribution of seismicity.

In the Alps, seismicity correlates spatially with a weaker crust and lithosphere, such as the Helvetic Alps. Such a clear distinction cannot be derived uniquely for both forelands, each showing a different pattern of seismic distribution, likely reflecting their different tectonic settings. In the southern foreland seismicity preferentially occurs across boundaries between rigid lithospheric blocks, such as the strong Adriatic indenter, whilst in the northern foreland seismicity localises beneath domains of crustal weakness as in the URG.

Chapter 6. Discussion

6.1. Lithospheric Structure and Validation

By using a fully 3D integrated modelling approach, encompassing gravity, thermal and rheological models, that are validated with external observations, we are able to interrogate the lithospheric structure beneath the Alps and their forelands. The workflow was found to be highly successful, with each progressive step adding to the available data such that it benefitted the later works. Quantitatively, the final results were found to respect seismic imaging, seismic velocities, gravity readings, wellbore temperature readings and mantle viscosities for the region as demonstrated throughout Chapters 2, 3, 4 and 5. The results were also validated with comparable findings to prior modelling works, either in 2D (e.g Okaya et al., 1996; Willingshofer and Cloetingh, 2003) or smaller 3D sections (e.g Ebbing, 2002; Przybycin et al., 2014; Freymark et al., 2017) of the study area. Additionally, the structural model has been further validated by independent work, that derives a structural and density model of the northern Adriatic region from seismic velocities (Magrin and Rossi, 2020). Both densities and Moho depths, return remarkably similar values to those derived within this work utilising this different methodology, with a Moho depth misfit of less than ±5km and a mean of density differences lower than 50 kg/m^3 throughout the region.

Prior to the completion of this work, one of the most poorly constrained features in the region was the Moho depth beneath the Eastern Alps, even represented as a 'Moho gap' by recent works (Spada et al., 2013). Through the generation of the 3D gravity constrained structural model presented in Chapter 2, we shed light on this previously ill-defined feature, showing that a Moho depth of ~47.5 km fits the observed gravity in the region and aligns well with other values from within the orogenic root. Further, the use of this Moho depth was found to: replicate observed temperatures in the shallow subsurface using standard thermal parameter values for upper (2.4 W/mK, 1.60E-06 W/m^3) and lower crust (2 W/mK, 3.00E-07 W/m^3); result in the same integrated lithospheric strength (10^{13} Pa) as previous work (Willingshofer and Cloetingh, 2003); and lead to similar mantle viscosities (~21 $\log_{10}$ Pa s) as prior studies (Norton and Hampel, 2010; Chéry et al., 2016; Mey et al., 2017; Sternai et al., 2019). Similarly, Mroczek et al. (2020) derive Moho depths of ~47.5 km for the Adriatic plate in the 'Moho gap' using receiver functions, despite their suggestion of a deeper underlying European Moho, a feature we have not incorporated.

As work from Lowe et al. (2020) shows that the maximum gravity effect plates could have at the surface is 40 mGal, similar to the maximum accuracy currently achievable from our structural model (~±25 mGal), deducing plate geometries with gravity observations alone is at present not possible. In order to accurately constrain geometry or polarity of plates directly, a significant increase in the availability of high resolution data coverage across the region is required. However, as neither plates nor subduction interfaces have been accounted for within any of the models generated for this work, their associated effects, most notably significant cooling of the mantle, are also not present within our results. As such, all instances of seismicity occurring at modelled temperatures in excess of 600 °C (maximum depth of seismicity, Emmerson and McKenzie, 2007) correspond to the location of a plate within the region, as derived from tomography (El-Sharkawy et al., 2020). Therefore, we show that an integrated geophysical modelling approach presents the ability to indirectly shed light on the location of some plates and subduction interfaces within the Alpine region.

Interestingly, how close the subduction zone is to thermal equilibrium also appears to be observable. Ongoing subduction between the Adria and Apennine plates, corresponding to the highest observable rate of convergence within the region (Sánchez et al., 2018), shows the highest amount of seismicity, occurring at temperatures above 600 °C even up to 1000 °C. In contrast, within the Alps or at the Alps-Dinarides junction where convergence rates are much lower and the nature of subduction is debated (Kästle et al., 2019), seismicity exceeds 600 °C infrequently. This suggests that subduction within the orogen likely no longer occurs at present day or is slow enough that thermal equilibrium is almost maintained. We therefore show that meaningful observations can still be derived from models that do not account for all possible physical process.

One of the most important features in controlling lithospheric strength in the region is the definition of the LAB itself. For modelling, we combined data from two different sources, depths from the seismically derived LAB of Geissler et al. (2010) and temperatures from converting the shear wave velocities of Schaeffer and Lebedev (2013). We found that both sources validated one another, with the temperatures derived at those depths deviating no more than 100 °C from 1300 °C and the majority of the area corresponding almost perfectly. Nevertheless, more recent shear wave velocity models have been published during the undertaking of this work, namely El-Sharkawy et al. (2020), previously discussed in regards to identifying plate locations.

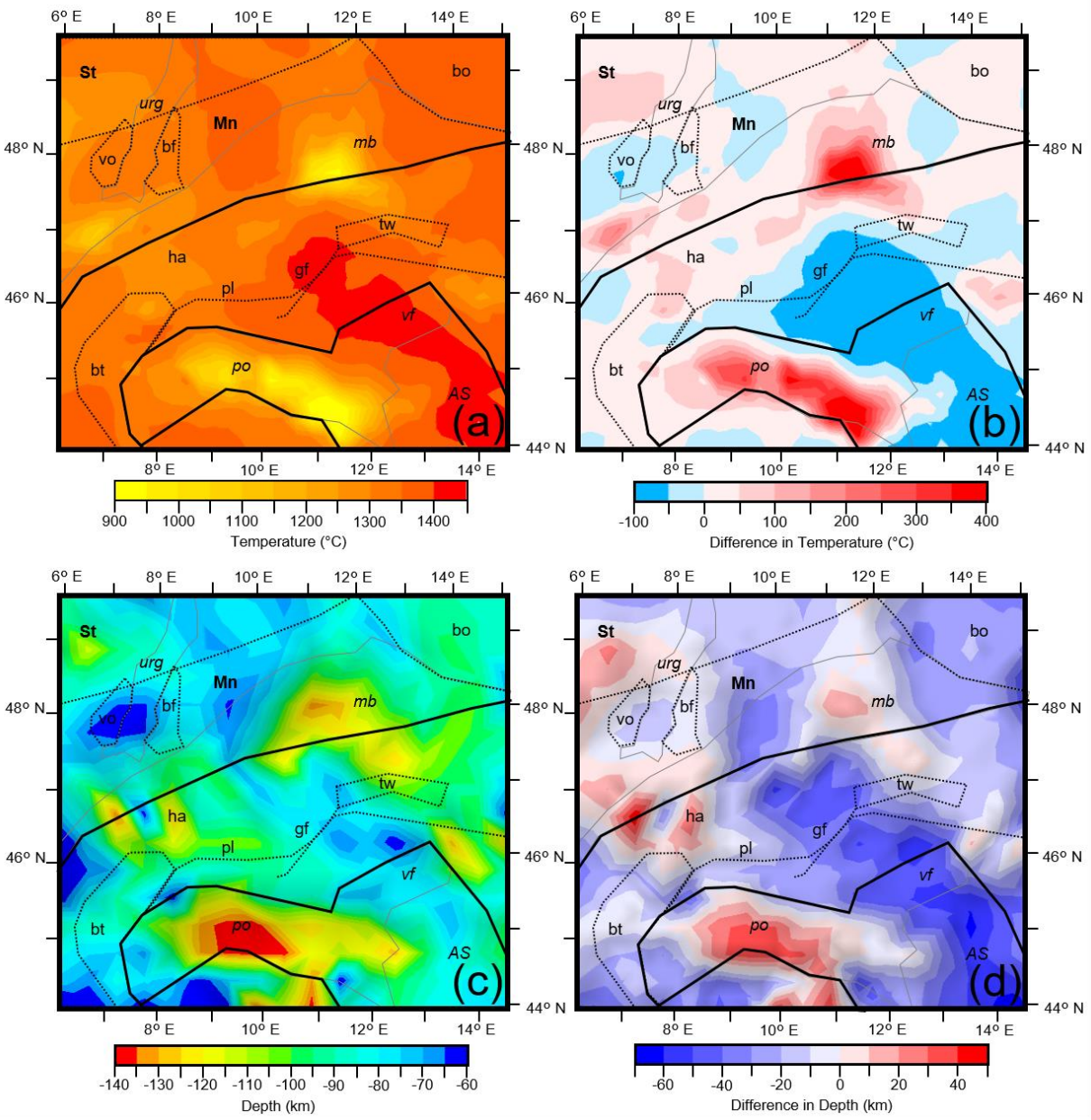

Figure 6.1. a) *Temperatures empirically derived from the El-Sharkawy et al. (2020) shear wave dataset at the depth of the Geissler et al (2010) LAB.* ***b)*** *Difference map between temperatures derived empirically from the El-Sharkawy et al. (2020) shear wave dataset and the Schaeffer and Lebedev (2013) dataset.* ***c)*** *Depth of the 1300 °C isotherm (LAB) extracted from the El-Sharkawy et al. (2020) dataset.* ***d)*** *Difference map between the LAB depth derived from the El-Sharkawy et al. (2020) dataset and from Geissler et al (2010). St – Saxothuringia; Mn – Moldanubia; bo – Bohemian Massif; vo – Vosges Massif; bf – Black Forest Massif; tw – Tauern Window; bt – Briançonnais Terrane; iz – Ivrea Zone; ha – Helvetic Alps; pl – Periadriatic Lineament; gf – Guidicarie Fault; urg – Upper Rhine Graben; mb – Molasse Basin; po – Po Basin; vf – Veneto-Friuli Plain; AS – Adriatic Sea.*

For comparison, shear wave velocities from El-Sharkawy et al. (2020) were converted to temperature at depths corresponding to the Geissler et al. (2010) LAB, in the same manner detailed in Chapter 3, with results shown plotted in Figure 6.1a. In contrast to the Schaeffer and Lebedev (2013) dataset, temperatures can be seen to deviate much further from 1300 °C. A difference map between temperatures derived from the Schaeffer and Lebedev (2013) and El-Sharkawy et al. (2020) datasets, calculated as the former minus the latter, is plotted in Figure 6.1b. The El-Sharkawy et al. (2020) values are observed to be consistently 100 °C warmer across the Adriatic plate, and 400 °C cooler in the Apennine and Alpine slabs. The depths of the 1300 °C isotherm from the El-Sharkawy et al. (2020) dataset, plotted in Figure 6.1c, in contrast to Geissler (2010), implies a largely flat LAB at around 80 km deep across the region, deepening to over 120 km only where plates are present. A difference map between the Geissler (2010) LAB depth and the 1300 °C isotherm from El-Sharkawy et al. (2020), calculated as the former minus the latter, is plotted in Figure 6.1d. The El-Sharkawy et al. (2020) dataset suggests the Adriatic LAB is 70km shallower than the Geisler (2020) LAB, whilst also being up to 50 km deeper in the regions where plates are present.

As we found that the Geissler (2010) and Schaeffer and Lebedev (2013) datasets complement one another, and that our thermal and rheological results were verified with outside measurements, such as wellbore temperature measurements and mantle viscosity values, we would suggest they represent a good approximation of the LAB depth within the region. Values derived from El-Sharkawy et al. (2020), deviate largely from this and would result in highly different thermal and rheological results, unlikely to fit the other independent data sources. They appear much more sensitive to the location of plates within the region, and as such they have been used for this purpose within our studies.

Lithospheric heterogeneity was represented through the definition of domains corresponding to different physical properties. These were constrained through gravity modelling alone, as current knowledge of Alpine tectonic features at depth in 3D is limited. Nevertheless, most correspond to locations of known features, such as the Brianconnais Terrain, the Tauern Window and the Adriatic and Apennine plates, lending validity to the results. As such, interfaces between domains also correspond to known fault systems such as the Alpine front and the Schio-Vicenza zone, allowing for the relationship between lithospheric structure and seismicity to be investigated.

6.2. Lithospheric Heterogeneity and Relation to Seismicity

Lithospheric heterogeneity is ubiquitous throughout the region, stemming from the different characteristics of the plates involved in orogenesis. This is exemplified in the present-day contrast between both the crust and upper mantle densities of the European (~2750 kg m^{-3}, 3305 kg m^{-3}) and Adriatic plates (~2800 kg m^{-3}, 3335 kg m^{-3}), of the northern and southern forelands respectively. The provenance of Alpine crustal blocks are also shown to be identifiable based on their densities, with zones of Adriatic provenance (Austro-Alpine unit and Southern Alps) found to be denser and those of European provenance (Helvetic zone and Tauern Window) to be less dense. This observation also encompasses thermal parameters, with the Adriatic crust producing less radiogenic heat (1.30E-06 W/m^3) than in the European crust (1.3–2.6E-06 W/m^3), consistent with the Adriatic crust being more mafic than the European crust, as suggested by their densities. This results in a stronger Adriatic crust (~13.1 $\log_{10}$ Pa m) in general than European crust (~13.05 $\log_{10}$ Pa m), demonstrating how different inherited physical properties like density and radiogenic heat production can impact strength.

Other inherited features, such as crustal thickness, also play a crucial role in contributing to the lithospheric strength distribution, with the thicker Bohemian crust (40 km) appearing stronger (13.15 $\log_{10}$ Pa m) than the thinner Moldanubian (30 km, 13.1 $\log_{10}$ Pa m), despite being represented with similar densities (Moldanubia: 2710 kg m^{-3}, Bohemia: 2720 kg m^{-3}) and the same thermal parameters (2.6 W/mK, 1.80E-06 W/m^3). The thicker radiogenic upper crust also results in raised crustal temperatures (500 °C at 20 km) and a deeper Moho (40 km) when compared to the adjacent Moldanubian domain (450 °C at 20 km, 30 km), leading to lower mantle strengths. As the lithospheric mantle has been shown in Chapter 5 to accommodate the majority of the lithospheric strength, this results in a lower integrated lithospheric strength for Bohemia (13.2 $\log_{10}$ Pa m) than Moldanubia (13.4 $\log_{10}$ Pa m). A similar effect is also observed in the Alpine orogen and other regions of thickened upper crust.

As lithospheric strengths are highly dependent on the thermal field, the lower thermal boundary condition also exerts a first order control on modelled strength trends. The hybrid LAB utilised within this work, the validation of which is discussed in the previous section, is highly variable throughout the study area as a result of regional tectonics. Its shallowest point (70 km), corresponds to the CERS, resulting in raised crustal temperatures (540 °C at 20 km), with the deepest point (140 km) corresponding to the Adriatic indenter and colder crustal temperatures (380 °C at 20 km). Inherited lithospheric thickness therefore also represents an important role in the observed strength contrast between the stronger crust of the Adriatic

(~13.1 $\log_{10}$ Pa m) plate and the weaker European crust (~13.05 $\log_{10}$ Pa m). As such, our results clearly show that observed heterogeneous lithospheric strength is heavily influenced by inherited crustal and lithospheric thicknesses along with inherited physical properties from both prior and present orogenies, leading to the possibility that they may also exert a control on regional deformation patterns.

This is continuously demonstrated throughout the work presented here, with seismicity shown to localise at the interfaces between blocks of different physical properties, such as corresponding to weaker integrated lithospheric strengths surrounding the rigid Adriatic indenter, which as with most regions of high lithospheric strength, appears largely aseismic. Within the Northern foreland however, the lithospheric strength does not vary pronouncedly, largely due to the intraplate setting resulting in consistently high mantle strengths. Nevertheless, the European crust does exhibit seismicity, specifically around the URG, largely due to crustal strength contrasts. Therefore, whilst differences in tectonic setting appear fundamental in controlling seismicity localisation, seismicity consistently corresponds to strength contrasts in the crust or lithosphere that likely lead to the formation of structures prone to accommodate seismicity.

With depth however, seismicity principally localises at depths corresponding to the highest strengths, often corresponding to phase transitions within the crust or upper mantle. Deeper regions of lower strength and viscosity, such as the lower crust, appear largely aseismic due to stresses being dissipated through creep processes, suggesting that the lower crust acts as an incompetent layer, decoupling the upper crust from the lithospheric mantle. This even appears to be the case in the Eastern part of the Southern Alps where Adria-Europe convergence is still active. As such, seismicity distribution appears largely controlled by the thermal field and resultant lithospheric strength, previously discussed to be heavily influenced by lithospheric heterogeneity from tectonic inheritance. This finding partly contrasts to recent work (Dal Zilio et al., 2018), that attributes the seismicity depth distribution across the region solely to the relatively low plate convergence rate, with negligible influence from tectonic inheritance, as we show that whilst tectonic inheritance is highly important, tectonics still play a role.

6.3. Crustal Focus Model

The Crustal Focus model in Chapter 4 was created due to indications from the thermal modelling results in Chapter 3 that the upper crust beneath the Po Basin may be slightly too

thick in the General Focus model (structural model from Chapters 2, 3 and 5). As such, the upper crust in this region was thinned, with the lower crust thickened to compensate. Further necessary alterations were made to the structural model using the same gravity modelling methodology described in Chapter 2, with the resulting model replicating seismic and gravity observations as well as the General Focus model. The thickness of the crust in the Crustal Focus model can be seen in Figure 6.2a, with a difference map of crustal thickness calculated as Crustal Focus model – General Focus model, plotted in Figure 6.2b.

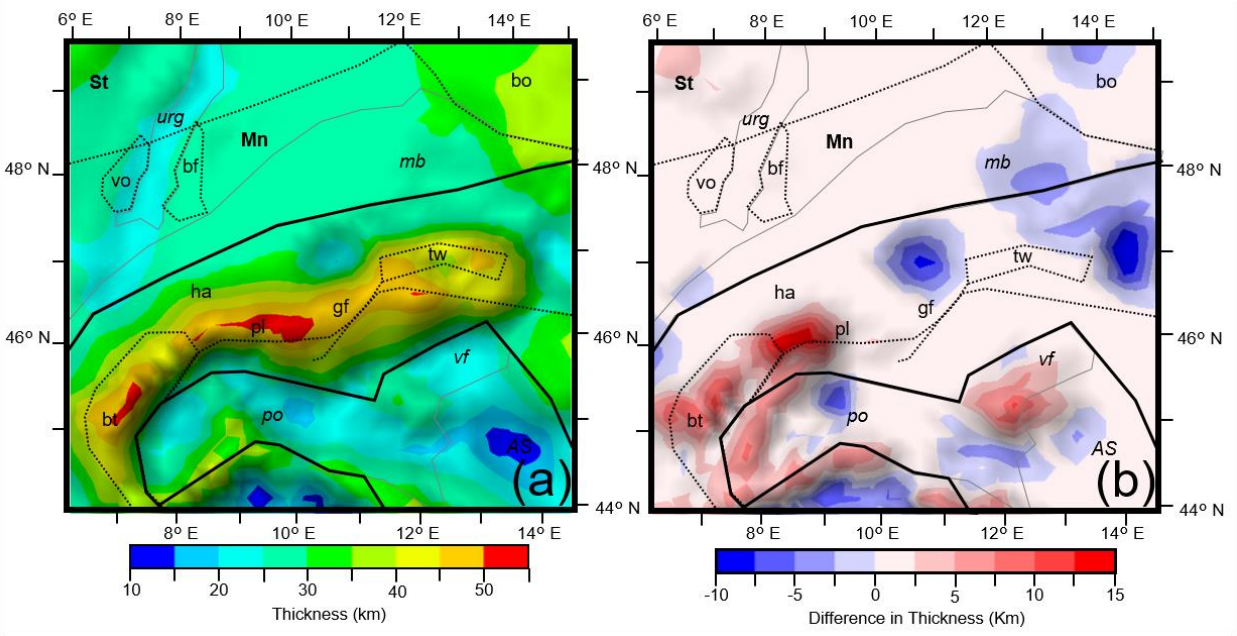

Figure 6.2. a) *Crustal thickness of the Crustal Focus model.* ***b)*** *Difference map between the crustal thickness of the Crustal Focus model and the General Focus model. Locations of key tectonic features are overlain (abbreviations shown in Figure 6.1 caption).*

The crustal thickness of the Crustal Focus model can be seen as largely the same as the General Focus model across the majority of the region, showing very similar overall trends. However, the modelled crust is thicker beneath the Brianconnais Terrain and Ivrea Zone (up to 15 km thicker) in the Crustal Focus model, whilst the crust on the Apennine plate and portions of the Central and Eastern Alps are thinned (up to 10 km thinner). The average density of the crust in the Crustal Focus model is shown in Figure 6.3a, with a difference map of average crustal density calculated as Crustal Focus model – General Focus model, plotted in Figure 6.3b.

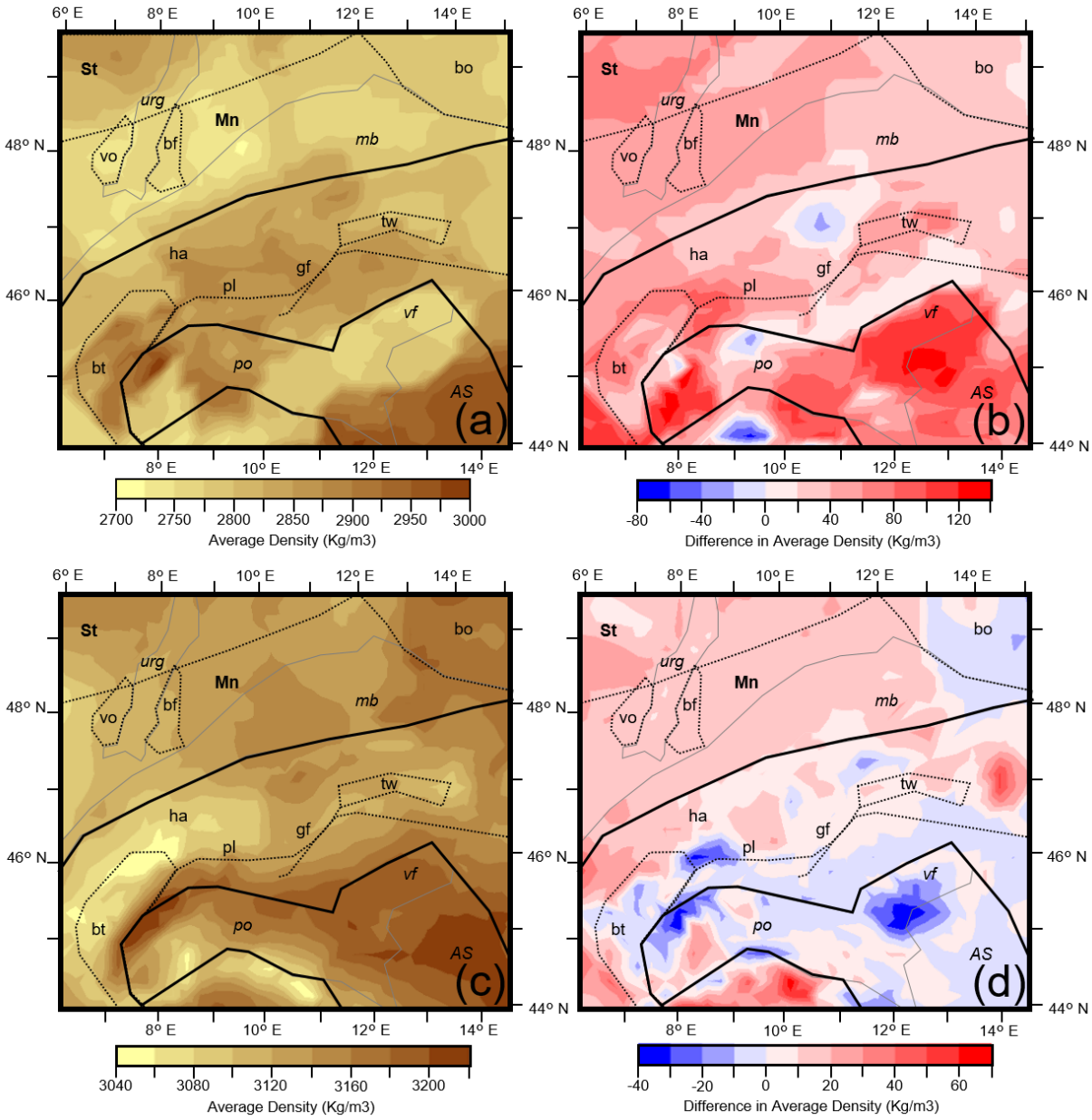

Figure 6.3. a) *Average density of the upper and lower crust for the Crustal Focus model.* ***b)*** *Difference map between the average density of the upper and lower crust of the Crustal Focus model and the General Focus model.* ***c)*** *Average density of the entire lithosphere for the Crustal Focus model.* ***d)*** *Difference map between the average density of the entire lithosphere for the Crustal Focus model and the General Focus model. Locations of key tectonic features are overlain (abbreviations shown in Figure 6.1 caption).*

It is evident how relatively localised alterations to the thickness of the crust, as shown in Figure 6.2, can require significant changes in density across the entire region's crust, in order to fit the observed gravity. As such, the importance of utilising a 3D approach for gravity constrained structural models is emphasised. However, as would be expected from the gravity constraint, the overall change in lithospheric density is very low, with the average lithospheric

density of the Crustal Focus model shown in Figure 6.3c, and a difference map of average lithospheric density calculated as Crustal Focus model – General Focus model, plotted in Figure 6.3d.

The thermal field of the Crustal Focus model was then generated using the same thermal parameters as Chapter 3. The thermal field of the Crustal Focus model was found to replicate thermal observations as well as the General Focus model. Neither is able to be classed as a definitely 'better' model, as both are focussed on different features, with the strengths and weaknesses of each discussed in the sensitivity analyses conducted in Chapter 4. The depth of the 600 °C isotherm from the Crustal Focus model is shown in Figure 6.4a, and a difference map of the depth of the 600 °C isotherm, calculated as Crustal Focus model – General Focus model, is plotted in Figure 6.4b.

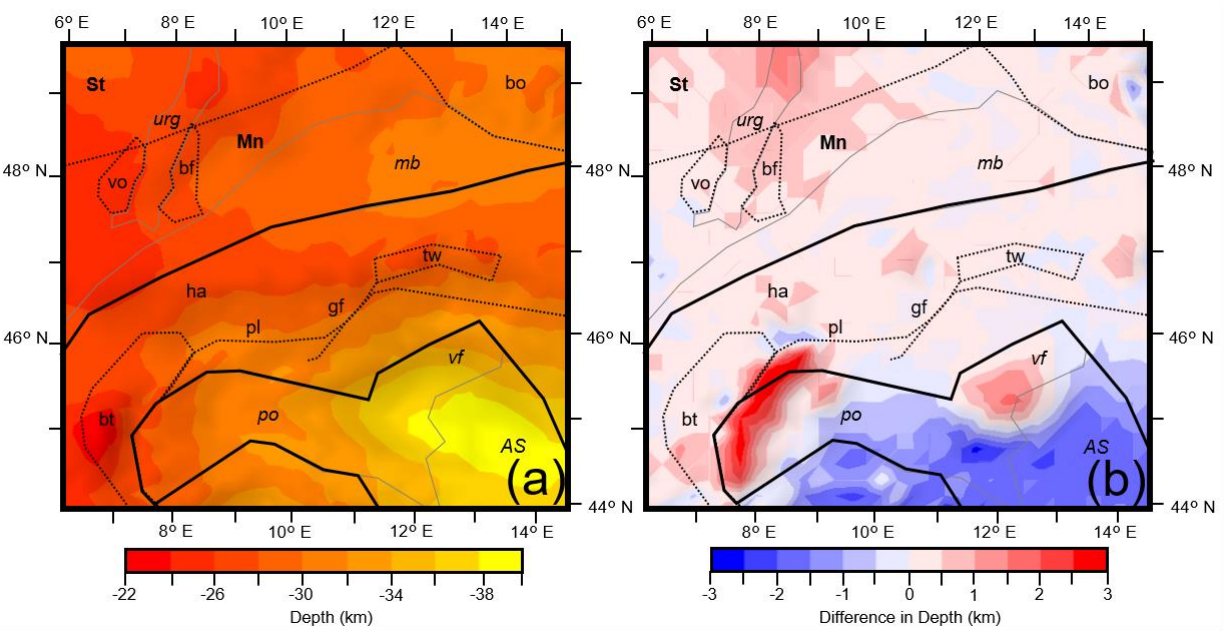

Figure 6.4. a) *Depth of the 600 °C isotherm from the Crustal Focus model.* ***b)*** *Difference map between the depth of the 600 °C isotherm from the Crustal Focus model and the General Focus model. Locations of key tectonic features are overlain (abbreviations shown in Figure 6.1 caption).*

As with the crustal thickness, the 600 °C isotherm depth across the majority of the region remains mostly unchanged in the Crustal Focus model. However, the isotherm does appear shallower beneath the URG, Ivrea Zone, and Venetto-Fruili plain (up to 3 km shallower) and deeper through the majority of the Adriatic plate (up to 3 km deeper). As strength is reliant on the thickness and density of layers as well as the thermal field, all of which have been demonstrated to be altered to varying degrees in the Crustal Focus model, the potential remains

that this model also leads to differing strength trends. To interrogate this the strengths for the Crustal Focus model were calculated using the workflow described in Chapter 5. The long term integrated strength of the crust and lithosphere are shown in Figures 6.5a and c respectively, and difference maps of integrated strengths of the crust and lithosphere, calculated as Crustal Focus model – General Focus model, are plotted in Figure 6.5b and d respectively.

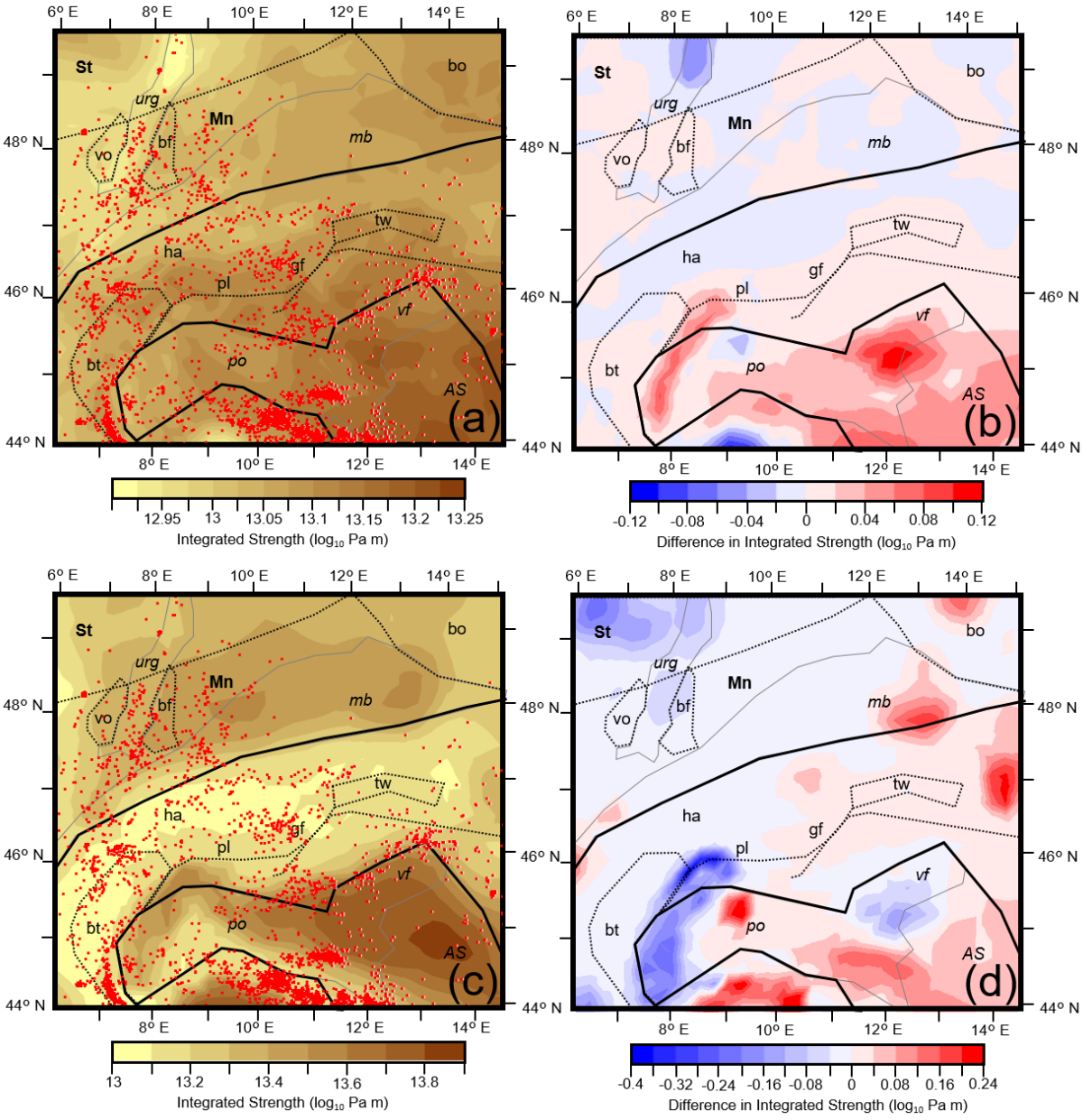

Figure 6.5. a) *Integrated strength of the upper and lower crust for the Crustal Focus model with seismicity > M2 shown in red dots.* ***b)*** *Difference map between the integrated strength of the upper and lower crust of the Crustal Focus model and the General Focus model.* ***c)*** *Integrated strength of the entire lithosphere for the Crustal Focus model with seismicity > M2 shown in red dots.* ***d)*** *Difference map between the integrated strength of the entire lithosphere for the Crustal Focus model and the General Focus model. Locations of key tectonic features are overlain (abbreviations shown in Figure 6.1 caption).*

Despite the absolute values of some features changing, such as a stronger crust in the Adriatic plate and a weaker lithosphere beneath the Saxothuringian terrain, the overall strength trends largely remain the same in the Crustal Focus model as the General Focus model and as such, the trends in relation to seismicity are largely the same. However, there are still localised improvements in the correlation between seismicity and strength along the southern extend of the Ivrea zone, the edges of the Adriatic indenter, and the URG, although these only serve to reinforce trends already identified and discussed previously from the General Focus model.

Our findings show that both the Crustal Focus model and General Focus model indicate a convergence in results despite different initial setups. Both models show consistent relationships between regional strength and seismicity even when features like crustal thickness and density were configured significantly different. The possibility therefore exists that the convergence of results is due to the enlargement of the parameter space through the integration of further data sources, in such a way that uncertainties in the model construction have been minimised, allowing for more consistent descriptions of the system state. This may suggest that unavoidable issues of non-uniqueness in the model generation workflow described here, can be dealt with through the use of additional constraining data at each stage of the modelling workflow.

This is explicitly discussed by Wellmann and Caumon (2018), as they show that one of the best ways to minimise uncertainty in geological modelling workflows, is to integrate distinct datasets of differing observations. This concept has been comprehensively carried out in the work described here, with different constraining datasets used at each stage in the modelling workflow and results of previously stages contributing to the available data such that they benefitted later works. Sensitivity work carried out in Chapter 2 also demonstrates the danger of using only one data source for the definition of physical properties, with lower crustal density values derived directly from p wave velocities alone resulting in large misfits from gravity observations.

However, as discussed in Chapter 4, the resolution and distribution of datasets used for model constraint also introduce an intrinsic bias into the workflow. As is typical in geoscience applications, this stems from certain regions possessing a high quality of data coverage, often in areas of interest to the hydrocarbon or other industries such as the Po Basin within our study area, whilst other regions possess much sparser coverage, such as within the Alps. The possibility therefore also exists that the converging results of the Crustal Focus and General Focus models represents the limitations exerted on model generation caused by the resolution and distribution of all datasets integrated during the modelling workflow. As such, whilst

enlarging the parameters space (with integrated data) could help downsize the intrinsic uncertainty in the model reconstruction, the data quality and distribution also comes with a bias in the tuning of the modelling outcomes, meaning that both likely exert a large degree of control in our results.

6.4 Limitations and Future Plans

Whilst the 3D workflow that has been utilised provides significant benefits, limitations in the coverage of available data presents challenges. Although gravity datasets of the region (e.g. Förste et al., 2014) allow for the validification of viable secondary data sources (e.g. Tesauro et al., 2008; Molinari and Morelli, 2011) to bridge gaps in deep seismic survey coverage, constraining thermal data is not present across the whole region. As the thermal field exerts a primary control on calculated lithospheric strengths, the most desirable additional data for the generation of better models, is therefore an improvement in the coverage of wellbore temperature measurements. This would further efforts to negate non-uniqueness in the modelling methodology through the use of a joint inversion workflow and allow for the ability to invert for solutions to gaps in our present day understanding of the Alpine subsurface geometries or properties, which was currently found not possible given the spread of available temperature measurements.

The availability of new datasets such as the Alp Array Gravity Research Group Bouguer map of the region (Zahorec et al., 2021), a state of the art compilation of terrestrial gravity observations with a resolution of 2km x 2km, and regional Moho maps (Mroczek et al., 2020) including features such as the depth of European Moho where it underlies the Adriatic Moho, will also facilitate the generation of higher fidelity structural models of the region. This would allow the workflow to identify smaller local features due to an increase in resolution, potentially allowing for the identification of plate geometries from gravity datasets, through a better resolved crustal model. In turn, it could also ultimately result in the calculation of more precise physical property values for the region and increase present-day knowledge on the continuation of tectonic boundaries at depth.

The models generated within this work heed recommendations from Wellmann and Caumon (2018) in regards to good modelling practice, by possessing a high level of geological realism, to account for the heterogeneity of physical properties within lithospheric layers. This is in contrast to most proceeding regional models of the Alps and their forelands that utilise homogenous values (e.g. Tesauro et al., 2009; Limberger et al., 2018). To emphasise the importance of representing lateral heterogeneity, Chapter 3 shows how the fit of calculated to

measured temperatures can be improved by altering the thermal properties of different tectonic domains away from a homogenous layer cake solution, especially in layers further from the surface (>3km).

To compliment this, a further improvement would be to integrate numeric datasets that describe the distribution of physical properties in 3D. In this way, regional velocity models of the crust (Jozi Najafabadi et al., 2020) or the mantle (El-Sharkawy et al., 2020) could be voxelised in order to constrain 3D property variation within a modelled layer, or supplement gaps in interface depths from other sources, such as deep seismic surveys. This would also dramatically increase the resolution of heterogeneity possible to incorporate within the modelling workflow and allow gradational change of physical properties laterally within a block to occur or with depth.

However, an increase in the fidelity of heterogeneity representable throughout the study area also poses additional challenges. Whilst lateral heterogeneity within layers was implemented in the gravity and thermal models, disagreement between experimentally derived flow law values from a laboratory setting and from lithospheric scale geodynamic models, meant homogenous flow laws were used for layers of the rheological model. Future work will be required in this field to tackle the challenges stemming from the difficulties on how to represent polymineralic lithospheric rocks using experimentally derived monomineralic values and with upscaling values from laboratory measurements to represent a tectonic block within the lithosphere.

Nevertheless, the creation of a model that perfectly replicates the present day lithospheric configuration, is by definition impossible (Box, 1979). The results described here however, show that despite present day data availability not supporting the constraint of all lithospheric and plate structures, methods of heat flow or rheological heterogeneity within model layers, meaningful information at an orogen scale is still provided. As such, the structural, density, thermal and rheological models produced using this workflow represent a significant improvement on the state of the art knowledge of Alpine lithospheric configuration and its relation to observed deformation within the region.

Whilst the results obtained here represent the state of the art understanding of the Alpine lithospheric state, increasing the complexity of the modelling workflow may lead to improved results, by accounting for additional physical processes such as: (i) the adoption of coupled fluid flow thermal models, in order to incorporate the effects of hydrothermal convection, such as in the URG (Koltzer et al., 2019), and the Schio-Vicenza fault zone (Pola et al., 2020), which could result in altered temperatures at shallow depths in these areas; (ii) by running transient

thermal models in order to account for regions not in thermal equilibrium, such as in the presently rifting URG (Heckenbach et al., 2021), which could result in altered temperatures at crustal and mantle depths beneath the rift; (ii) the use of variable strain rates to account for changes both laterally and with depth, also demonstrated in the URG (Heckenbach et al., 2021), which would result in lower surface strain rates but higher mantle strain rates. All of these effects have the potential to alter calculated strengths, however more data regionwide is required before models of this complexity can be carried out. Nevertheless, the results generated here provide a solid backbone for these additional studies in the future.

Rheological results obtained in this work also present the opportunity to contribute to the ongoing debate on the relative impact of glacial isostatic adjustment versus tectonic and mantle dynamic processes as causes of the observed present-day kinematic state of the Alpine region. Calculated mantle viscosity values (~21 $\log_{10}$ Pa s) are broadly in line with values used by others (20-22 $\log_{10}$ Pa s, Norton and Hampel, 2010; Chéry et al., 2016; Mey et al., 2017; Sternai et al., 2019). In contrast to other works, we present here, variable mantle viscosities throughout the region that are validated through multiple independent data sources, which can act as important observations for future works constraining Alpine glacial isostasy.

Work towards comparing relationships between lithospheric strength and seismicity, utilising a similar integrated gravity, thermal and rheological modelling workflow is also being carried out in other orogens, such as the Andes (e.g. Rodriguez Piceda, 2020). Comparison between the results generated here and from other regions of the world, allow for the interrogation of commonalities. As such, conclusions could be made about whether the identified trends relating to lithospheric strength and deformation in the Alpine subsurface are unique to the region or applicable globally, furthering our understanding of the fundamental processes that lead to seismicity localisation and how it relates to lithospheric configuration.

Chapter 7. Conclusions

The overall aim of this dissertation was to interrogate how lithospheric configuration controls the patterns of observed seismicity within the Alps and their forelands. The main outcomes of this work can be summarised as:

1. The Adriatic crust is thinner and more mafic (~22.5 km, 2800 kg m^{-3}, 1.30E^{-06} W m^{-3}) than the thicker and more felsic European crust (~27.5 km, 2750 kg m^{-3}, 1.3–2.6E^{-06} W m^{-3}), with the provenance of Alpine domains also identifiable based on their physical properties.
2. Inherited heterogeneous features such as crustal and lithospheric thickness have a large impact on resultant lithospheric strength trends, largely due to the impact they have on the thermal field.
3. Long term strength trends in the crust and lithosphere closely correspond to the location of seismicity throughout the region.
4. The relationship between long term strength and seismicity differs by tectonic setting, with events in the plate boundary setting of the southern foreland corresponding to weak integrated lithospheric strengths, and events in the intraplate setting of the northern foreland, instead corresponding to weak crustal strengths.
5. Seismicity within the crust or upper mantle localises at depths corresponding to the highest strengths, often corresponding to phase transitions (felsic crust: 200–400 °C; mafic crust and upper mantle: ~600 °C), with no seismicity present in very weak regions due to stresses being dissipated through creep processes.
6. Through the generation of 2 models with different initial lithospheric configurations that are both constrained by the same data observations and result in consistent relationships between regional strength and seismicity, it is demonstrated that whilst non-uniqueness is an unavoidable component in the model generation workflow described here, the integration of multiple observation based datasets helps minimize this uncertainty.
7. Locations where seismicity appears to occur above 600 °C based on steady state thermal calculations, are demonstrated to correspond to the locations of slabs within the region, due to those systems not being in thermal equilibrium yet.

Acknowledgments

This thesis represents the findings of the project INTEGRATE (Integrated 3D structural, thermal, gravity and rheological modeling of the Alps and their forelands), that was carried out as part of the 4D-MB (Mountain building processes in 4D) SPP funded by the DFG (Deutsche Forschungsgemeinschaft) as part of the international AlpArray initiative. My thanks go out to everyone from these institutions and projects involved in granting or securing funding for this work, I quite literally couldn't have done it without you. To Mark Handy and Emanuel Kästle for organising all of the Alpine meetings, sessions and field trips I had the pleasure to take part in over the course of my project I offer sincere thanks. I would also like to thank all of my colleagues from these projects, for all the interesting discussions we have had over a pint, be it in Bratislava, Frankfurt, Vienna or Heiligenblut.

I would like to thank all of those involved in the supervision of this work, Sascha Brune, Michael Weber and particularly Magdalena Scheck-Wenderoth, who definitely had to put up with the lion's share of questions and constantly encouraged me to "Go for Gold!". Your combined guidance has proved invaluable. Thanks to every co-author I had the pleasure of publishing alongside, Hans-Jürgen Götze, Jörg Ebbing, György Hetényi and Elco Luijendijk, your contributions, be it from datasets, previous models or constructive comments, were crucial in shaping this work into what it became. Particular thanks are extended to Denise Degen who's patience, hardwork and expertise resulted in a paper that really brings a lot to this work.

To all of you Basin Modellers from GFZ Section 4.5 I also extend my sincerest gratitude, your advice, comments, support and friendship throughout has helped me get by, not just in work but also outside of it. Thanks to Mauro Cacace for his support with almost every model ran, talk given and paper written during my PhD, and for providing links to good techno throughout. Thanks to Denis Anikiev for his support everytime something went wrong, for helping prepare the nicest figures in this whole work and helping me move flat in Berlin. Thanks to Judith Bott for her support and advice, especially in the first year of my project by helping me get set up in Germany and transition into academic life. Thanks to Max Frick for helping me every time I needed support navigating the weird world of German bureaucracy. And thanks to everyone else in the section, past and present: Antoine, Lew, Constanza, Ershad, Nora, Federico, Jan Ine, Angela, Katharina, Sebastian, Christian, Maria Laura and Michael, you all helped the office to feel like one big family. And thanks again to Leni, not just for her

countless contributions to this work but also for bringing the family together, the summer parties in Werder and the Betriebsausflug boating trips were some of the best times I have had in Germany.

Finally, thanks to poor Gabi, who had to put up with me working from home for over a year, in the middle of a pandemic, in a small Berlin studio flat that only has 2 rooms and paper thin walls. I promise I will never tell you to turn down Grey's Anatomy ever again in your life. Thanks for supporting and encouraging me to keep going each day.

Bibliography

- Aichroth, B., Prodehl, C. and Thybo, H.: Crustal structure along the Central Segment of the EGT from seismic-refraction studies. Tectonophysics, 207(1-2), pp.43-64, https://doi.org/10.1016/0040-1951(92)90471-h, 1992.

- Alger, B., Andrš, D., Carlsen, R. W., Gaston, D. R., Kong, F., Lindsay, A. D., Miller, J. M., Permann, C. J., Peterson, J. W., Slaughter, A. E., and Stogner, R. MOOSE Web page, https://mooseframework.org, 2019.

- Allen, P. and Allen, J. Basin Analysis. 3rd ed. Somerset: Wiley, 2013.

- Amante, C. and Eakins, B. W.: ETOPO1 1 Arc-Minute Global Relief Model: Procedures, Data Sources and Analysis. NOAA Technical Memorandum NESDIS NGDC-24, National Geophysical Data Center, NOAA, https://doi.org/10.1594/PANGAEA.769615, 2009.

- Aretz-Nellesen, N., Grepl, M. and Veroy, K. 3D-VAR for parameterized partial differential equations: a certified reduced basis approach. Advances in Computational Mathematics, 45(5-6), pp.2369-2400, https://doi.org/10.1007/s10444-019-09713-w, 2019.

- Babuška, V. and Plomerová, J. The lithosphere in central Europe—seismological and petrological aspects. Tectonophysics, 207(1-2), pp.141-163, https://doi.org/10.1016/0040-1951(92)90475-l, 1992.

- Bächler, D., Kohl, T. and Rybach, L. Impact of graben-parallel faults on hydrothermal convection—Rhine Graben case study. Physics and Chemistry of the Earth, Parts A/B/C, 28(9-11), pp.431-441, https://doi.org/10.1016/s1474-7065(03)00063-9, 2003.

- Baroni, G. and Tarantola, S. A General Probabilistic Framework for uncertainty and global sensitivity analysis of deterministic models: A hydrological case study. Environmental Modelling & Software, 51, pp.26-34, https://doi.org/ 10.1016/j.envsoft.2013.09.022, 2014.

- Baş, D. and Boyacı, İ. Modeling and optimization I: Usability of response surface methodology. Journal of Food Engineering, 78(3), pp.836-845, https://doi.org/10.1016/j.jfoodeng.2005.11.024, 2007.

- Benner, P., Gugercin, S. and Willcox, K. A Survey of Projection-Based Model Reduction Methods for Parametric Dynamical Systems. SIAM Review, 57(4), pp.483-531, https://doi.org/10.1137/130932715, 2015.

- Bezerra, M., Santelli, R., Oliveira, E., Villar, L. and Escaleira, L. Response surface methodology (RSM) as a tool for optimization in analytical chemistry. Talanta, 76(5), pp.965-977, https://doi.org/10.1016/j.talanta.2008.05.019, 2008.

- Bleibinhaus, F. and Gebrande, H. Crustal structure of the Eastern Alps along the TRANSALP profile from wide-angle seismic tomography. Tectonophysics, 414(1-4), pp.51-69, https://doi.org/10.1016/j.tecto.2005.10.028, 2006.

- Böhm, R., Auer, I., Schöner, W., Ganekind, M., Gruber, C., Jurkovic, A., Orlik, A., Ungersböck, M. Eine neue Webseite mit instrumentellen Qualitäts-Klimadaten für den Grossraum Alpen zurück bis 1760. Wiener Mitteilungen Band 216: Hochwässer: Bemessung, Risikoanalyse und Vorhersage, 2009.

- Boettcher, M., Hirth, G. and Evans, B. Olivine friction at the base of oceanic seismogenic zones. Journal of Geophysical Research, 112(B1), https://doi.org/10.1029/2006jb004301, 2007.

- Bonjer, K. Seismicity pattern and style of seismic faulting at the eastern borderfault of the southern Rhine Graben. Tectonophysics, 275(1-3), pp.41-69, https://doi.org/10.1016/s0040-1951(97)00015-2, 1997.

- Box, G. E. Robustness in the Strategy of Scientific Model Building, in: Robustness in statistics, pp. 201–236, Elsevier, 1979.

- Brace, W. and Kohlstedt, D. Limits on lithospheric stress imposed by laboratory experiments. Journal of Geophysical Research: Solid Earth, 85(B11), pp.6248-6252, https://doi.org/10.1029/jb085ib11p06248, 1980.

- Brocher, T.: Empirical Relations between Elastic Wavespeeds and Density in the Earth's Crust. Bulletin of the Seismological Society of America, 95(6), pp.2081-2092, https://doi.org/10.1785/0120050077, 2005.

- Brückl, E., Bleibinhaus, F., Gosar, A., Grad, M., Guterch, A., Hrubcová, P., Keller, G., Majdański, M., Šumanovac, F., Tiira, T., Yliniemi, J., Hegedűs, E. and Thybo, H. Crustal structure due to collisional and escape tectonics in the Eastern Alps region based on profiles Alp01 and Alp02 from the ALP 2002 seismic experiment. Journal of Geophysical Research, 112(B6), https://doi.org/10.1029/2006jb004687, 2007.

- Burov, E. Rheology and strength of the lithosphere. Marine and Petroleum Geology, 28(8), pp.1402-1443, https://doi.org/10.1016/j.marpetgeo.2011.05.008, 2011.

- Byerlee, J. Friction of rocks. Pure and Applied Geophysics PAGEOPH, 116(4-5), pp.615-626, https://doi.org/10.1007/bf00876528, 1978.

- Cacace, M. and Jacquey, A. Flexible parallel implicit modelling of coupled thermal–hydraulic–mechanical processes in fractured rocks. Solid Earth, 8(5), pp.921-941, https://doi.org/10.5194/se-8-921-2017, 2017.

- Cacace, M. and Scheck-Wenderoth, M. Why intracontinental basins subside longer: 3-D feedback effects of lithospheric cooling and sedimentation on the flexural strength of the lithosphere. Journal of Geophysical Research: Solid Earth, 121(5), pp.3742-3761, http://doi.org/10.1002/2015jb012682, 2016.

- Cannavó, F. Sensitivity analysis for volcanic source modeling quality assessment and model selection. Computers & Geosciences, 44, pp.52-59, https:// doi.org/10.1016/j.cageo.2012.03.008, 2012.

- Castellarin, A., Vai, G. and Cantelli, L. The Alpine evolution of the Southern Alps around the Giudicarie faults: A Late Cretaceous to Early Eocene transfer zone. Tectonophysics, 414(1-4), pp.203-223, https://doi.org/10.1016/j.tecto.2005.10.019, 2006.

- Cattaneo, M., Augliera, P., Parolai, S. and Spallarossa, D. Anomalously deep earthquakes in northwestern Italy. Journal of Seismology 3, pp.421–435, https://doi.org/10.1023/A:1009899214734, 1999.

- Cherpeau, N. and Caumon, G. Stochastic structural modelling in sparse data situations. Petroleum Geoscience, 21(4), pp.233-247, http://doi.org/10.1144/petgeo2013-030, 2015.

- Chéry, J., Genti, M. and Vernant, P. Ice cap melting and low-viscosity crustal root explain the narrow geodetic uplift of the Western Alps. Geophysical Research Letters, 43(7), pp.3193-3200, http://doi.org/10.1002/2016gl067821, 2016.

- Chiarabba, C., Jovane, L. and DiStefano, R. A new view of Italian seismicity using 20 years of instrumental recordings. Tectonophysics, 395(3-4), pp.251-268, http://doi.org/10.1016/j.tecto.2004.09.013, 2005.

- Cloke, H., Pappenberger, F. and Renaud, J. Multi-method global sensitivity analysis (MMGSA) for modelling floodplain hydrological processes. Hydrological Processes, 22(11), pp.1660-1674, https://doi.org/10.1002/hyp.6734, 2008.

- D'Agostino, N., Avallone, A., Cheloni, D., D'Anastasio, E., Mantenuto, S. and Selvaggi, G. Active tectonics of the Adriatic region from GPS and earthquake slip vectors. Journal of Geophysical Research, 113(B12), https://doi.org/10.1029/2008jb005860, 2008.

- Dal Zilio, L., van Dinther, Y., Gerya, T. and Pranger, C. Seismic behaviour of mountain belts controlled by plate convergence rate. Earth and Planetary Science Letters, 482, pp.81-92, https://doi.org/10.1016/j.epsl.2017.10.053, 2018.

- Degen, D., Veroy, K. and Wellmann, F. Certified reduced basis method in geosciences. Computational Geosciences, 24(1), pp.241-259, https://doi.org/10.1007/s10596-019-09916-6, 2019.

- Degen, D., Veroy, K., Freymark, J., Scheck-Wenderoth, M., and Wellmann, F. Global Sensitivity Analysis to Optimize Basin-Scale Conductive Model Calibration - Insights on the Upper Rhine Graben, https://doi.org/10.31223/osf.io/b7pgs, 2020a.

- Degen, D., Veroy, K., and Wellmann, F. cgre-aachen/DwarfElephant: DwarfElephant 1.0, https://doi.org/10.5281/zenodo.4074777, 2020b.

- Deichmann, N., Ansorge, J. and Mueller, S.: Crustal structure of the Southern Alps beneath the intersection with the European Geotraverse. Tectonophysics, 126(1), pp.57-83, https://doi.org/10.1016/0040-1951(86)90220-9, 1986.

- Deichmann, N. Structural and rheological implications of lower-crustal earthquakes below northern Switzerland. Physics of the Earth and Planetary Interiors, 69(3-4), pp.270-280, https://doi.org/10.1016/0031-9201(92)90146-m, 1992.

- Dentith, M. and Featherstone, W.: Controls on intra-plate seismicity in southwestern Australia. Tectonophysics, 376(3-4), pp.167-184, https://doi.org/10.1016/j.tecto.2003.10.002, 2003.

- Deutsch, C.: 2D Gravity Modeling and Evaluation of the Lithospheric Structure of the Alpine Collision Zone along the TRANSALP Profile. Masters Thesis. Freien Universität Berlin, 2014.

- Dèzes, P., Schmid, S. and Ziegler, P. Evolution of the European Cenozoic Rift System: interaction of the Alpine and Pyrenean orogens with their foreland lithosphere. Tectonophysics, 389(1-2), pp.1-33, https://doi.org/10.1016/j.tecto.2004.06.011, 2004.

- Doherty, J., Hunt, R. and Tonkin, M. Approaches to highly parameterized inversion: A guide to using PEST for model-parameter and predictive-uncertainty analysis. Scientific Investigations Report, p.i-71, https://doi.org/10.3133/sir20105211, 2010.

- Ebbing, J. 3-D Dichteverteilung und isostatisches Verhalten der Lithosphäre in den Ostalpen. Ph.D Thesis. Freien Universität Berlin, 2002.

- Ebbing, J., Braitenberg, C. and Götze, H. The lithospheric density structure of the Eastern Alps. Tectonophysics, 414(1-4), pp.145-155, https://doi.org/10.1016/j.tecto.2005.10.015, 2006.

- Ehlers, T. and Chapman, D. Normal fault thermal regimes: conductive and hydrothermal heat transfer surrounding the Wasatch fault, Utah. Tectonophysics, 312(2-4), pp.217-234, https://doi.org/10.1016/s0040-1951(99)00203-6, 1999.

- Ehlers, T. Crustal Thermal Processes and the Interpretation of Thermochronometer Data. Reviews in Mineralogy and Geochemistry, 58(1), pp.315-350, https://doi.org/10.2138/rmg.2005.58.12, 2005.

- El-Sharkawy, A., Meier, T., Lebedev, S., Behrmann, J., Hamada, M., Cristiano, L., Weidle, C. and Köhn, D. The Slab Puzzle of the Alpine-Mediterranean Region: Insights From a New, High-Resolution, Shear Wave Velocity Model of the Upper Mantle. Geochemistry, Geophysics, Geosystems, 21(8), http://doi.org/10.1029/2020gc008993, 2020.

- Elison, P., Niederau, J., Vogt, C. and Clauser, C. Quantification of thermal conductivity uncertainty for basin modeling. AAPG Bulletin, 103(8), pp.1787-1809, http://doi.org/10.1306/12181818038, 2019.

- Emmerson, B. and McKenzie, D. Thermal structure and seismicity of subducting lithosphere. Physics of the Earth and Planetary Interiors, 163(1-4), pp.191-208, https://doi.org/10.1016/j.pepi.2007.05.007, 2007.

- Enderle, U., Schuster, K., Prodehl, C., Schulze, A. and Bribach, J.: The refraction seismic experiment GRANU95 in the Saxothuringian belt, southeastern Germany. Geophysical Journal International, 133(2), pp.245-259, https://doi.org/10.1046/j.1365-246x.1998.00462.x, 1998.

- Eva, E., Malusà, M. and Solarino, S. A seismotectonic picture of the inner southern Western Alps based on the analysis of anomalously deep earthquakes. Tectonophysics, 661, pp.190-199, http://doi.org/10.1016/j.tecto.2015.08.040, 2015.

- Evans, B., Fredrich, J. and Wong, T. The brittle-ductile transition in rocks: Recent experimental and theoretical progress. The Brittle-Ductile Transition in Rocks, pp.1-20, https://doi.org/10.1029/GM056p0001, 1990.

- Fäh, D., Giardini, D., Kästli, P., Deichmann, N., Gisler, M., Schwarz-Zanetti, G., Alvarez-Rubio, S., Sellami, S., Edwards, B., Allmann, B., Bethmann, F., Wössner, J., Gassner-Stamm, G., Fritsche, S., Eberhard, D. ECOS-09 Earthquake Catalogue of Switzerland Release 2011 Report and Database. Public catalogue, 17. 4. 2011. Swiss Seismological Service ETH Zurich, Report SED/RISK/R/001/20110417, 2011.

- Fairley, J. Models And Modeling: An Introduction For Earth And Environmental Scientists. Wiley-Blackwell, 2016.

- Fan, Y., and H. van den Dool, A global monthly land surface air temperature analysis for 1948-present, J. Geophys. Res., 113, D01103, https://doi.org/10.1029/2007JD008470, 2008.

- Feng, L., Palmer, P., Parker, R., Deutscher, N., Feist, D., Kivi, R., Morino, I. and Sussmann, R. Estimates of European uptake of CO 2 inferred from GOSAT X CO 2 retrievals: sensitivity to measurement bias inside and outside Europe. Atmospheric Chemistry and Physics, 16(3), pp.1289-1302, https://doi.org/10.5194/acp-16-1289-2016, 2016.

- Fernández, M., Eguía, P., Granada, E. and Febrero, L. Sensitivity analysis of a vertical geothermal heat exchanger dynamic simulation: Calibration and error determination. Geothermics, 70, pp.249-259, https://doi.org/10.1016/j.geothermics.2017.06.012, 2017.

- Feyen, L. and Caers, J. Quantifying geological uncertainty for flow and transport modeling in multi-modal heterogeneous formations. Advances in Water Resources, 29(6), pp.912-929, https://doi.org/10.1016/j.advwatres.2005.08.002, 2006.

- Floris, F., Bush, M., Cuypers, M., Roggero, F. and Syversveen, A. Methods for quantifying the uncertainty of production forecasts: a comparative study. Petroleum Geoscience, 7(S), pp.S87-S96, https://doi.org/10.1144/petgeo.7.s.s87, 2001.

- Förste, C., Bruinsma, S. L., Abrikosov, O., Lemoine, J. M., Marty, J. C., Flechtner, F., Balmino, G., Barthelmes, F., Biancale, R.: EIGEN-6C4 The latest combined global gravity field model including GOCE data up to degree and order 2190 of GFZ Potsdam and GRGS Toulouse. GFZ Data Services, http://doi.org/10.5880/icgem.2015.1, 2014.

- Fox, M., Herman, F., Kissling, E. and Willett, S. Rapid exhumation in the Western Alps driven by slab detachment and glacial erosion. Geology, 43(5), pp.379-382, https://doi.org/10.1130/g36411.1, 2015.

- Fox, M., Herman, F., Willett, S. and Schmid, S. The Exhumation history of the European Alps inferred from linear inversion of thermochronometric data. American Journal of Science, 316(6), pp.505-541, https://doi.org/10.2475/06.2016.01, 2016.

- Frangos, M., Marzouk, Y., Willcox, K. and van Bloemen Waanders, B. Surrogate and Reduced-Order Modeling: A Comparison of Approaches for Large-Scale Statistical Inverse Problems. Large-Scale Inverse Problems and Quantification of Uncertainty, pp.123-149, https://doi.org/10.1002/9780470685853.ch7, 2010.

- Franke, W. The mid-European segment of the Variscides: tectonostratigraphic units, terrane boundaries and plate tectonic evolution. Geological Society, London, Special Publications, 179(1), pp.35-61, https://doi.org/10.1144/gsl.sp.2000.179.01.05, 2000.

- Freymark, J., Sippel, J., Scheck-Wenderoth, M., Bär, K., Stiller, M., Fritsche, J. and Kracht, M. The deep thermal field of the Upper Rhine Graben. Tectonophysics, 694, pp.114-129, https://doi.org/10.1016/j.tecto.2016.11.013, 2017.

- Freymark, J., Bott, J., Cacace, M., Ziegler, M. and Scheck-Wenderoth, M. Influence of the Main Border Faults on the 3D Hydraulic Field of the Central Upper Rhine Graben. Geofluids, 2019, pp.1-21, https://doi.org/10.1155/2019/7520714, 2019.

- Frisch, W. Tectonic progradation and plate tectonic evolution of the Alps. Tectonophysics, 60(3-4), pp.121-139, https://doi.org/10.1016/0040-1951(79)90155-0, 1979.

- Fuchs, S. and Balling, N. Improving the temperature predictions of subsurface thermal models by using high-quality input data. Part 1: Uncertainty analysis of the thermal-conductivity parameterization. Geothermics, 64, pp.42-54, https://doi.org/10.1016/j.geothermics.2016.04.010, 2016.

- Gajewski, D. and Prodehl, C. Crustal structure beneath the Swabian Jura, SW Germany, from seismic refraction investigations. Journal of Geophysics, 56, pp.69-80, 1985.

- Gajewski, D. and Prodehl, C. Seismic refraction investigation of the Black Forest. Tectonophysics, 142(1), pp.27-48, https://doi.org/10.1016/0040-1951(87)90293-9, 1987.

- Gajewski, D., Holbrook, W. and Prodehl, C.: A three-dimensional crustal model of southwest Germany derived from seismic refraction data. Tectonophysics, 142(1), pp.49-70, https://doi.org/10.1016/0040-1951(87)90294-0, 1987.

- Geissler, W., Sodoudi, F. and Kind, R. Thickness of the central and eastern European lithosphere as seen by S receiver functions. Geophysical Journal International, https://doi.org/10.1111/j.1365-246x.2010.04548.x, 2010.

- Ghasemi, M. and Gildin, E. Model order reduction in porous media flow simulation using quadratic bilinear formulation. Computational Geosciences, 20(3), pp.723-735, https://doi.org/10.1007/s10596-015-9529-0, 2015.

- Goetze, C. and Evans, B. Stress and temperature in the bending lithosphere as constrained by experimental rock mechanics. Geophysical Journal International, 59(3), pp.463-478, https://doi.org/10.1111/j.1365-246x.1979.tb02567.x, 1979.

- González, Á. The Spanish National Earthquake Catalogue: Evolution, precision and completeness. Journal of Seismology, 21(3), pp.435-471, https://doi.org/10.1007/s10950-016-9610-8, 2016.

- Gosses, M., Nowak, W. and Wöhling, T. Explicit treatment for Dirichlet, Neumann and Cauchy boundary conditions in POD-based reduction of groundwater models. Advances in Water Resources, 115, pp.160-171, https://doi.org/10.1016/j.advwatres.2018.03.011, 2018.

- Grepl, M. Reduced-basis Approximation and A Posteriori Error Estimation for Parabolic Partial Differential Equations, Ph.D. thesis, Massachusetts Institute of Technology, 2005.

- Grünthal, G., Wahlström, R. and Stromeyer, D. The SHARE European Earthquake Catalogue (SHEEC) for the time period 1900–2006 and its comparison to the European-Mediterranean Earthquake Catalogue (EMEC). Journal of Seismology, 17(4), pp.1339-1344, https://doi.org/10.1007/s10950-013-9379-y, 2013.

- Guterch, A., Grad, M., Janik, T., Materzok, R., Luosto, U., Yliniemi, J., Lück, E., Schulze, A. and Förste, K.: Crustal structure of the transition zone between Precambrian and Variscan Europe from new seismic data along LT-7 profile (NW Poland and eastern Germany). C. R. Acad. Sci. Paris, 319, pp.1489–1496, 1994.

- Handy, M., M. Schmid, S., Bousquet, R., Kissling, E. and Bernoulli, D. Reconciling plate-tectonic reconstructions of Alpine Tethys with the geological–geophysical record of spreading and subduction in the Alps. Earth-Science Reviews, 102(3-4), pp.121-158, https://doi.org/10.1016/j.earscirev.2010.06.002, 2010.

- Handy, M., Ustaszewski, K. and Kissling, E. Reconstructing the Alps–Carpathians–Dinarides as a key to understanding switches in subduction polarity, slab gaps and surface motion. International Journal of Earth Sciences, 104(1), pp.1-26, https://doi.org/10.1007/s00531-014-1060-3, 2014.

- Hasterok, D. and Webb, J. On the radiogenic heat production of igneous rocks. Geoscience Frontiers, 8(5), pp.919-940, https://doi.org/10.1016/j.gsf.2017.03.006, 2017.

- Heckenbach, E., Brune, S., Glerum, A. and Bott, J. Is there a Speed Limit for the Thermal Steady-State Assumption in Continental Rifts?. Geochemistry, Geophysics, Geosystems, https://doi.org/10.1029/2020GC009577, 2021.

- Herman, J. and Usher, W. SALib: An open-source Python library for Sensitivity Analysis. The Journal of Open Source Software, 2(9), p.97, https://doi.org/10.21105/joss.00097, 2017.

- Hesthaven, J., Rozza, G. and Stamm, B. Certified Reduced Basis Methods for Parametrized Partial Differential Equations. Cham: Springer International Publishing, 2016.

- Hetényi, G., Plomerová, J., Bianchi, I., Kampfová-Exnerová, H., Bokelmann, G., Handy, M. and Babuška, V. From mountain summits to roots: Crustal structure of the Eastern Alps and Bohemian Massif along longitude 13.3°E. Tectonophysics, 744, pp.239-255, https://doi.org/10.1016/j.tecto.2018.07.001, 2018a.

- Hetényi, G., Epard, J.L., Colavitti, L., Hirzel, A.H., Kiss, D., Petri, B., Scarponi, M., Schmalholz, S.M., Subedi, S.: Spatial relation of surface faults and crustal seismicity: a first comparison in the region of Switzerland. Acta Geod Geophys, 53, pp.39-461, https://doi.org/10.1007/s40328-018-0229-9, 2018b.

- Hill, M. and Tiedeman, C. Effective groundwater model calibration: with analysis of data, sensitivities, predictions, and uncertainty. New Jersey: John Wiley, 2006.

- Houghton, J., Ding, Y., Griggs, D. J., Noguer, M., van der Linden, P. J., Dai, X., Maskell, K., and Johnson, C. Climate change 2001. Cambridge: Cambridge University Press, 2001.

- Houlié, N., Woessner, J., Giardini, D. and Rothacher, M. Lithosphere strain rate and stress field orientations near the Alpine arc in Switzerland. Scientific Reports, 8(1), https://doi.org/10.1038/s41598-018-20253-z, 2018.

- Hyndman, R., Wang, K. and Yamano, M. Thermal constraints on the seismogenic portion of the southwestern Japan subduction thrust. Journal of Geophysical Research: Solid Earth, 100(B8), pp.15373-15392, https://doi.org/10.1029/95jb00153, 1995.

- IESG: Alp 75 d-h. Boll. di Geofisica Teorica ed Applicata, 20, pp.287-302, 1978.

- IESG and ETH: Südalp 77 b-d. Boll. di Geofisica Teorica ed Applicata, 23, pp.297-330, 1981.

- Iglesias, M. and Stuart, A. M. Inverse Problems and Uncertainty Quantification, SIAM News, pp. 2–3, 2014.

- Ince, E., Barthelmes, F., Reißland, S., Elger, K., Förste, C., Flechtner, F. and Schuh, H.: ICGEM - 15 years of successful collection and distribution of global gravitational models, associated services and future plans. Earth System Science Data Discussions, pp.1-61, https://doi.org/10.5194/essd-11-647-2019, 2019.

- International Seismological Centre, On-line Bulletin, https://doi.org/10.31905/D808B830, 2020.

- Jones, E., Oliphant, T., and Peterson, P.: SciPy: Open source scientific tools for Python, 2014.

- Jozi Najafabadi, A., Haberland, C., Ryberg, T., Verwater, V., Le Breton, E., Handy, M. R., Weber, M., and the AlpArray working group: Relocation of earthquakes in the Southern and Eastern Alps (Austria, Italy) recorded by the dense, temporary SWATH–D network using a Markov chain Monte Carlo inversion, Solid Earth Discuss. [preprint], https://doi.org/10.5194/se-2020-192, in review, 2020.

- Jülich Supercomputing Centre. JUWELS: Modular Tier-0/1 Supercomputer at the Jülich Supercomputing Centre, Journal of large-scale research facilities, 5, https://doi.org/10.17815/jlsrf-5-171, 2019.

- Kärcher, M., Boyaval, S., Grepl, M. and Veroy, K. Reduced basis approximation and a posteriori error bounds for 4D-Var data assimilation. Optimization and Engineering, 19(3), pp.663-695, https://doi.org/10.1007/s11081-018-9389-2, 2018.

- Kästle, E., Rosenberg, C., Boschi, L., Bellahsen, N., Meier, T. and El-Sharkawy, A. Slab Break-offs in the Alpine Subduction Zone. Solid Earth Discussions, pp.1-16, https://doi.org/10.5194/se-2019-17, 2019.

- Karato, S. and Wu, P. Rheology of the Upper Mantle: A Synthesis. Science, 260(5109), pp.771-778, https://doi.org/10.1126/science.260.5109.771, 1993.

- Katayama, I. and Karato, S. Low-temperature, high-stress deformation of olivine under water-saturated conditions. Physics of the Earth and Planetary Interiors, 168(3-4), pp.125-133, https://doi.org/10.1016/j.pepi.2008.05.019, 2008.

- Khuri, A. and Mukhopadhyay, S. Response surface methodology. Wiley Interdisciplinary Reviews: Computational Statistics, 2(2), pp.128-149, https://doi.org/10.1002/wics.73, 2010.

- Kissling, E., Schmid, S., Lippitsch, R., Ansorge, J. and Fügenschuh, B. Lithosphere structure and tectonic evolution of the Alpine arc: new evidence from high-resolution teleseismic tomography. Geological Society, London, Memoirs, 32(1), pp.129-145, https://doi.org/10.1144/gsl.mem.2006.032.01.08, 2006.

- Kahle, H.G., Geiger, A., Buerki, B., Gubler, E., Marti, U., Wirth, B., Rothacher,M., Gurtner, W., Beutler, G., Bauersima, I., Pfiffner, O.A. Recent crustal movements, geoid and density distribution: Contribution from integrated satellite and terrestrial measurements, in Pfiffner, O.A., et al., (eds), Results of NRP 20: Deep structure of the Swiss Alps: Basel, Boston, Berlin, Birkhaüser, pp. 251–259, 1997.

- Koltzer, N., Scheck-Wenderoth, M., Bott, J., Cacace, M., Frick, M., Sass, I., Fritsche, J. and Bär, K. The Effects of Regional Fluid Flow on Deep Temperatures (Hesse, Germany). Energies, 12(11), p.2081, https://doi.org/10.3390/en12112081, 2019.

- Kuhlemann, J., Frisch, W., Székely, B., Dunkl, I. & Kázmér, M. Post-collisional sediment budget history of the Alps: tectonic versus climatic control. Int J Earth Sci (Geol Rundsch) 91, pp.818–837, https://doi.org/10.1007/s00531-002-0266-y, 2002.

- Kummerow, J., Kind, R., Oncken, O., Giese, P., Ryberg, T., Wylegalla, K. and Scherbaum, F. A natural and controlled source seismic profile through the Eastern Alps: TRANSALP. Earth and Planetary Science Letters, 225(1-2), pp.115-129, https://doi.org/10.1016/j.epsl.2004.05.040, 2004.

- Lehmann, H., Wang, K. and Clauser, C. Parameter identification and uncertainty analysis for heat transfer at the KTB drill site using a 2-D inverse method. Tectonophysics, 291(1-4), pp.179-194, https://doi.org/10.1016/s0040-1951(98)00039-0, 1998.

- Lerch, F., 1991. Optimum data weighting and error calibration for estimation of gravitational parameters. Bulletin Géodésique, 65(1), pp.44-52, https://doi.org/10.1007/bf00806341, 1991.

- Limberger, J., van Wees, J., Tesauro, M., Smit, J., Bonté, D., Békési, E., Pluymaekers, M., Struijk, M., Vrijlandt, M., Beekman, F. and Cloetingh, S., 2018. Refining the thermal structure of the European lithosphere by inversion of subsurface temperature data. Global and Planetary Change, 171, pp.18-47, https://doi.org/10.1016/j.gloplacha.2018.07.009, 2018.

- Linde, N., Ginsbourger, D., Irving, J., Nobile, F. and Doucet, A. On uncertainty quantification in hydrogeology and hydrogeophysics. Advances in Water Resources, 110, pp.166-181, https://doi.org/10.1016/j.advwatres.2017.10.014, 2017.

- Lippitsch, R., Kissling, E. and Ansorge, J. Upper mantle structure beneath the Alpine orogen from high-resolution teleseismic tomography. Journal of Geophysical Research, 108(B8), https://doi.org/10.1029/2002jb002016, 2003.

- Locarnini, R. A., A. V. Mishonov, J. I. Antonov, T. P. Boyer, H. E. Garcia, O. K. Baranova, M. M. Zweng, C. R. Paver, J. R. Reagan, D. R. Johnson, M. Hamilton, and D. Seidov. World Ocean Atlas 2013, Volume 1: Temperature. S. Levitus, Ed., A. Mishonov Technical Ed.; NOAA Atlas NESDIS 73, 40 pp, 2013.

- Lowe, M. Sensitivity study on separation of crustal and mantle contribution to the Alpine gravity field. Masters Thesis. Christian-Albrechts-Universität Kiel. 2019.

- Lowe, M., Ebbing, J., El-Sharkawy, A., and Meier, T. Gravity Effect of Alpine Slab Segments Based on Geophysical and Petrological Modelling, Solid Earth Discuss. [preprint], https://doi.org/10.5194/se-2020-145, in review, 2020.

- Lucazeau, F. and Le Douaran, S. The blanketing effect of sediments in basins formed by extension: a numerical model. Application to the Gulf of Lion and Viking graben. Earth and Planetary Science Letters, 74(1), pp.92-102, https://doi.org/10.1016/0012-821x(85)90169-4, 1985.

- Lüschen, E., Borrini, D., Gebrande, H., Lammerer, B., Millahn, K., Neubauer, F. and Nicolich, R. TRANSALP—deep crustal Vibroseis and explosive seismic profiling in the Eastern Alps. Tectonophysics, 414(1-4), pp.9-38, https://doi.org/10.1016/j.tecto.2005.10.014, 2006.

- Luijendijk, E., Winter, T., Köhler, S., Ferguson, G., von Hagke, C., Scibek, J. Using thermal springs to quantify groundwater flow and its thermal footprint in the Alps and North American orogens. Manuscript in preparation, 2020.

- Magrin, A. and Rossi, G. Deriving a New Crustal Model of Northern Adria: The Northern Adria Crust (NAC) Model. Frontiers in Earth Science, 8, https://doi.org/10.3389/feart.2020.00089, 2020.

- Marotta, A. and Splendore, R. 3D mechanical structure of the lithosphere below the Alps and the role of gravitational body forces in the regional present-day stress field. Tectonophysics, 631, pp.117-129, https://doi.org/10.1016/j.tecto.2014.04.038, 2014.

- McKenzie, D., Jackson, J. and Priestley, K. Thermal structure of oceanic and continental lithosphere. Earth and Planetary Science Letters, 233(3-4), pp.337-349, https://doi.org/10.1016/j.epsl.2005.02.005, 2005.

- Mechie, J., Prodehl, C. and Fuchs, K.: Seismic refraction investigations of crust and uppermost mantle structure beneath the Rhenish Massif. Tectonophysics, 118(1-2), pp.159-160, https://doi.org/10.1016/0040-1951(85)90165-9, 1985.

- Meeßen, C. VeloDT. https://doi.org/10.5281/zenodo.1172628, 2018.

- Mey, J., Scherler, D., Wickert, A., Egholm, D., Tesauro, M., Schildgen, T. and Strecker, M. Erratum: Corrigendum: Glacial isostatic uplift of the European Alps. Nature Communications, 8(1), https://doi.org/10.1038/ncomms16138, 2017.

- Miao, T., Lu, W., Lin, J., Guo, J. and Liu, T. Modeling and uncertainty analysis of seawater intrusion in coastal aquifers using a surrogate model: a case study in Longkou, China. Arabian Journal of Geosciences, 12(1), https://doi.org/10.1007/s12517-018-4128-8, 2018.

- Mitterbauer, U., Behm, M., Brückl, E., Lippitsch, R., Guterch, A., Keller, G., Koslovskaya, E., Rumpfhuber, E. and Šumanovac, F. Shape and origin of the East-Alpine slab constrained by the ALPASS teleseismic model. Tectonophysics, 510(1-2), pp.195-206, https://doi.org/10.1016/j.tecto.2011.07.001, 2011.

- Mo, S., Shi, X., Lu, D., Ye, M. and Wu, J. An adaptive Kriging surrogate method for efficient uncertainty quantification with an application to geological carbon sequestration modeling. Computers & Geosciences, 125, pp.69-77, https://doi.org/10.1016/j.cageo.2019.01.012, 2019.

- Molinari, I. and Morelli, A.: EPcrust: a reference crustal model for the European Plate. Geophysical Journal International, 185(1), pp.352-364, https://doi.org/10.1111/j.1365-246x.2011.04940.x, 2011.

- Molinari, I., Argnani, A., Morelli, A. and Basini, P.: Development and Testing of a 3D Seismic Velocity Model of the Po Plain Sedimentary Basin, Italy. Bulletin of the Seismological Society of America, 105(2A), pp.753-764, https://doi.org/10.1785/0120140204, 2015.

- Molli, G., Crispini, L., Malusà, M., Mosca, P., Piana, F. and Federico, L. Geology of the Western Alps-Northern Apennine junction area: a regional review. Journal of the Virtual Explorer, 36, https://doi.org/10.3809/jvirtex.2010.00215, 2010.

- Mroczek, S., Tilmann, F., Pleuger, J., Yuan, X., Heit, B. and the AlpArray Working Group, Filling the Moho gap: High resolution crustal structure of the Eastern Alps, T047-04 presented at 2020 Fall Meeting, AGU, 1-17 Dec, 2020.

- Murphy, J., Sexton, D., Barnett, D., Jones, G., Webb, M., Collins, M. and Stainforth, D. Quantification of modelling uncertainties in a large ensemble of climate change simulations. Nature, 430(7001), pp.768-772, https://doi.org/10.1038/nature02771, 2004.

- Myers, R., Montgomery, D. and Anderson-Cook, C. Response surface methodology: Process and Product Optimization Using Designed Experiments. Hoboken: Wiley, 2016.

- Navarro, M., Le Maître, O., Hoteit, I., George, D., Mandli, K. and Knio, O. Surrogate-based parameter inference in debris flow model. Computational Geosciences, 22(6), pp.1447-1463, https://doi.org/10.1007/s10596-018-9765-1, 2018.

- Nocquet, J. and Calais, E. Geodetic Measurements of Crustal Deformation in the Western Mediterranean and Europe. Pure and Applied Geophysics, 161(3), pp.661-681, https://doi.org/10.1007/s00024-003-2468-z, 2004.

- Norton, K. and Hampel, A. Postglacial rebound promotes glacial re-advances - a case study from the European Alps. Terra Nova, https://doi.org/10.1007/10.1111/j.1365-3121.2010.00946.x, 2010.

- Norton, K., von Blanckenburg, F., DiBiase, R., Schlunegger, F. and Kubik, P. Erratum to: Cosmogenic 10Be-derived denudation rates of the Eastern and Southern European Alps. International Journal of Earth Sciences, 100(5), pp.1225-1226, https://doi.org/10.1007/s00531-011-0655-1, 2011.

- Okaya, N., Cloetingh, S. and Mueller, S. A lithospheric cross-section through the Swiss Alps-II. Constraints on the mechanical structure of a continent-continent collision zone. Geophysical Journal International, 127(2), pp.399-414, https://doi.org/10.1111/j.1365-246x.1996.tb04729.x, 1996.

- Pesaresi, M., Ehrlich, D., Kemper, T., Siragusa, A., Florczyk, A.J., Freire, S., Corbane, C., Atlas of the Human Planet 2017: Global Exposure to Natural Hazards, EUR 28556 EN, https://doi.org/10.2760/19837, 2017.

- Piana Agostinetti, N. and Faccenna, C. Deep Structure of Northern Apennines Subduction Orogen (Italy) as Revealed by a Joint Interpretation of Passive and Active Seismic Data. Geophysical Research Letters, 45(9), pp.4017-4024, https://doi.org/10.1029/2018gl077640, 2018.

- Pistone, M., Müntener, O., Ziberna, L., Hetényi, G. and Zanetti, A. Report on the ICDP workshop DIVE (Drilling the Ivrea–Verbano zone). Scientific Drilling, 23, pp.47-56, https://doi.org/10.5194/sd-23-47-2017, 2017.

- Pola, M., Cacace, M., Fabbri, P., Piccinini, L., Zampieri, D. and Torresan, F. Fault Control on a Thermal Anomaly: Conceptual and Numerical Modeling of a Low-Temperature Geothermal System in the Southern Alps Foreland Basin (NE Italy). Journal of Geophysical Research: Solid Earth, 125(5), https://doi.org/10.1029/2019jb017394, 2020.

- Pomella, H., Klötzli, U., Scholger, R., Stipp, M. and Fügenschuh, B. The Northern Giudicarie and the Meran-Mauls fault (Alps, Northern Italy) in the light of new paleomagnetic and geochronological data from boudinaged Eo-/Oligocene tonalites. International Journal of Earth Sciences, 100(8), pp.1827-1850, https://doi.org/10.1007/s00531-010-0612-4, 2010.

- Priestly, K. and McKenzie, D. The thermal structure of the lithosphere from shear wave velocities. Earth and Planetary Science Letters, 244(1-2), pp.285-301, https://doi.org/10.1016/j.epsl.2006.01.008, 2006.

- Prud'homme, C., Rovas, D., Veroy, K., Machiels, L., Maday, Y., Patera, A. and Turinici, G. Reliable Real-Time Solution of Parametrized Partial Differential Equations: Reduced-Basis Output Bound Methods. Journal of Fluids Engineering, 124(1), pp.70-80, https://doi.org/10.1115/1.1448332, 2001.

- Przybycin, A., Scheck-Wenderoth, M. and Schneider, M.: Assessment of the isostatic state and the load distribution of the European Molasse basin by means of lithospheric-scale 3D structural and 3D gravity modelling. International Journal of Earth Sciences, 104(5), pp.1405-1424, https://doi.org/10.1007/s00531-014-1132-4, 2014.

- Przybycin, A., Scheck-Wenderoth, M. and Schneider, M. The 3D conductive thermal field of the North Alpine Foreland Basin: influence of the deep structure and the adjacent European Alps. Geothermal Energy, 3(1), https://doi.org/10.1186/s40517-015-0038-0, 2015.

- Quarteroni, A., Manzoni, A., and Negri, F. Reduced Basis Methods for Partial Differential Equations: An Introduction, UNITEXT, Springer International Publishing, 2015.

- Ranalli, G. Rheology of The Earth. London: Chapman & Hall, 1995.

- Ranalli, G. and Murphy, D. Rheological stratification of the lithosphere. Tectonophysics, 132(4), pp.281-295, https://doi.org/10.1016/0040-1951(87)90348-9, 1987.

- Refsgaard, J., van der Sluijs, J., Højberg, A. and Vanrolleghem, P. Uncertainty in the environmental modelling process – A framework and guidance. Environmental Modelling & Software, 22(11), pp.1543-1556, https://doi.org/10.1016/j.envsoft.2007.02.004, 2007.

- Restivo, A., Bressan, G. and Sugan, M. Stress and strain patterns in the Venetian Prealps (north-eastern Italy) based on focal-mechanism solutions. Bollettino di Geofisica Teorica ed Applicata, 57(1), pp.13-30, 2016.

- Reinecker, J. and Lenhardt, W. Present-day stress field and deformation in eastern Austria. International Journal of Earth Sciences, 88(3), pp.532-550, https://doi.org/10.1007/s005310050283, 1999.

- Rizzo, C., de Barros, F., Perotto, S., Oldani, L. and Guadagnini, A. Adaptive POD model reduction for solute transport in heterogeneous porous media. Computational Geosciences, 22(1), pp.297-308, https://doi.org/10.1007/s10596-017-9693-5, 2017.

- Rodriguez Piceda, C., Scheck Wenderoth, M., Gomez Dacal, M., Bott, J., Prezzi, C. and Strecker, M. Lithospheric density structure of the southern Central Andes constrained by 3D data-integrative gravity modelling. International Journal of Earth Sciences, https://doi.org/10.1007/s00531-020-01962-1, 2020.

- Rousset, M., Huang, C., Klie, H. and Durlofsky, L. Reduced-order modeling for thermal recovery processes. Computational Geosciences, 18(3-4), pp.401-415, https://doi.org/10.1007/s10596-013-9369-8, 2013.

- Rozza, G., Huynh, D. and Patera, A. Reduced basis approximation and a posteriori error estimation for affinely parametrized elliptic coercive partial differential equations. Archives of Computational Methods in Engineering, 15(3), pp.1-47, https://doi.org/10.1007/bf03024948, 2007.

- Saltelli, A. Making best use of model evaluations to compute sensitivity indices. Computer Physics Communications, 145(2), pp.280-297, https://doi.org/10.1016/s0010-4655(02)00280-1, 2002.

- Saltelli, A., Annoni, P., Azzini, I., Campolongo, F., Ratto, M. and Tarantola, S. Variance based sensitivity analysis of model output. Design and estimator for the total sensitivity index. Computer Physics Communications, 181(2), pp.259-270, https://doi.org/10.1016/j.cpc.2009.09.018, 2010.

- Sánchez, L., Völksen, C., Sokolov, A., Arenz, H. and Seitz, F. Present-day surface deformation of the Alpine region inferred from geodetic techniques. Earth System Science Data, 10(3), pp.1503-1526, https://doi.org/10.5194/essd-10-1503-2018, 2018.

- Scarascia, S. and Cassinis, R.: Crustal structures in the central-eastern Alpine sector: A revision of the available DSS data. Tectonophysics, 271(1-2), pp.157-188, https://doi.org/10.1016/s0040-1951(96)00206-5, 1997.

- Schaeffer, A. and Lebedev, S. Global shear speed structure of the upper mantle and transition zone. Geophysical Journal International, 194(1), pp.417-449, https://doi.org/10.1093/gji/ggt095, 2013.

- Scharf, A., Handy, M., Favaro, S., Schmid, S. and Bertrand, A. Modes of orogen-parallel stretching and extensional exhumation in response to microplate indentation and roll-back subduction (Tauern Window, Eastern Alps). International Journal of Earth Sciences, 102(6), pp.1627-1654, https://doi.org/10.1007/s00531-013-0894-4, 2013.

- Scheck-Wenderoth, M., Cacace, M., Maystrenko, Y., Cherubini, Y., Noack, V., Kaiser, B., Sippel, J. and Björn, L. Models of heat transport in the Central European Basin System: Effective mechanisms at different scales. Marine and Petroleum Geology, 55, pp.315-331, https://doi.org/10.1016/j.marpetgeo.2014.03.009, 2014.

- Schlumburger.: Petrel (2011.1.2) [Computer program], 1998.

- Schlunegger, F., Willett, S. Spatial and temporal variations in exhumation of the central Swiss Alps and implications for exhumation mechanisms, in Exhumation Processes: Normal Faulting, Ductile Flow and Erosion, U. Ring et al. (eds), Geol. Soc. London Sp Pub, 154, 157–179, 1999.

- Schmid, S., Aebli, H., Heller, F. and Zingg, A. The role of the Periadriatic Line in the tectonic evolution of the Alps. Geological Society, London, Special Publications, 45(1), pp.153-171, https://doi.org/10.1144/gsl.sp.1989.045.01.08, 1989.

- Schmid, S., Fügenschuh, B., Kissling, E. and Schuster, R. Tectonic map and overall architecture of the Alpine orogen. Eclogae Geologicae Helvetiae, 97(1), pp.93-117, https://doi.org/10.1007/s00015-004-1113-x, 2004.

- Schmidt, S., Götze, H. J., Fichler, C, Ebbing, J., Alvers, M. R.: 3D Gravity, FTG and magnetic modeling: the new IGMAS + software. Geoinformatik 2010, 2010.

- Schmidt, S., Anikiev, D., Götze, H.-J., Gomez Garcia, À., Gomez Dacal, M. L., Meeßen, C., Plonka, C., Rodriguez Piceda, C., Spooner, C., and Scheck-Wenderoth, M.: IGMAS+ – a tool for interdisciplinary 3D potential field modelling of complex geological structures., EGU General Assembly 2020, Online, 4–8 May 2020, EGU2020-8383, https://doi.org/10.5194/egusphere-egu2020-8383, 2020

- Schwarz, R., Pfeifer, N., Pfennigbauer, M. and Mandlburger, G. Depth Measurement Bias in Pulsed Airborne Laser Hydrography Induced by Chromatic Dispersion. IEEE Geoscience and Remote Sensing Letters, pp.1-5, https://doi.org/10.1109/lgrs.2020.3003088, 2020.

- Serpelloni, E., Vannucci, G., Anderlini, L. and Bennett, R. Kinematics, seismotectonics and seismic potential of the eastern sector of the European Alps from GPS and seismic deformation data. Tectonophysics, 688, pp.157-181, https://doi.org/10.1016/j.tecto.2016.09.026, 2016.

- Sibson, R. H. Fault zone models, heat flow, and the depth distribution of earthquakes in the continental crust of the United States, Bull. Seismol. Soc. Am., 72(1), 151–163, 1982.

- Simpson, F. Surveys in Geophysics, 20(3/4), pp.201-227, https://doi.org/10.1023/A:1006641922180, 1999.

- Sinclair, H., D. Tectonostratigraphic model for underfilled peripheral foreland basins: An Alpine perspective. GSA Bulletin, 109(3), pp.324–346, https://doi.org/10.1130/0016-7606(1997)109<0324:TMFUPF>2.3.CO;2, 1997.

- Singer, J., Diehl, T., Husen, S., Kissling, E. and Duretz, T. Alpine lithosphere slab rollback causing lower crustal seismicity in northern foreland. Earth and Planetary Science Letters, 397, pp.42-56, https://doi.org/10.1016/j.epsl.2014.04.002, 2014.

- Sippel, J., Scheck-Wenderoth, M., Lewerenz, B. and Klitzke, P. Deep vs. shallow controlling factors of the crustal thermal field - insights from 3D modelling of the Beaufort-Mackenzie Basin (Arctic Canada). Basin Research, 27(1), pp.102-123, https://doi.org/10.1111/bre.12075, 2014.

- Smith, L. and Chapman, D. On the thermal effects of groundwater flow: 1. Regional scale systems. Journal of Geophysical Research, 88(B1), p.593, https://doi.org/10.1029/jb088ib01p00593, 1983.

- Sobol, I. Global sensitivity indices for nonlinear mathematical models and their Monte Carlo estimates. Mathematics and Computers in Simulation, 55(1-3), pp.271-280, https://doi.org/10.1016/s0378-4754(00)00270-6, 2001.

- Song, X., Zhang, J., Zhan, C., Xuan, Y., Ye, M. and Xu, C. Global sensitivity analysis in hydrological modeling: Review of concepts, methods, theoretical framework, and applications. Journal of Hydrology, 523, pp.739-757, https://doi.org/10.1016/j.jhydrol.2015.02.013, 2015.

- Spada, M., Bianchi, I., Kissling, E., Agostinetti, N. and Wiemer, S. Combining controlled-source seismology and receiver function information to derive 3-D Moho topography for Italy. Geophysical Journal International, 194(2), pp.1050-1068, https://doi.org/10.1093/gji/ggt148, 2013.

- Spiegel, C., Kuhlemann, J., Dunkl, I., Frisch, W., von Eynatten, H. and Balogh, K. The erosion history of the Central Alps: evidence from zircon fission track data of the foreland basin sediments. Terra Nova, 12(4), pp.163-170, https://doi.org/10.1046/j.1365-3121.2000.00289.x, 2000.

- Spiegel, C., Siebel, W., Frisch, W. and Berner, Z. Nd and Sr isotopic ratios and trace element geochemistry of epidote from the Swiss Molasse Basin as provenance indicators: implications for the reconstruction of the exhumation history of the Central Alps. Chemical Geology, 189(3-4), pp.231-250, https://doi.org/10.1016/s0009-2541(02)00132-8, 2002.

- Spooner, C., Scheck-Wenderoth, M., Götze, H., Ebbing, J. and Hetényi, G. Density distribution across the Alpine lithosphere constrained by 3-D gravity modelling and relation to seismicity and deformation. Solid Earth, 10(6), pp.2073-2088, https://doi.org/10.5194/se-10-2073-2019, 2019.

- Spooner, C., Scheck-Wenderoth, M., Cacace, M., Götze, H. and Luijendijk, E. The 3D thermal field across the Alpine orogen and its forelands and the relation to seismicity. Global and Planetary Change, 193, p.103288, https://doi.org/10.1016/j.gloplacha.2020.103288, 2020.

- Sternai, P., Sue, C., Husson, L., Serpelloni, E., Becker, T., Willett, S., Faccenna, C., Di Giulio, A., Spada, G., Jolivet, L., Valla, P., Petit, C., Nocquet, J., Walpersdorf, A. and Castelltort, S. Present-day uplift of the European Alps: Evaluating mechanisms and models of their relative contributions. Earth-Science Reviews, 190, pp.589-604, https://doi.org/10.1016/j.earscirev.2019.01.005, 2019.

- Stephenson, R., Egholm, D., Nielsen, S. and Stovba, S. Role of thermal refraction in localizing intraplate deformation in southeastern Ukraine. Nature Geoscience, 2(4), pp.290-293, https://doi.org/10.1038/ngeo479, 2009.

- Strößenreuther, U.: Die Struktur der Erdkruste am Südwestrand der Böhmischen Masse, abgeleitet aus refraktionsseismischen Messungen der Jahre 1970 und 1978/79. Ph.D. Thesis, Universität München, 1982.

- Stucchi, M., Rovida, A., Gomez Capera, A., Alexandre, P., Camelbeeck, T., Demircioglu, M., Gasperini, P., Kouskouna, V., Musson, R., Radulian, M., Sesetyan, K., Vilanova, S., Baumont, D., Bungum, H., Fäh, D., Lenhardt, W., Makropoulos, K., Martinez Solares, J., Scotti, O., Živčić, M., Albini, P., Batllo, J., Papaioannou,

C., Tatevossian, R., Locati, M., Meletti, C., Viganò, D. and Giardini, D. The SHARE European Earthquake Catalogue (SHEEC) 1000–1899. Journal of Seismology, 17(2), pp.523-544, https://doi.org/10.1007/s10950-012-9335-2, 2012.

- Sue, C. and Tricart, P. Neogene to ongoing normal faulting in the inner western Alps: A major evolution of the late alpine tectonics. Tectonics, 22(5), https://doi.org/10.1029/2002tc001426, 2003.

- Tang, Y., Reed, P., van Werkhoven, K. and Wagener, T. Advancing the identification and evaluation of distributed rainfall-runoff models using global sensitivity analysis. Water Resources Research, 43(6), https://doi.org/10.1029/2006wr005813, 2007.

- Tesauro, M., Hollenstein, C., Egli, R., Geiger, A. and Kahle, H. Continuous GPS and broad-scale deformation across the Rhine Graben and the Alps. International Journal of Earth Sciences, 94(4), pp.525-537, https://doi.org/10.1007/s00531-004-0453-0, 2005.

- Tesauro, M., Kaban, M. and Cloetingh, S. EuCRUST-07: A new reference model for the European crust. Geophysical Research Letters, 35(5), https://doi.org/10.1029/2007gl032244, 2008.

- Tesauro, M., Kaban, M. and Cloetingh, S. A new thermal and rheological model of the European lithosphere. Tectonophysics, 476(3-4), pp.478-495, https://doi.org/10.1016/j.tecto.2009.07.022, 2009.

- Tesauro, M., Burov, E., Kaban, M. and Cloetingh, S. Ductile crustal flow in Europe's lithosphere. Earth and Planetary Science Letters, 312(1-2), pp.254-265, https://doi.org/10.1016/j.epsl.2011.09.055, 2011.

- Trumpy, E. and Manzella, A. Geothopica and the interactive analysis and visualization of the updated Italian National Geothermal Database. International Journal of Applied Earth Observation and Geoinformation, 54, pp.28-37, https://doi.org/10.1016/j.jag.2016.09.004, 2017.

- Turcotte, D. and Schubert, G., 2002. Geodynamics. Cambridge: Cambridge Univ. Press.

- Turrini, C., Lacombe, O. and Roure, F.: Present-day 3D structural model of the Po Valley basin, Northern Italy. Marine and Petroleum Geology, 56, pp.266-289, https://doi.org/10.1016/j.marpetgeo.2014.02.006, 2014.

- Ustaszewski, K. and Schmid, S. Latest Pliocene to recent thick-skinned tectonics at the Upper Rhine Graben – Jura Mountains junction. Swiss Journal of Geosciences, 100(2), pp.293-312, https://doi.org/10.1007/s00015-007-1226-0, 2007.

- van Griensven, A., Meixner, T., Grunwald, S., Bishop, T., Diluzio, M. and Srinivasan, R. A global sensitivity analysis tool for the parameters of multi-variable catchment models. Journal of Hydrology, 324(1-4), pp.10-23, https://doi.org/10.1016/j.jhydrol.2005.09.008, 2006.

- Vignaroli, G., Faccenna, C., Jolivet, L., Piromallo, C. and Rossetti, F. Subduction polarity reversal at the junction between the Western Alps and the Northern Apennines, Italy. Tectonophysics, 450(1-4), pp.34-50, https://doi.org/10.1016/j.tecto.2007.12.012, 2008.

- Vogt, C., Mottaghy, D., Wolf, A., Rath, V., Pechnig, R. and Clauser, C. Reducing temperature uncertainties by stochastic geothermal reservoir modelling. Geophysical Journal International, 181(1), pp.321-333, https://doi.org/10.1111/j.1365-246x.2009.04498.x, 2010.

- von Blanckenburg, F. and Davies, J. Slab breakoff: A model for syncollisional magmatism and tectonics in the Alps. Tectonics, 14(1), pp.120-131, https://doi.org/10.1029/94tc02051, 1995.

- Vrabec M, Fodor L. Late Cenozoic tectonics of Slovenia: structural styles at the northeastern corner of the Adriatic microplate. In: Pinter N, Grenerczy G, Weber J, Stein S, Medak D (eds) The Adria microplate: GPS geodesy, tectonics and hazards, vol 61: Nato Scie Series, IV, earth and environmental science, vol 61. Springer, Dordrecht, pp 151–158, 2006.

- Vrabec, M., Pavlovcic Preseren, P., Stopar, B. GPS study (1996-2002) of active deformation along the Periadriatic fault system in northeastern Slovenia: tectonic model. Geol. Carpathica, 57, 1, 57-65, 2006.

- Wagner, R. and Clauser, C. Evaluating thermal response tests using parameter estimation for thermal conductivity and thermal capacity. Journal of Geophysics and Engineering, 2(4), pp.349-356, https://doi.org/10.1088/1742-2132/2/4/s08, 2005.

- Wainwright, H., Finsterle, S., Jung, Y., Zhou, Q. and Birkholzer, J. Making sense of global sensitivity analyses. Computers & Geosciences, 65, pp.84-94, https://doi.org/10.1016/j.cageo.2013.06.006, 2014.

- Wellmann, J. and Reid, L. Basin-scale Geothermal Model Calibration: Experience from the Perth Basin, Australia. Energy Procedia, 59, pp.382-389, https://doi.org/10.1016/j.egypro.2014.10.392, 2014.

- Wellmann, F. and Caumon, G. 3-D Structural geological models: Concepts, methods, and uncertainties. Advances in Geophysics, pp.1-121, https://doi.org/10.1016/bs.agph.2018.09.001, 2018.

- Wiemer, S., Kraft, T., Trutnevyte, E., & Roth, P. "Good Practice " Guide for Managing Induced Seismicity in Deep Geothermal Energy Projects in Switzerland, SED, Swiss Seismological Service at ETH Zürich, https://doi.org/10.3929/ethz-b-000254161, 2017

- Willingshofer, E. and Cloetingh, S. Present-day lithospheric strength of the Eastern Alps and its relationship to neotectonics. Tectonics, 22(6), https://doi.org/10.1029/2002tc001463, 2003.

Wittmann, H., von Blanckenburg, F., Kruesmann, T., Norton, K. and Kubik, P. Relation between rock uplift and denudation from cosmogenic nuclides in river sediment in the Central Alps of Switzerland. Journal of Geophysical Research, 112(F4), https://doi.org/10.1029/2006jf000729, 2007.

- Yan, Q. and Mechie, J.: A fine structural section through the crust and lower lithosphere along the axial region of the Alps. Geophysical Journal International, 98(3), pp.465-488, https://doi.org/10.1111/j.1365-246x.1989.tb02284.x, 1989.

- Ye, S., Ansorge, J., Kissling, E. and Mueller, S.: Crustal structure beneath the eastern Swiss Alps derived from seismic refraction data. Tectonophysics, 242(3-4), pp.199-221, https://doi.org/10.1016/0040-1951(94)00209-r, 1995.

- Zahorec, P., Papčo, J., Pašteka, R., Bielik, M., Bonvalot, S., Braitenberg, C., Ebbing, J., Gabriel, G., Gosar, A., Grand, A., Götze, H.-J., Hetényi, G., Holzrichter, N., Kissling, E., Marti, U., Meurers, B., Mrlina, J., Nogová, E., Pastorutti, A., Scarponi, M., Sebera, J., Seoane, L., Skiba, P., Szűcs, E., and Varga, M. The first pan-Alpine surface-gravity database, a modern compilation that crosses frontiers, Earth Syst. Sci. Data Discuss. [preprint], https://doi.org/10.5194/essd-2020-375, in review, 2021.

- Zehner, B., Watanabe, N. and Kolditz, O. Visualization of gridded scalar data with uncertainty in geosciences. Computers & Geosciences, 36(10), pp.1268-1275, https://doi.org/10.1016/j.cageo.2010.02.010, 2010.

- Zeis, S., Gajewski, D. and Prodehl, C.: Crustal structure of southern Germany from seismic refraction data. Tectonophysics, 176(1-2), pp.59-86, https://doi.org/10.1016/0040-1951(90)90259-b, 1990.

- Zhan, C., Song, X., Xia, J. and Tong, C. An efficient integrated approach for global sensitivity analysis of hydrological model parameters. Environmental Modelling & Software, 41, pp.39-52, https://doi.org/10.1016/j.envsoft.2012.10.009, 2013.

- Zhao, L., Paul, A., Guillot, S., Solarino, S., Malusà, M., Zheng, T., Aubert, C., Salimbeni, S., Dumont, T., Schwartz, S., Zhu, R. and Wang, Q. First seismic evidence for continental subduction beneath the Western Alps. Geology, 43(9), pp.815-818, https://doi.org/10.1130/g36833.1, 2015.

- Zingg, A., Handy, M., Hunziker, J. and Schmid, S. Tectonometamorphic history of the Ivrea Zone and its relationship to the crustal evolution of the Southern Alps. Tectonophysics, 182(1-2), pp.169-192, https://doi.org/10.1016/0040-1951(90)90349-d, 1990.

- Zlotnik, S., Díez, P., Modesto, D. and Huerta, A. Proper generalized decomposition of a geometrically parametrized heat problem with geophysical applications. International Journal for Numerical Methods in Engineering, 103(10), pp.737-758, https://doi.org/10.1002/nme.4909, 2015.

-Zucca, J.J.: The crustal structure of the southern Rhine graben from the reinterpretation of seismic refraction data. Journal of Geophysics - Zeitschrift für Geophysik, 55, pp.13-22, https://doi.org/10.23689/fidgeo-3178, 1984.